UCGE Reports

Number 20388

Department of Geomatics Engineering

GNSS Signal Acquisition in The Presence of Narrowband Interference

by

Mohammad Abdizadeh

September 2013

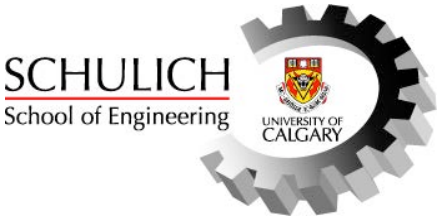

UNIVERSITY OF CALGARY

GNSS Signal Acquisition in The Presence of Narrowband Interference

by

Mohammad Abdizadeh

A THESIS

SUBMITTED TO THE FACULTY OF GRADUATE STUDIES

IN PARTIAL FULFILMENT OF THE REQUIREMENTS FOR THE

DEGREE OF DOCTOR OF PHILOSOPHY

DEPARTMENT OF GEOMATICS ENGINEERING

CALGARY, ALBERTA

SEPTEMBER, 2013

Abstract

GNSS system vulnerability to interference is a major concern for civil applications particularly for either weak signal environment or consumer-grade receivers. This thesis provides a comprehensive analysis of the quantization and acquisition loss incurred in a conventional GNSS receiver in the presence of CW interference. It also proposes some low complexity solutions to improve the receiver performance in terms of quantization and acquisition metrics.

This work contributes to the field of interference resilience consumer-grade GNSS receiver in three different ways. First, a general framework for quantization loss in a low resolution GNSS receiver is developed. Simulation results show that traditional techniques used to estimate C/N_0 are unreliable when interference is present. To avoid this problem, the BER metric is employed in this work. Afterwards, it is shown that in this case, there is an optimum configuration in terms of BER and detection probability performance for a quantization process in which the AGC is allowed to dynamically adjust the gain applied to the input signal.

Second, an LMS-based adaptive FIR notch filter is proposed and developed to adaptively detect, locate and reject the narrowband interference signal with negligible side effects on desired GNSS signal. Next, this NF is modified to have linear-phase response in order to eliminate the bias and distortion on pseudorange measurements. Compared to IIR notch filters, an FIR notch filter is always stable and induces less numerical errors into the filtered signal.

Third, the problem of GNSS signal acquisition using a consumer-grade receiver is investigated. After proposing a general framework for cell-level and system-level signal

acquisition of a GNSS receiver, a detailed model of the impact of interference signals on the CAF of a GNSS signal is presented, and is employed in the development of novel acquisition strategies. These new strategies are examined under a selection of operating scenarios including: acquisition in the presence of interference when the receiver has some, or no *a priori* information regarding the interference. It is shown that, by employing these new schemes, a receiver can operate under a *JNR* 20 dB higher than when using traditional schemes.

Preface

This thesis includes some materials (e.g. figures, tables and texts) previously published, accepted or submitted in two conference papers and two journal paper as follows:

1. **M. Abdizadeh**, J. T. Curran, and G. Lachapelle, "Acquisition of GNSS Signals in The Presence of Continuous Wave Interference," submitted to *IEEE Transactions on Aerospace and Electronic Systems*, 12 pages.

2. **M. Abdizadeh**, J. T. Curran, and G. Lachapelle, "Quantization Loss in GNSS Receivers Due to Narrowband Interference," submitted to *International Journal of Navigation and Observation*, 11 pages.

3. **M. Abdizadeh**, J. T. Curran, and G. Lachapelle, "Quantization Effects in GNSS Receivers in The Presence of Interference," ION/ITM'12, Newport Beach, California, 29 Jan.-2 Feb. 2012.

4. Tao Lin, **M. Abdizadeh**, A. Broumandan, D. Wang, K. O'Keefe, and Gérard Lachapelle, "Interference Suppression for High Precision Navigation Using Vector-Based and Ultra-Tight GNSS Software Receivers," ION GNSS 2011, Portland, Or., Sep. 20-23, 2011.

The above papers were produced by the author during the research phase of this thesis.

The co-authors' valuable feedback on the above materials is acknowledged. Use of the above material in this thesis is allowed by the co-authors and the journal/proceedings publishers.

Acknowledgements

I would like to express the deepest appreciation to my supervisor, Professor Gérard Lachapelle for his generous support and persistent guidance throughout my PhD studies. His sincere kindness and continuous invaluable encouragement over the last three years have helped me to shape my professional career.

In addition, I would like to sincerely thank my advisor, Dr. James T. Curran who has generously shared his precious time and expertise during this research. It's been an honor for me to work with him while his guidance and profound knowledge helped me throughout my studies. I would also like to thank Dr. Ali Boroumandan and Dr. Daniele Borio for their valuable advice during my research.

I would also like to thank my colleagues and dear friends in the PLAN group, in particular Dr. Saeed Daneshmand and Negin Sokhandan who provided me with a pleasant and peaceful environment to live and study. Special thanks to Dr. Benyamin Yadali for his editorial comments on the final copy.

Finally and most importantly, I would like to thank my parents and my brothers and sisters without whose support, warm encouragement and motivation throughout my research I would never have been able to finish my dissertation. I would never have gotten this far without them.

To my lovely mother, Fatemeh

Table of Contents

List of Tables

List of Figures and Illustrations

List of Acronyms

ACF	Autocorrelation Function
ADC	Analogue to Digital Converter
AGC	Automatic Gain Control
AM	Amplitude Modulation
ARMA	Autoregressive Moving Average
AR	Autoregressive
AWGN	Additive White Gaussian Noise
BER	Bit Error Rate
BPSK	Binary Phase Shift Keying
BW	Bandwidth
C/A	Coarse/Acquisition
C/N_0	Carrier-to-Noise-Ratio
CAF	Cross Ambiguity Function
CDMA	Code Division Multiple Access
CW	Continuous Wave
dBic	dB (isotropic circular)
DFT	Discrete Fourier Transform
DME	Distance Measuring Equipment
DMF	Digital Matched Filter
DS/CDMA	Direct Sequence CDMA
DSSS	Direct Sequence Spread Spectrum
FFT	Fast Fourier Transform

FIR	Finite Impulse Response
FIR-ANF	Adaptive FIR Notch Filters
FM	Frequency Modulation
GNSS	Global Navigation Satellite System
GPS	Global Positioning System
IF	Intermediate Frequency
IIR	Infinite Impulse Response
JNR	Jammer-to-Noise-Ratio
JSNR	Jammer-to-Signal-and-Noise-Ratio
LNA	Low Noise Amplifier
LOS	Line of Sight
LP-FIR	Linear-Phase FIR
LMS	Least Mean Squares
MA	Moving Average
MSE	Mean Square Error
NB	Narrowband
NF	Notch Filter
NI	National Instrument
NRZ	Non-Return to Zero
PDF	Probability Density Function
PG	Plain Gradient
PLL	Phase Lock Loop
PRN	Pseudo Random Noise

PSD	Power Spectral Density
PVT	Position, Velocity and Time
RF	Radio Frequency
ROC	Receiver Operating Characteristic
SINR	Signal-to-Interference-and-Noise-Ratio
SNR	Signal-to-Noise-Ratio
STFT	Short Time Fourier Transform
TACAN	Tactical Air Navigation
TOA	Time of Arrival
WT	Wavelet Transform

List of Symbols and Notations

$*$	Conjugate operator
$\bigstar$	Convolution operator
$\langle\cdot\rangle_W$	Average of input calculated across a window of W cells
∇	Gradient operator
∇^2	Laplacian operator
β	Decision constant threshold
δx	Error in the receivers estimate
$\Delta\tau$	Code bin width
ΔF	Doppler bin width
$\eta_{\mathrm{IF}}(t)$	Additive noise
θ	IF carrier phase
θ_{int}	Interference random initial phase
λ	L1 Wavelength
$\mu[k]$	Normalized LMS step size
ρ	Pole contraction factor
ρ_∞	Coherent SINR for a no-quantizing receiver
ρ_B	Coherent SINR for a B-bit quantizer
σ_n^2	Noise variance
τ	Code phase
τ_g	Group delay
A_g	AGC gain
$A_{g,\mathrm{opt}}$	Optimum AGC gain

A_{int}	Transmitted interference amplitude
A_s	Amplitude of the received signal after the IF stage
B	Quantizer's bit resolution
B_{IF}	IF front-end bandwidth
c	Speed of light
C	Received power of the desired signal
$c(t)$	Spreading code
$\text{chip}(t)$	Unit amplitude rectangular pulse
D	*Decision variable*
D_0	Null hypothesis
D_1	Alternative hypothesis
D^{τ}	Curvature of *decision variable* in the τ dimension
D^{IntR}	Direct interference removal *decision variable*
D^{Lap}	Laplacian of *decision variable*
D^{Pair}	Frequency-pair *decision variable*
D^{Wind}	Window-based *decision variable*
$d(t)$	Data modulation
$e[k]$	Notch filter output or the error signal of the filter
$\text{erfc}(\cdot)$	Complementary error function
f_{Δ}	Interference frequency offset
f_c	L1 frequency (1575.42 MHz)
f_{D}	Doppler shift/frequency
$F_{\text{D, jammer}}$	Doppler frequency of jammer

f_{IF}	Intermediate frequency
F_s	Sampling rate
$g[k]$	Impulse response of the gradient system
G_r	Receiver antenna gain for jammer
G_t	Jammer antenna gain
$G_s(f)$	Power spectral density of the GNSS signal
H_0	Null hypothesis
H_1	Alternative hypothesis
$h_c[n]$	Impulse response of equivalent demodulation process
$H_c(f)$	Fourier transform of $h_c[n]$
$H_{\mathrm{FIR}}(z)$	*T*ransfer function of complex FIR notch filter
$h_{\mathrm{FIR-LP}}$	Impulse response of linear-phase NF
$H_{\mathrm{IIR}}(z)$	Transfer function of complex IIR notch filter
$H_{\mathrm{LP-FIR}}(z)$	Transfer function of linear-phase NF
I_2	2×2 identity matrix
I_n	Real part of $S(\tau, f_{\mathrm{D}})$
$i_{\mathrm{IF}}(t)$	Narrowband interference
J[k]	Cost function
K	Non-coherent combinations
L1	GPS L1 center frequency, 1575.42 MHz
L_B	Quantization loss for a B-bit quantizer
M	Number of continuous wave interferences
N	FIR NF filter order

N_0 (W/Hz)	AWGN single-sided power spectral density
$N(\mu, \sigma^2)$	Gaussian random variable with mean μ and variance of σ^2
P_{D}	Detection probability
P_e	Bit error rate
P_{fa}	Probability of false-alarm
P_{cw}	Interference power
P_j	Transmitted jammer power
P_{jammer}	Received jammer power
$Q(x)$	Quantized value of input x
$Q_B^{Ag}[x]$	B-bit symmetric quantizer
Q_n	Imaginary part of $S(\tau, f_{\mathrm{D}})$
$r_B[n]$	Sampled and quantized version of received signal
$r_{\mathrm{IF}}(t)$	IF signal at the input of a GNSS receiver
$R(\tau)$	Autocorrelation function of the spreading codes
$R_{c,x}$	Correlation between the interference and spreading code
$s_{\mathrm{IF}}(t)$	Desired GNSS signal
S_{sv}	Set of all the visible satellites
$S(\tau, f_{\mathrm{D}})$	Cross ambiguity function
S_η	Contribution of the noise signal in CAF
S_{int}	Contribution of the interference signal in CAF
S_y	Contribution of the GNSS signal in CAF
T_0	*Decision metric*
T_1	*Decision metric*

T_b	GNSS bit period
T_c	Chip period
T_I	Coherent integration time
T_{SW}	Interference swept time
$u(\cdot)$	Unit step function
V_{rel}	Relative velocity
V_T	Decision threshold
W	Window length of window-based *decision variable*
$\hat{x}$	Estimate value of x
z_0	Notch filer zero
$\hat{z}_0[k]$	NF zero estimate
$z_{0,\ \mathrm{Wiener}}$	Wiener solution for notch filter

Chapter One: Thesis Introduction

As radio frequency (RF) interference becomes more recognized as a threat, the challenge of its detection and mitigation in global navigation satellite system (GNSS) receivers is becoming ever more important and receiving more attention. It is evident that virtually no GNSS system is impervious to the effects of interference, intentional or otherwise (Abdizadeh et al 2012, Arribas et al 2012, Balaei et al 2008, Betz 2000). The exact impact of interference on receiver performance is heavily dependent on the receiver configuration. Specifically, the carrier-to-noise ratio (C/N_0) of all GPS satellite signals is reduced in the presence of interference. Furthermore, this effect degrades the code correlation, acquisition, and loop filtering performance (Kaplan & Hegarty 2006). Hence, the overall system performance decreases in terms of acquisition loss, tracking loop error, and navigation solution error.

The objective of this study is to provide a cohesive and complete analysis of the quantization and acquisition process of GNSS receiver in the presence of narrowband (NB) interference. Specifically, this study provides the statistical and mathematical tools required to design, and predict the performance of both the cell-level and system-level acquisition schemes that can mitigate the effect of interfering signals.

1.1 Background and Motivation

Interference signals can affect different processes and different parameters of a typical GNSS receiver. Specifically, the performance of the quantization process, acquisition process and tracking loops can be severely affected by interference. Interference

detection and mitigation techniques are widely employed to detect the interference signal, estimate some of its characteristics, and remove the interference signal (Kaplan & Hegarty 2006). However, the proposed algorithms do not work perfectly and, due to missed detection and residual interference signal, the GNSS receiver may not provide the desired performance.

This study targets the quantization process, interference detection and mitigation scheme, and acquisition process of the receiver in the presence of interference. In addition, receiver design guidelines, which provide reasonable performance in terms of acquisition metrics and reception quality, are presented and analyzed. Appendix A presents a review of some interference and jammers that have been observed in the GPS band. Among different types of interference signals, continuous wave (CW) interference and swept interference are the two most common types of interference observed in the GPS band. Thus, this study focuses on CW interference and swept/chirp interference detection and mitigation techniques.

1.2 Relevant Research

This research evaluates the performance of the digital GNSS receiver and proposes new methods to enhance the performance. The following section presents a review of the literature on the functionality of these receiver operations in the presence of interference. Additionally, the existing opportunities to improve the GNSS receiver performance in the presence of harmful interference are introduced.

1.2.1 IF Signal Quantization

The study of quantization of a signal is a widely discussed subject that has been considered in many different fields. In terms of performance measures, traditional techniques have focused on the "minimum average distortion" metric where the best quantizer is that which minimizes the expected value of $\left(x - Q(x)\right)^2$, where $Q(x)$ represents the quantized value of input x. While effective in high signal-to-noise-ratio environments (Echard 1992, Gandhi 1996, Gray & Neuhoff 1998), this metric is not necessarily useful for weaker signals, especially for GNSS, where the desired signal is often below the noise floor.

In the case of GNSS, the noise is the dominant part of the received signal and, therefore, the minimum distortion metric simply measures the distortion of the noise. More appropriate for the GNSS application is a metric that measures the receiver's ability to estimate a parameter of a received signal from a quantized sample of signal-plus-noise. This criterion has not really been considered in any of the early quantization work. In the GNSS literature, this criterion can be related to an effective C/N_0 and, therefore, C/N_0 results are mostly considered to evaluate the performance of GNSS quantizers. As it has been shown over the last ten years, this metric generally results in quite different losses and design rationales (e.g. Curran et al (2010) and Borio (2008)). In the absence of interference, this has been examined by various researchers (Dierendonck et al 1996, Borio 2008, Parkinson & Spilker 1996, Zhe et al 2008, Hegarty 2011). However, in the presence of interference, this has only been briefly touched upon and is currently

receiving a considerable attention in the GPS community, including, for example, work by (Hegarty 2011, Betz 2000, Sharawi et al 2007, Balaei et al 2009).

Typically, a low resolution quantizer is utilized in consumer-grade GNSS receivers (Curran et al 2010). The reasons for such a choice include the facts that employing a low resolution quantizer is efficient in the sense of cost, computational requirement, and data-throughput limitations. Furthermore, with an appropriate sampling rate, the quantizer degradation in the presence of a Gaussian noise alone is not significant, being 1.96 dB, 0.55 dB, and 0.16 dB for 1-, 2-, and 3-bit quantizers, respectively (Kaplan & Hegarty 2006). Appendix B provides some specifications for common consumer-grade GPS receivers describing the range of quantizer resolutions employed.

Needless to say, the quantization process does degrade the received signal quality and the presence of interference intensifies this effect. Hence, the configuration of the signal quantizer can have a significant effect on the performance of interference-suffering GNSS receiver. In order to provide reliable receiver performance under strong jamming/interference conditions, the design of the receiver quantizer should be carefully considered.

The processing loss for a given number of quantization levels and certain quantizer gain is well understood in the absence of interference, and is a receiver feature that can be readily optimized (Sharawi et al 2007, Borio 2008, Zhe et al 2008, Hegarty 2011, Curran et al 2010). The mathematical model for quantization loss in the absence of interference is derived in Borio (2008) for any given number of quantizer bits as a function of the maximum input threshold level for the additive white Gaussian noise (AWGN) case. This

work was then generalized to consider the effect of front-end filtering parameters such as center frequency and bandwidth in Curran (2010). Moreover, these contributions and several previous studies (Kaplan & Hegarty 2006, Parkinson & Spilker 1996, Chang 1982) showed that there is an optimum automatic control gain for multi-bit quantizers which results in a minimum bit error rate (BER) or, equivalently, a maximum effective carrier-to-noise-ratio.

However, these results are not applicable to interference-suffering receivers and, to the best of the author's knowledge, a comprehensive analysis and optimization of the quantization loss incurred in a conventional GNSS receiver in the presence of interference is lacking. Also, the quantization literature of GNSS is lacking a model for the effect of interference power and frequency on quantization configuration. In fact, the presence of interference changes the statistics and model of the received signal at the quantizer input. This effect has serious implications for the design of quantizers for interference-suffering receivers.

1.2.2 Interference Detection & Mitigation

In the literature, numerous solutions have been proposed to alleviate the challenges of RF interference. The first step to deal with the problem of interference is to effectively detect its presence. In Ndili & Enge (1998), CW, broadband and pulsed interference are considered to test the detection metrics. Correlator output power, correlator output power variation, carrier phase vacillation and automatic gain control (AGC) control loop gain are suggested as test statistics to monitor the operation integrity of the GPS receiver.

In Borio (2008), a detection scheme for narrowband interference is proposed based on an adaptive infinite impulse response (IIR) notch filter (NF) that adaptively estimates the notch frequency. The notch frequency estimation is based on the fact that the magnitude of estimated zero of notch filter migrates toward unity in the presence of CW interference and otherwise it remains close to zero.

With the intention of eliminating the interference within the GNSS receiver, several interference mitigation techniques including time domain and frequency domain filtering have been proposed and investigated. In Capozza et al (2000), a discrete Fourier transform (DFT) based algorithm is employed to detect and remove any abnormal spectral line from the received signal's band. Moreover, some work focuses on using Kalman and Weiner based filtering (Fasihuddin et al 2005). Other current approaches include interference mitigation employing the transform domain filtering, e.g. wavelet transform (WT) domain, as well as methods based on the adaptive array antennas (Arribas et al 2012, Savasta et al 2013). Compared to other interference mitigation techniques, notch filtering algorithm is the lowest cost, computationally efficient and appropriate for in-band and out of band CW interference (Borio 2008).

To summarize, before applying any interference mitigation algorithm, an interference presence detector and characteristics estimator might be employed. The task of an “interference characteristics estimator” is to extract required information about the interference present in the received signal. This information may include interference type, interference frequency and power. Subsequently, based on the interference

characteristics, appropriate interference mitigation algorithms can be applied by the receiver to reduce the interference effect on the signal.

1.2.3 The Acquisition Process

The presence of interference within a received signal increases the challenge of acquisition of the desired GNSS signal. Previous work has mainly considered the effect of interference on the conventional acquisition schemes of the GNSS receiver (Arribas et al 2012, Savasta et al 2013, Deshapande 2004, Borio 2010). However, the effect of interference detection and mitigation is not considered. In Deshapande (2004), the effect of CW, amplitude modulation (AM) and frequency modulation (FM) interference on the acquisition process of a receiver employing different values of coherent and non-coherent integration time is presented based on a software receiver implementation. It was shown that CW interference introduces more damage into the acquisition process compared to AM/FM interference sources. This work will be extended to consider the effect of quantization and the interference detection process as well.

In Borio (2010), a statistical model is presented to describe the effect of narrowband CW interference on the acquisition process of the GNSS receiver. Theoretical results of probability of detection and false-alarm of a GNSS receiver are given in the presence of CW interference. However, this work does not consider the effect of quantization and interference detection/mitigation techniques.

To the best of the author's knowledge, the effect of interference detection/mitigation on the acquisition process is not considered in the literature. In addition, knowledge of the

presence of interference in the received signal, not only reduces the likelihood of acquiring false signals, but can also increase the probability of detecting the correct signal by employing some decision techniques. Moreover, acquisition of the quantized signal needs to be studied and analyzed in the presence of interference.

1.3 Research Motivation, Objectives & Proposed Research

In recent years, GNSS system vulnerability to interference has become a major concern for military and civil applications especially for weak signal environment or consumer-grade receivers (Mitch et al 2011). The main reasons are the increasing threat of interference and the challenge of its mitigation in receivers. The main objective of this thesis is to study the effect of interference signals on the GNSS signal quantization and acquisition process and to investigate some low complexity solutions to improve the receiver performance in terms of quantization and acquisition metrics.

The theoretical part of this thesis includes signal and interference modeling, characterization of the effects of signal quantization process, the analysis and development of interference detection/mitigation algorithms and the performance analysis of GPS signal acquisition. In areas where a theoretical study is deemed unsuitable, the study is conducted via the use of numerical simulations and real signal experimentations.

The proposed work and the details of the contributions of each section of the thesis are presented as follows.

1.3.1 IF Signal Quantization

This research seeks to extend the analysis of quantization loss in the interference-free case (Curran et al 2010) to consider the interference characteristics. In this thesis, a model for the receiver quantization loss is developed in terms of both receiver and signal parameters, including interference power, thermal noise floor, quantizer resolution, and quantizer gain. In this work, a consumer-grade GNSS receiver with 1-, 2-, 3-, and 4-bit resolution and a fixed/Swept CW interference model is considered. Details of a typical consumer-grade GNSS receiver are presented in Appendix B (Curran et al 2010).

It is expected that a receiver can adaptively adjust the quantizer gain both in the presence and absence of interference to minimize the total processing losses. This will provide some associated improvements in acquisition and tracking performance. This gain is a function of noise and interference power with respect to desired signal power. In order to set the AGC gain optimally, not only should the noise level be estimated, but also the interference power must be determined.

Moreover, the impact of optimal quantization design and configuration on the overall acquisition process is investigated. It is shown that the quantizer configuration that yields optimal performance in terms of the BER metric also provides optimal receiver operating characteristics (ROC) performance. The data collection scenario, the equipment used, and the interference replication method are discussed in detail in Chapter Three.

1.3.2 Interference Detection & Mitigation

Interference detection is required to enable the receiver to apply appropriate interference mitigation schemes (Thompson et al 2011). That is, employing incorrect interference mitigation technique does not provide expected improvements. Once the interference has been detected and characterized, then based on its characteristics, appropriate narrowband/broadband, fixed/adaptive, or time domain/transform domain interference mitigation algorithm could be applied by the receiver. Interference detection not only determines which interference mitigation technique should be employed, but also can be utilized to improve the acquisition process resiliency. Knowing the type of interference, for example whether it is fixed or swept, will be used to enhance the ROC results in the cell-level or determining a searching algorithm in system-level acquisition. In this thesis, a detection algorithm based on notch frequency estimation and AGC input histogram based interfering signals discrimination is considered. This approach is straightforward and effective in the sense of testing and software implementation.

To mitigate narrowband interference signals, notch filtering is considered in this thesis. To improve the receiver performance in terms of BER and C/N_0, an adaptive finite impulse response (FIR) notch filtering scheme is developed and implemented in the GSNRx-vb software receiver (Petovello et al 2008). It is shown that this scheme provides improved acquisition, tracking, and position domain performance compared to those of IIR notch filtering (Lin et al 2011, Montloin 2010). The data collection scenario, the equipment used, and the interference mitigation method are discussed in Chapter Four.

1.3.3 The Acquisition Process

The performance of the GNSS receiver acquisition process in the presence of interference is then evaluated. First, the acquisition model is extended to account for the impact of fixed/swept CW interference on the receiver. This model specifies the receiver detection performance at the cell-level. Furthermore, the effect of interference power on the ROC functionality of the receiver is investigated. The ROC results are generally used to evaluate the performance of the acquisition process. ROC results for this model are derived and compared through Monte-Carlo simulations. The level of performance degradation due to the addition of narrowband CW interference to the received signal is studied in detail.

Secondly, this thesis employs the results of interference detection/mitigation block to enhance the acquisition process of a GNSS signal suffering from interference. Knowledge of the interference type and its characteristics such as amplitude and frequency can improve the acquisition performance in the cell-level in terms of the probabilities of false-alarm and correct detection and the estimation of desired signal parameters.

Thirdly, the effect of the quantization process is taken into account at the cell-level. Quantization process results in a distortion on the received signal, which degrades the ROC performance of the acquisition process. For a multi-bit quantizer, it is shown that applying the optimum quantization gain could improve the acquisition performance in the sense of ROC as well. The ROC results of 1-bit, 2-bit, 3-bit, and 4-bit quantization is

computed to evaluate the benefit of employing such quantizers for different values of quantization gain.

Finally, the system-level detection performance of the GNSS receiver is investigated. Specifically, two acquisition search methods (i.e. serial search, parallel search) are considered in the fixed/swept interference case. It is possible for the serial search to fail in the presence of time varying interference. That is, the serial search algorithm searches one cell at a given time, thus the cell containing time varying interference might change in each search step.

1.3.4 System-Level Optimization: Real-Signal Test and Evaluation

Based on the research work presented here, first a MATLAB test-bench is developed to evaluate the developed mathematical models for the GPS receiver in the presence of interference. In this section, field test results are presented based on real GPS data. To collect real GPS data containing interference, a hardware simulator is employed to generate different types of interference. This generated interference is amplified and combined with a real GPS signal received from the antenna by means of a RF combiner. This signal is then be input to a National Instrument (NI) digitalizer to be filtered, down-converted, sampled and recorded into hardware storage (National Instruments 2013). This stored data is further analyzed via a developed MATLAB script as well as GSNRx software receiver to compute the quantization, acquisition and position domain results.

This study presents a comparison between theoretical and real signal experimental results to verify and analyze the theoretical results. The main goal is first to evaluate the whole

system functionality, i.e. quantization, interference detection/mitigation and signal acquisition, and next, to provide a comparison between the whole system optimization performance and separate optimization of each block. In particular, this section endeavors to quantify the total performance improvement gained through the design optimization of each of the processing stages of the receiver.

1.3.5 Experimental Measurement and Procedure

In order to collect and process the interfered GPS data, the latter is generated by combining emulated interference with real GNSS signals. The interference generation is performed with a Spirent simulator (Spirent 2008). This simulator is reconfigurable and can emulate various types of interference, i.e. fixed, swept-like CW and pulsed interference.

The GPS interference experimental test bed is comprised of three segments, namely a Spirent simulator, RF Combiner and Amplifier, and NI system. Each of the contributing signals (i.e., GPS, and Spirent signal) is filtered, amplified and combined prior to input into the NI system. The power of the generated signal can be controlled using amplifier/attenuators. The NI receiver is capable of sampling the combined signal as well as interference only signal via its different channels with a 16-bit resolution. These recorded signals are used to perform post-mission testing of the developed algorithms.

1.4 Summary of Thesis Contributions

This thesis treats different parts of an interference-suffering GNSS system. Specifically, the quantization process, interference detection and mitigation schemes, and acquisition

process are investigated and evaluated through numerical simulations and real data analyses. The main contributions of this thesis are summarized as follows:

- Analysis of the output C/N_0 and the quantization loss for low resolution GNSS receiver and proposal of a BER metric as an alternative to better represent the effect of performance degradation due to the interference. Moreover, the loss incurred through signal quantization in the presence of interference is evaluated based on the research in Chapter Three. The results of simulated signal experimentation in this work demonstrates that, for a given interference power and received signal strength, a properly designed quantizer configuration can have a significant effect on GNSS receiver performance, especially in the presence of interference. This configuration is presented in the form of design guidelines for quantizer configuration.
- A detection/mitigation algorithm based on adaptive linear-phase FIR notch filtering is designed and presented in Chapter Four. In this chapter, after investigating the performance of FIR NF, an adaptive linear-phase FIR NF is developed and implemented in a GNSS vector-based software receiver to mitigate the fixed/swept CW interference signal. The results of this work show that the linear-phase FIR notch filter provides better navigation domain results compared to that of the FIR/IIR notch filters because the group delay of linear-phase filter is frequency independent.
- The effect of the AGC gain on cell-level detection probability is studied in Chapter Five. It is shown that adjusting the AGC gain to its optimal value in

terms of BER, also results in better cell-level detection statistics of the desired signal.

- Chapter Five investigates the problem of GNSS signal acquisition using a low-resolution receiver in the presence of CW interference. After presenting a detailed model of the impact of interference signals on the cross ambiguity function of a GNSS CDMA signal, this model is employed in the development of novel acquisition strategies. These new strategies are then examined under a selection of operating scenarios including acquisition in the presence of interference when the receiver has some or no a priori information regarding the interference.
- The overall receiver performance in terms of acquisition metrics and BER in the presence of interference is evaluated. Here, the effect of quantization loss and interference mitigation schemes on the acquisition process is investigated. In Chapter Six, the total performance of the receiver is examined by considering all of the effects in previous chapters so as to improve the overall acquisition performance in the presence of interference.

1.5 Thesis Outline

The objective of this thesis is to provide a performance analysis of the acquisition of a consumer-grade GNSS receiver in the presence of NB interference. In particular, efforts are focused on the performance improvement by optimally adjusting the quantizer and modifying the acquisition search scheme.

The remaining chapters are as follows:

In Chapter Two, a short review of direct sequence spread spectrum (DSSS) modulation is provided as well as the basic models for GNSS signals. Furthermore, the considered receiver structure and the interference models are presented.

Chapter Three presents different losses in the presence of interference that are introduced in the quantization process. In this chapter, the effect of receiver's number of quantization levels and the automatic gain control process are examined.

Chapter Four discusses the characteristics of different sources of interfering signals. It presents a newly proposed NF based interference detection and mitigation method. Specifically, the interference mitigation technique based on adaptive linear-phase FIR notch filtering is proposed and developed in this chapter.

Chapter Five deals with the study of techniques for acquiring GPS L1 C/A (Coarse/Acquisition) in the presence of interference signals. The interference impact on the acquisition process is characterized and different countermeasures are considered.

Chapter Six investigates the overall GNSS receivers performance. The considered approach is to combine the proposed methods of previous chapters in order to improve receiver's performance. In this chapter, system-level optimization and real signal test are conducted. The performance of interference mitigation algorithm in the presence of quantization loss on the ROC performance is also investigated.

Finally, in Chapter Seven, conclusions as well as some future directions are provided.

Chapter Two: GNSS Signals and Receiver Model

GNSS systems are designed to provide user positioning anywhere at any time. In general, these systems are based on code division multiple access (CDMA) direct sequence spread spectrum (DSSS) modulation. Generally, spreading codes have a good correlation/cross-correlation property that makes it possible to measure the transmission time from satellites to a GNSS receiver. In addition to the transmit time, information describing the satellite's orbit, position and signal transmission time is also provided within the transmitted signal. The geometric range, which is the distance between satellite and receiver, can be estimated based on the difference between the transmission time and the time of arrival of the signal. Different spreading codes are assigned to each satellite utilized to identify them. These spreading codes are quasi-orthogonal, that is the cross-correlation between each two of them is bounded.

In this chapter, a detailed overview of the GNSS signal structure and receiver scenario is presented. Moreover, the concepts, models and notations of the GNSS systems are introduced as used throughout the rest of the thesis. Here, we focus on a consumer-grade GNSS receivers with cell-phone quality, which employs a low resolution quantizer and a low sampling frequency. After presenting the GNSS signal model and quantization process, interference signal structure with the analysis of conventional acquisition strategies are described.

2.1 GNSS Signal Structure

Figure 2.1 depicts a generic situation wherein a typical GNSS receiver tries to acquire transmitted signals from each visible satellite. In this figure, the received signal by GNSS receiver includes the desired GNSS signal, the channel noise and other undesired signals in the GNSS band. These undesired signals are considered as interference and their source is almost always closer to the receiver than the satellites. Generally, the user's position can be calculated given the range measurements to a minimum of four satellites. To ascertain the time of arrival (TOA) information within a receiver clock bias, which is estimated as part of the navigation solution, the receiver must first remove the carrier and the code modulation of the received signal.

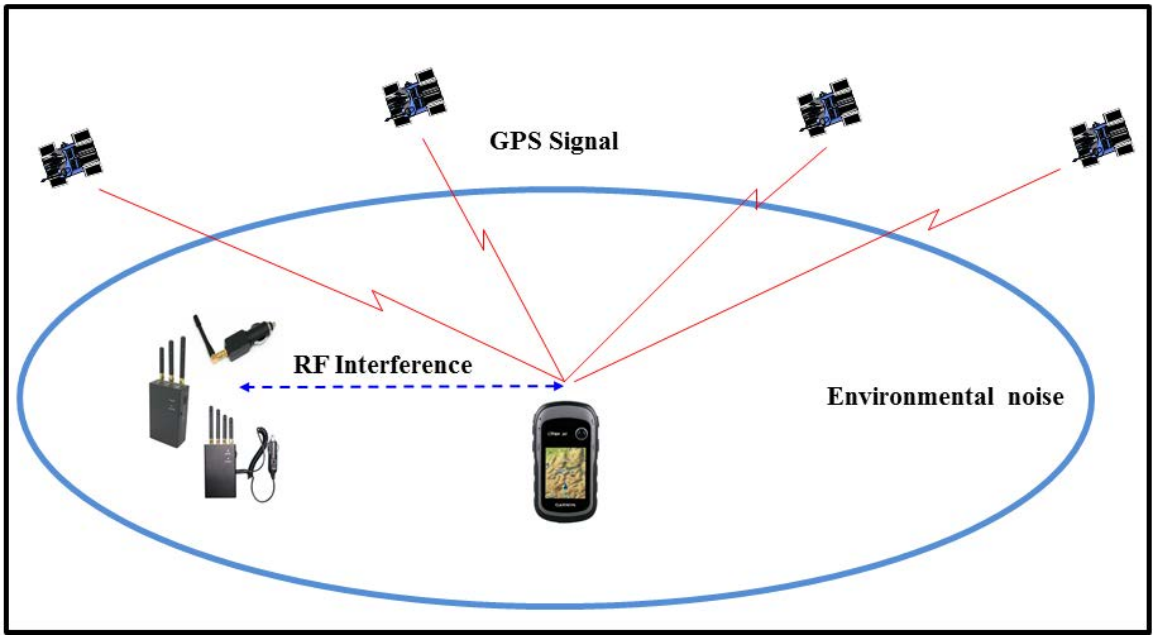

Figure 2.1: Basic principles of GNSS

The spreading code correlation property is used to estimate the time that the satellite transmitted signals reach the receiver. An overview of the principles of TOA ranging and satellite positioning is given in Kaplan & Hegarty (2006), Misra & Enge (2010) and Tsui (2004). In the following, the signal model for the direct sequence CDMA (DS/CDMA) GNSS system is presented. This model will be used in the next chapters.

In this thesis, a simplified GNSS signal model is adopted. A single path additive white Gaussian noise is assumed. After radio frequency processing that may include multiple down conversions and filtering stages, the complex intermediate frequency (IF) signal at the input of a GNSS receiver can be modeled as

$$r_{\mathrm{IF}}(t) = s_{\mathrm{IF}}(t) + i_{\mathrm{IF}}(t) + \eta_{\mathrm{IF}}(t). \tag{2.1}$$

This signal is comprised of a GNSS signal, $s_{\mathrm{IF}}(t)$, a narrowband interference, $i_{\mathrm{IF}}(t)$, and an additive noise, $\eta_{\mathrm{IF}}(t)$. The desired signal is a compound of all the signals from visible satellites. That is, $s_{IF}(t)$ can be represented as

$$s_{\mathrm{IF}}(t) = \sum_{i=1}^{S_{sv}} s_{\mathrm{IF},\,i}(t) \tag{2.2}$$

where S_{sv} is the number of all the visible satellites. Since the spreading codes have a good correlation/cross-correlation property, it is assumed that the received signal at the antenna is a single satellite signal distorted by a zero mean AWGN and narrowband interference. In the rest of this thesis, the satellite index is omitted for the sake of simplicity. The received GNSS signal component from the satellite has the following structure (Parkinson & Spilker 1996):

$$s_{\mathrm{IF}}(t) = A_s c(t-\tau) d(t-\tau) cos(2\pi(f_{\mathrm{IF}} + f_{\mathrm{D}})t + \theta) \tag{2.3}$$

where A_s is the amplitude of the received signal after the IF stage, $c(t)$ is the spreading code with chip period T_c, $d(t)$ represents the data modulation, τ is the initial code phase, f_{IF} is the IF frequency, i.e. carrier frequency minus the frequency of local oscillator, f_{D} is the Doppler shift, and θ is the initial IF carrier phase. The noise component is assumed to be a zero mean AWGN with a single-sided power spectral density of N_0 W/Hz. The interference signal is modeled as a simple multi-tone as described in Section 2.4. In this model, the effect of the front-end filter is ignored. The front-end filter limits the bandwidth of the signal and noise components in the receiver. Figure 2.2 shows a block diagram of the signal processing module within a typical GNSS receiver.

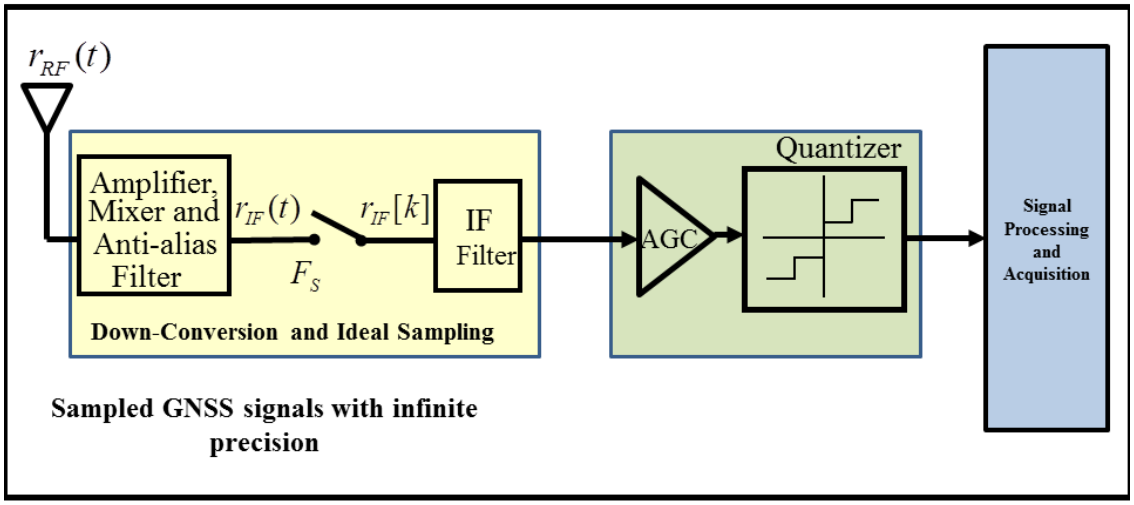

Figure 2.2: Generic block diagram of a GNSS receiver

GNSS operation is based on good correlation characteristics of the spreading codes. The spreading code properties are (Ziemer et al 1995):

- TOA measurements based on these codes;

- Good autocorrelation property: spreading code has one autocorrelation peak and it has low autocorrelation values for offsets greater than zero;
- Good cross correlation property: quasi-orthogonality property between two different satellite signals allowing for discrimination between their signals;
- Interference rejection and anti-jamming capability;
- Approximately zero mean property.

The spreading code is a non-return to zero (NRZ) pseudo random noise (PRN) sequence known as Gold codes for GPS application (Proakis & Salehi 2007, Gold 1967). Each satellite employs a unique spreading sequence with a nominal rate of 1023 kchip/s. The spreading code can be written as

$$c(t) = \sum_{i=-\infty}^{\infty} c_i \text{chip}(t - iT_c) \tag{2.4}$$

where N is the spreading code length, c_i denotes the i^{th} element of the code sequence and $\text{chip}(t)$ is the unit amplitude rectangular pulse of duration $T_c = 1/1.023\ 10^{-6}$ s. The spreading code is periodic in time with period of $T_{code} = NT_c$. Thus, the autocorrelation function (ACF) of the spreading codes, $R(\tau)$, is defined as

$$R(\tau) = \frac{1}{T_{code}} \int_0^{T_{code}} c(t)c(t-\tau)dt \tag{2.5}$$

This function is shown in Figure 2.3 for first GPS PRN.

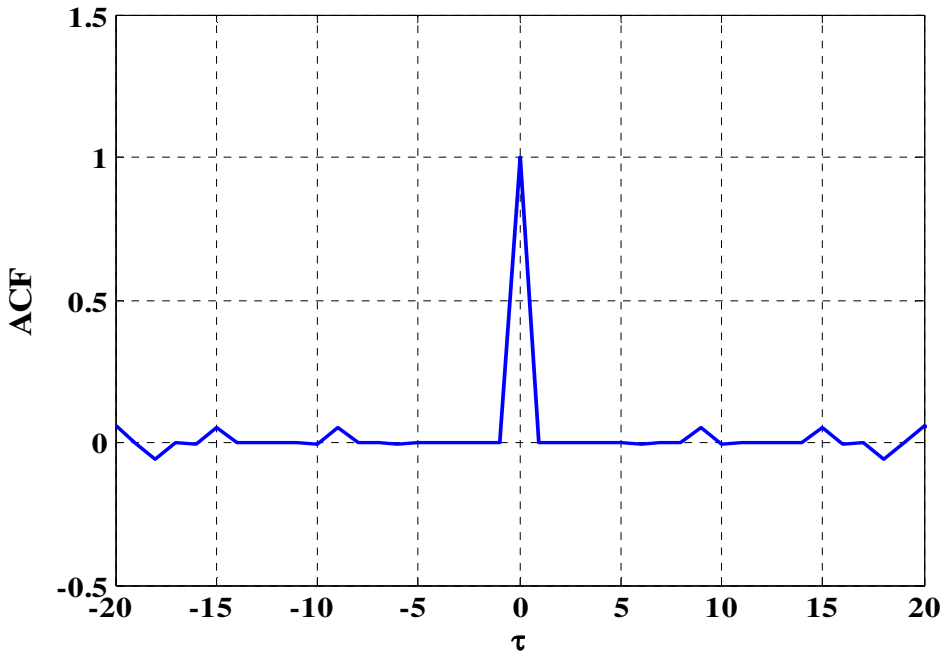

Figure 2.3: An example of autocorrelation function for Gold Codes

2.2 Received Signal Power

Several factors impact the received signal power. Transmitter and receiver antennas gains and space propagation loss mostly determine the line of sight (LOS) received power. The GNSS transmitted power is approximately 27 W (Misra & Enge 2010, Curran 2010). The received power of Eq. (2.3) is given by

$$C = \frac{A_s^2}{2} \tag{2.6}$$

The typical antenna gain for consumer-grade receivers is from -5 dBic[1] to 4 dBic depending on the satellite elevation angle seen at the receiver antenna. Thus, the received

[1] dBic: dB (isotropic circular) – The forward gain of an antenna above the gain of a circularly polarized isotropic antenna.

signal power at the receiver antenna output is approximately -160 dBW (Curran 2010, Sarantel 2010).

2.3 Thermal Noise

The noise component is assumed to be a zero mean complex AWGN with a single-sided power spectral density of N_0 W/Hz, with variance denoted by σ_n^2. Here, it is assumed that the sampling rate, $F_s = 1/T_s$, of the IF signal is equal to twice that of the IF front-end bandwidth, B_{IF}. Thus, the power of $\eta_{IF}(t)$, can be given by

$$\sigma_n^2 = B_{\mathrm{IF}} N_0 = \frac{F_s}{2} N_0 \tag{2.7}$$

2.4 Continuous Wave Interference

The performance of GNSS navigation and positioning depends upon the quality of the received signal and geometry. Thus, due to the low power level of the received GNSS signal at the earth's surface (see Section 2.2), radio frequency interference represents a significant impairing factor in GNSS applications. Interference can affect several blocks and parameters of a GNSS receiver. This effect can be on synchronization and acquisition steps, pseudorange measurements and positioning solutions (Kaplan & Hegarty 2006, Poisel 2011, Borio 2008). This kind of interference can be generated by a wide variety of electronic systems.

Figure 2.4 shows the short time Fourier transform (STFT) of these jammers. Specifically, the jammer referred in Mitch et al (2011) as "*Jammer 1"* is considered here as a swept jammer (see Figure 2.4). It has a jamming bandwidth of

$[L_1 - 25.4\,MHz,\ L_1 + 31.3\,MHz]$ and a sweeping period of 26 µs. The power of this jammer is 30 mW. Although due to low bandwidth of the consumer-grade receiver, just a portion of this interference is introduced to the receiver.

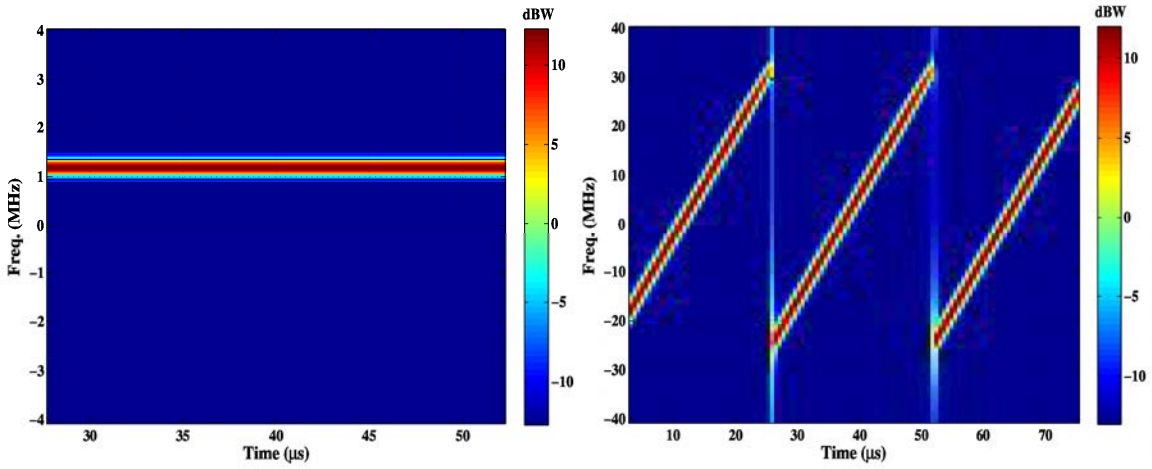

(a) STFT of fixed CW interference (b) STFT of swept CW interference

Figure 2.4: STFT of fixed and swept CW jammers

The interference component, $i_{\mathrm{IF}}(t)$, of Eq. (2.1) is assumed to be a fixed frequency CW interference modeled here as a pure sinusoidal tone having a frequency offset of f_Δ relative to the nominal IF frequency, such that $f_{\mathrm{int}} = f_{\mathrm{IF}} + f_\Delta$, where f_{int} is the frequency of the IF interference. The transmitted interference amplitude, A_{int}, is assumed constant. The fixed frequency CW interference signal can therefore be represented by

$$i_{\mathrm{IF}}(t) = A_{\mathrm{int}}\sin(2\pi f_{\mathrm{int}}t + \theta_{\mathrm{int}}) \tag{2.8}$$

where, θ_{int} is a random initial phase uniformly distributed on the interval $(-\pi,\ \pi]$.

Similar to the common signal-to-noise-ratio metric, a jammer-to-noise-ratio (*JNR*) can be defined. Assuming that the sampling rate, $F_s = 1/T_s$, of the IF signal is equal to twice

that of the IF front-end bandwidth, B_{IF}, the power of $\eta_{IF}(t)$, can be given by Eq. (2.7). Moreover, the *JNR* can be defined as

$$\mathrm{JNR} = \frac{\frac{1}{2}A_{\mathrm{int}}^2}{\sigma_n^2} = \frac{A_{\mathrm{int}}^2}{F_s N_0} \tag{2.9}$$

For multiple-interference cases, the interference component, $i_{\mathrm{IF}}(t)$, of Eq. (2.1) is assumed to consist of M continuous waves entering the GNSS front-end. The CW interference signal, modeled here as a pure sinusoidal tone, can be represented by

$$i_{\mathrm{IF}}(t) = \sum_{i=1}^{M} A_{\mathrm{int},\,i} \sin\left(2\pi f_{\mathrm{int},\,i} t + \theta_{\mathrm{int},\,i}\right) \tag{2.10}$$

where $A_{\mathrm{int},\,i}$ and $f_{\mathrm{int},\,i}t$ are amplitude and frequency of i^{th} CW interference, respectively, and $\theta_{\mathrm{int},\,i}$ is a random initial phase uniformly distributed over the interval $(-\pi,\ \pi]$.

The carrier-to-noise-ratio *C/N₀*, interference/jammer to noise ratio *JNR* and interference/jammer-to-signal-and-noise-ratio *JSNR* for this case are given by

$$\mathrm{C/N_0} = \frac{C}{N_0} = \frac{A_{\mathrm{s}}^2}{2N_0} \tag{2.11}$$

$$\mathrm{JNR} = \frac{J}{N} = \frac{\sum_{i=1}^{M} A_{\mathrm{int},\,i}^2}{2N_0 B_{\mathrm{IF}}} \tag{2.12}$$

$$\mathrm{JSNR} = \frac{J}{S+N} = \frac{\sum_{i=1}^{M} A_{\mathrm{int},\,i}^2}{A_{\mathrm{s}}^2 + 2N_0 B_{\mathrm{IF}}} \tag{2.13}$$

The swept interference is assumed to be a linear swept CW, i.e. in-car chirp jammers, having frequency of $f_{\mathrm{int}}(t) = f_1 + kt,\ \forall\ 0 \le t \le T_{\mathrm{SW}}$, where, f_1 is the lower frequency component, k is chip rate, and T_{SW} is swept time. The interference amplitude, A_{int}, is

usually constant for in-car jammers. The swept CW interference signals are represented as

$$r_{\text{IF-Swept CW}}(t) = A_{\text{int}}\cos\left(2\pi\left(f_1 + \frac{k}{2}t\right)t + \theta_{\text{int}}\right) \tag{2.14}$$

where θ_{int} is a random phase uniformly distributed on the interval $(-\pi,\ \pi]$.

2.5 Sampling and Quantization Process Non-Idealities in GNSS Receiver and Their Associated Loss

In this section, a description of analogue to digital converter component and its associated loss in a consumer-grade receiver is presented. In general, sampling/quantization process is a nonlinear operation introducing harmonics and distortion to the input signal in the form of quantization and clipping noise.

Typically, a low resolution quantizer is utilized in consumer-grade GNSS receivers (Curran et al 2010, Dierendonck et al 1996). The reasons for such a choice include the facts that employing a low resolution quantizer is efficient in the sense of cost, computational requirement and data-throughput. Furthermore, with an appropriate sampling rate, the quantizer degradation, for a purely AWGN channel, is not significant, being 1.96 dB, 0.55 dB, and 0.16 dB for 1-, 2-, and 3-bit quantizers, respectively (Parkinson & Spilker 1996, Curran et al 2010). Figure 2.5 shows the simulated C/N_0 loss versus $A_g\sigma_n$ due to quantization for 2-, 3-, and 4-it quantization schemes, where A_g is the AGC gain applied to the received signal prior to quantization. As it can be seen for multi-bit quantization, there is an optimum AGC gain that results in a minimum C/N_0 loss.

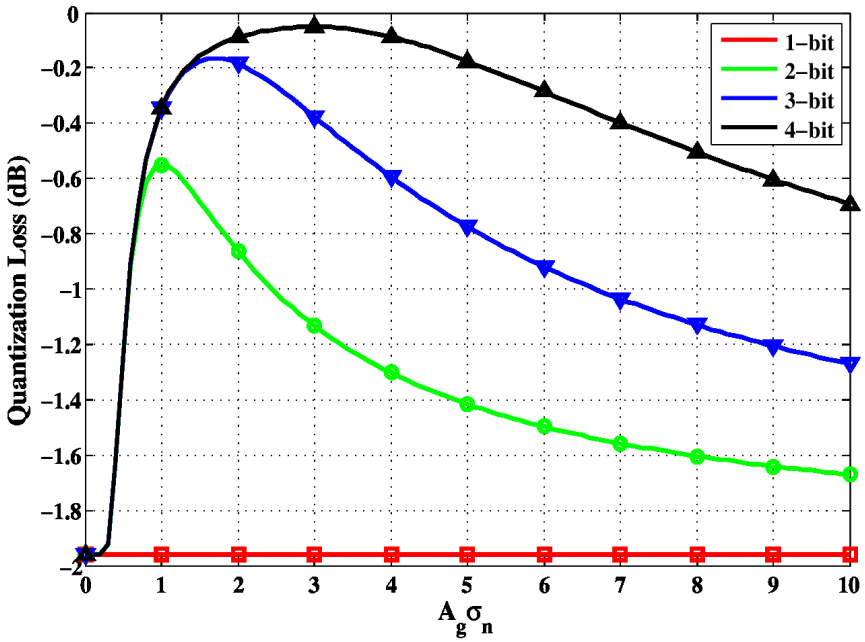

Figure 2.5: Simulated C/N_0 loss for 1-, 2-, 3-, and 4-bit quantizers

While this degradation is quite benign, it is intensified in the presence of interference (Balaei et al 2008). Hence, the configuration of the quantizer can have a significant effect on the performance of interference-suffering GNSS receivers. Figure 2.6 shows the effect of 4-bit quantizer on tone interference. As can be seen, quantization introduces several harmonics into the received spectrum. In order to provide reliable receiver performance under strong jamming/interference conditions, the design of the AGC system and the quantizer should be carefully considered.

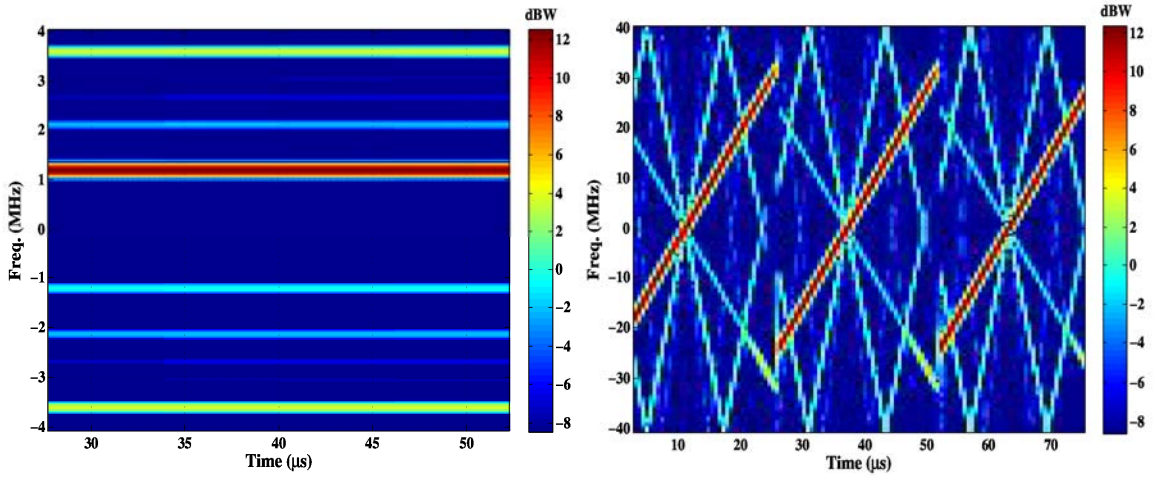

(a) STFT of fixed CW interference (b) STFT of swept CW interference

Figure 2.6: STFT of 4-bit quantized fixed and swept CW jammers

In this thesis, it is assumed that the IF signal is uniformly sampled at a rate of F_s and quantized with a B-bit symmetric quantizer, denoted by $Q_B^{A_g}[x]$. The quantizer is modeled as an odd-symmetric, uniform, memory-less operation. The input-output relation of such a quantizer is given by (Kaplan & Hegarty 2006)

$$Q_B^{A_g}[x] = -(2^B - 1) + 2\sum_{i=-L}^{L} u\big(A_g x - i\big) \tag{2.15}$$

where, $u(\cdot)$ is the unit step function, and $L = 2^{B-1} - 1$. Figure 2.7 shows the uniform quantizers input-output relationship for 1-, 2- and 3-bit quantizers. The sampled and quantized signal is therefore given by

$$\begin{aligned} r_B[n] &= Q_B^{A_g}[r_{\mathrm{IF}}(nT_s)] \\ &= Q_B^{A_g}[s_{\mathrm{IF}}(nT_s) + i_{\mathrm{IF}}(nT_s) + \eta_{\mathrm{IF}}(nT_s)] \end{aligned} \tag{2.16}$$

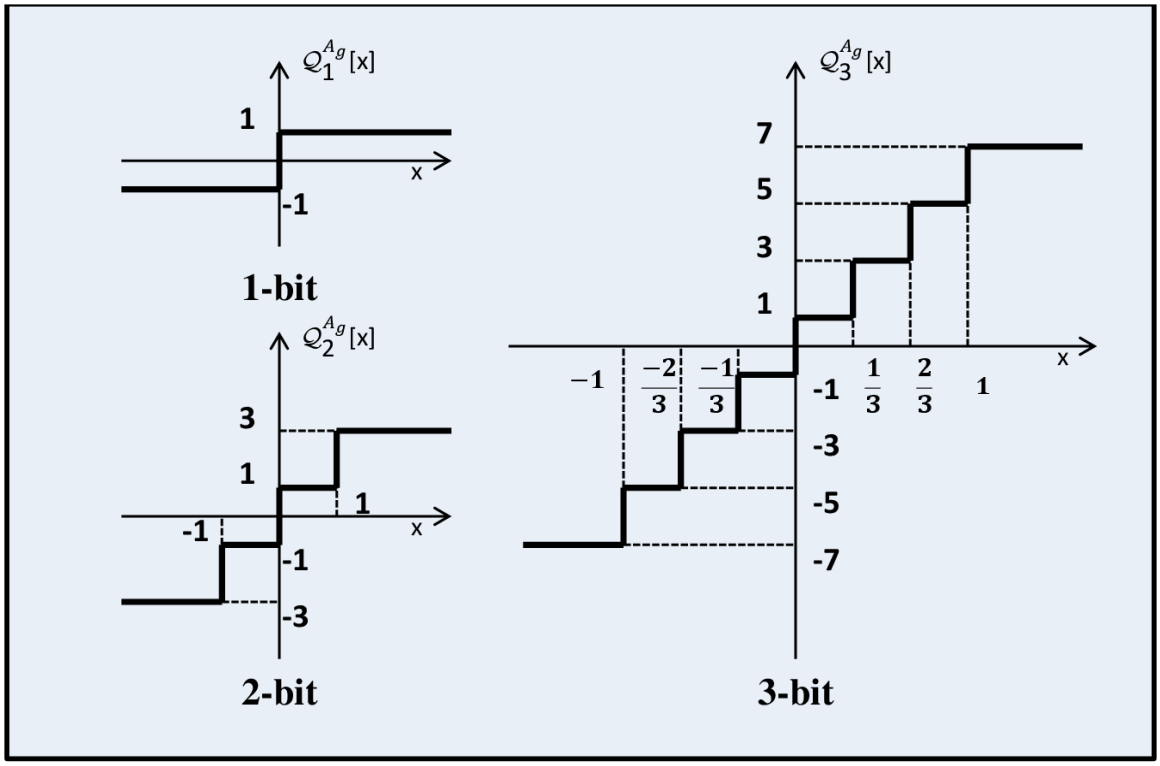

Figure 2.7: Input-output relationship for 1-, 2- and 3-bit quantizers

2.6 Interference Detection and Mitigation

One common method to detect the interference presence especially for consumer grade receivers is based on AGC output histograms. Figure 2.8 shows a typical histogram of the AGC output in the absence and presence of a relatively strong narrowband interference, i.e. *JNR* = 85 dB. As can be seen, for the interference-free case, the histogram shows the normal distribution pattern. That is, as the GPS signal is weaker than the noise level, the noise signal is prevalent and determines the statistics of the AGC output. Thus, the histogram shows a unimodal pattern. However, as strong narrowband interference emerges, the probability density function (PDF) otherwise follows that of the CW interference amplitude given by (Kaplan & Hegarty 2006, Balaei et al 2008) as:

$$p(x) = \begin{cases} \dfrac{1}{\pi\sqrt{A_{\text{int}}^2 - \text{x}^2}} & -A_{\text{int}} \le x \le A_{\text{int}} \\ 0 \end{cases} \tag{2.17}$$

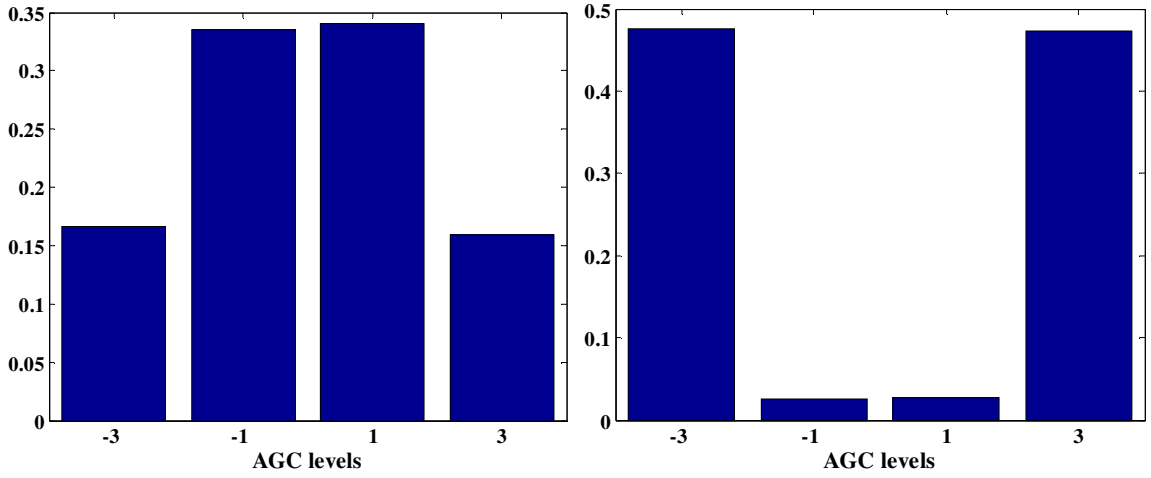

(a) Interference-free case (b) Interfered signal

Figure 2.8: Quantizer's output histogram in the absence and presence of narrowband interference

As mentioned in Section 2.5, for the 2-bit quantizer case, the receiver tries to maintain AGC gain as to have the highest output C/N_0. That is, the AGC gain is set to a value to have 16.7 % on the first bin (Bastide et al 2003). This bin distribution is shown in Figure 2.9. It can be concluded that any deviation from this percentage is an interference threatening situation.

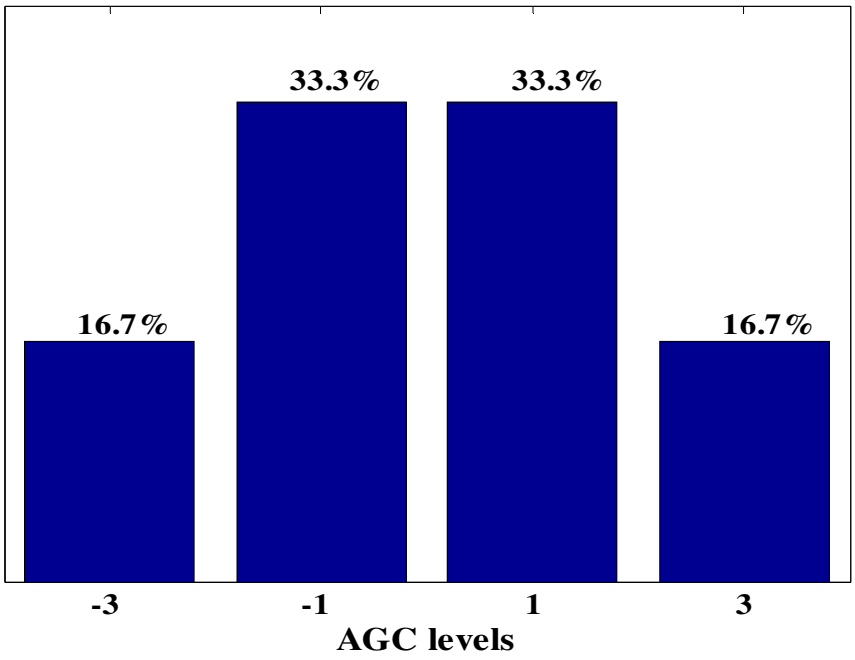

Figure 2.9: Histogram of optimum 2-bit quantizer for the interference-free case

In this work, an interference detection scheme based on notch filtering is considered in Chapter Four. This scheme is based on this fact that the magnitude of the estimate zero of the notch filter goes to zero for the interference-free case. On the other hand, when the narrowband interference is present, this magnitude converges to one. Thus, interference can be detected by comparing the magnitude of the estimated zero to a threshold.

2.7 DSSS Code Despreading and Acquisition

Figure 2.10 depicts a conventional acquisition scheme of a GNSS receiver (Kaplan & Hegarty 2006). Generally a digital matched filter (DMF) is employed by a GNSS receiver to estimate the required parameters of the desired GNSS signal (Curran 2010). To perform signal acquisition, the receiver must first demodulate the received signal using

an estimate of the received signals code phase and carrier Doppler. In a conventional receiver, the received signal is multiplied by a delayed version of the local replica of the GNSS signal, comprising of a replica spreading code, with initial code phase τ, a replica carrier with frequency $f_{\mathrm{IF}} + f_{\mathrm{D}}$, and an arbitrary initial carrier phase. This product is then coherently integrated over a fixed period, denoted here by T_{I}, to produce a cross ambiguity function (CAF), $S(\tau, f_{\mathrm{D}})$. The complex valued function, i.e. $S(\tau, f_{\mathrm{D}})$, in the absence of both noise and interference, will generally have maximum amplitude when the code phase and carrier frequencies of the received and local replica signals coincide. Therefore, the square magnitude of the CAF value is typically examined by a detection scheme. Although the CAF is a continuous function in τ and f_{D}, it is generally evaluated at discrete intervals where each (τ, f_{D}) pair is referred to as a cell. The CAF value for a given cell, (τ, f_{D}), can be rewritten as

$$\begin{aligned} S(\tau, f_{\mathrm{D}}) &= S_y(\tau, f_{\mathrm{D}}) + S_{\mathrm{int}}(\tau, f_{\mathrm{D}}) + S_\eta(\tau, f_{\mathrm{D}}) \\ &= I_n + jQ_n \end{aligned} \tag{2.18}$$

where, S_y, S_{int} and S_η are the contribution of the GNSS signal, the interference and noise, respectively. I_n and Q_n samples are real and imaginary parts of $S(\tau, f_{\mathrm{D}})$ values, where the subscript, n, denotes the interval, $nT_I \leq t < (n+1)T_I$, over which the CAF is calculated.

As a mathematical convenience, the demodulation process is often represented by an equivalent filter with impulse response (Misra & Enge 2010):

$$h_c[n] = \begin{cases} c(nT_s - \tau)e^{j2\pi(f_{\mathrm{IF}} + f_{\mathrm{D}})nT_s + \theta} & \forall\ 0 \leq n \leq \dfrac{T_I}{T_s} \\ 0 & \text{otherwise,} \end{cases} \tag{2.19}$$

which has a Fourier transform $H_c(f)$.

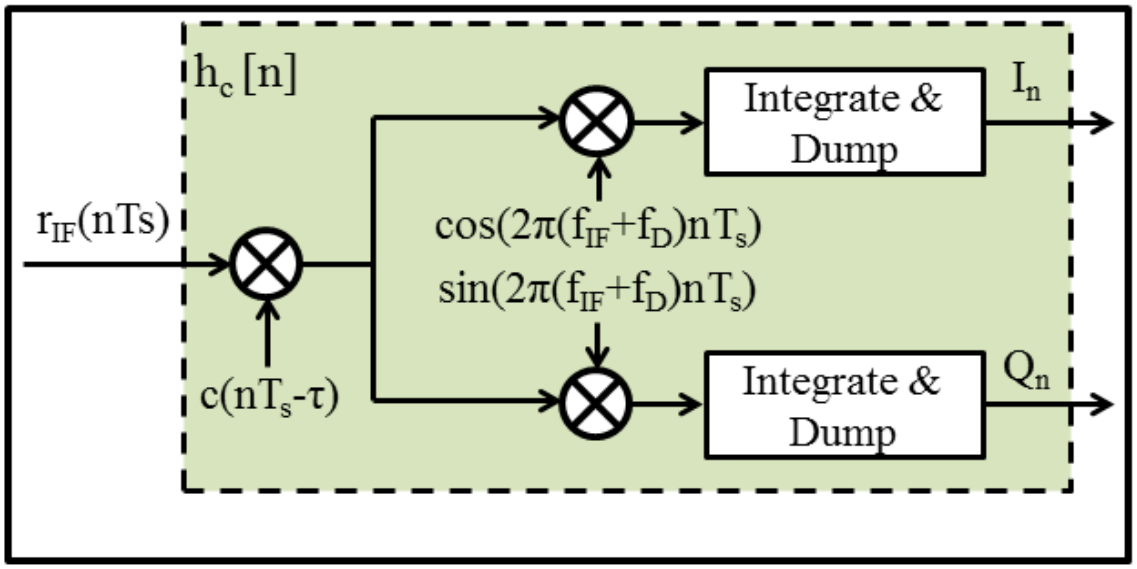

Figure 2.10: Generic block diagram of a GNSS correlator

From Eq. (2.19), the contribution to Eq. (2.18) from the GNSS signal can be represented by:

$$S_y(\tau, f_{\mathrm{D}}) = \frac{A_s}{2} R(\delta\tau)\mathrm{sinc}(\pi\delta f_{\mathrm{D}} T_I) e^{-j(\pi\delta f_{\mathrm{D}} T_I + \theta_0)} \tag{2.20}$$

where δx represents the error in the receivers estimate, $\hat{x}$, of the parameter x, such that $\delta x = x - \hat{x}$.

The interference component of $S(\tau, f_{\mathrm{D}})$, is given by (Oppenheim & Schafer 2009):

$$\begin{aligned} S_{\mathrm{int}}(\tau, f_{\mathrm{D}}) &= h_c[n] \bigstar i_{\mathrm{int}}(nT_s) \\ &= \frac{A_{\mathrm{int}}}{2}\{H_c(f_{\mathrm{IF}} + f_{\mathrm{int}} + f_{\mathrm{D}}) e^{j(2\pi(f_{\mathrm{IF}} + f_{\mathrm{int}} + f_{\mathrm{D}})\tau + \theta_{\mathrm{int}})} \\ &+ H_c(f_{\mathrm{IF}} - f_{\mathrm{int}} + f_{\mathrm{D}}) e^{j(2\pi(f_{\mathrm{IF}} - f_{\mathrm{int}} + f_{\mathrm{D}})\tau + \theta_{\mathrm{int}})}\} \end{aligned} \tag{2.21}$$

where ★ represents the convolution operator. For the no-quantizing receiver, this component has been thoroughly analyzed in Borio (2008). For a quantizing receiver this interference will be distorted and will no longer resemble a pure sinusoid. By considering its Fourier series expansion, however, it may be represented as a linear combination of weighted sinusoids. In this way, Eq. (2.21) may be utilized to evaluate the contribution of each element in the series and $S_{\text{int}}(\tau, f_{\text{D}})$ can be evaluated as their linear combination.

The contribution of the noise term, $\eta_{IF}(t)$, to $S(\tau, f_{\text{D}})$, is a zero mean circularly symmetric complex Gaussian random variable and is given by

$$S_{\eta}(\tau, f_{\text{D}}) = N\left(0, \frac{N_0}{4T_I} I_2\right) \tag{2.22}$$

where I_2 is the 2×2 identity matrix and $N(\mu, \sigma^2)$ represents a Gaussian random variable with mean μ and variance of σ^2. Although the noise contribution in adjacent cells in the search space will be correlated, this correlation is negligible in comparison to that of the interference and so, for simplicity, it is neglected here.

After computing CAF values, a signal acquisition scheme is applied which includes detecting the presence of the desired signal and estimating the signal code phase and Doppler frequency. The typical approach to implement the acquisition scheme is to compare the *decision variable*, here the magnitude of CAF value, to a threshold for a number of Doppler frequencies and code phases. This bi-dimensional grid of τ and f_{D} is usually referred to as the *search space*. Each τ and f_{D} of this grid defines a *cell* of the search space.

Within this work, the cell-level performance relates to the effective probability of false-alarm when the signal is absent and the probability of detection when the signal is present (O'Driscoll 2007, Corazza & Caini 2004). Another useful and related metric, known as the system-level performance, is defined in terms of the overall probability of correct detection of the signal, considering the entire search space (O'Driscoll 2007, Corazza & Caini 2004). In this case the detection probability is a function of (i) the cell-level probability of detection for the cell which contains the signal, (ii) the cell-level false-alarm probability for all other cells in the search space and (iii) on the particular sequence in which the cells are tested; the simplest case, the parallel search, is employed in this work (O'Driscoll 2007, Corazza & Caini 2004).

Figure 2.11 shows a typical real collected data power spectrum of GPS L1 C/A signal for interference-free and interference-corrupted cases. Interference is adjusted to have $JNR = 50$ dB and $f_{\Delta} \approx 100$ Hz. Corresponding normalized CAF results are shown in Figure 2.12. For the interference-free case, the CAF results demonstrate a peak related to correct delay and Doppler frequency. In this case, conventional methods, e.g. parallel and serial searching, based on comparing the CAF value to a threshold can be employed. However, as it can be seen for CAF values in the presence of interference, threshold checking is no longer applicable and some more intelligent scheme might be useful.

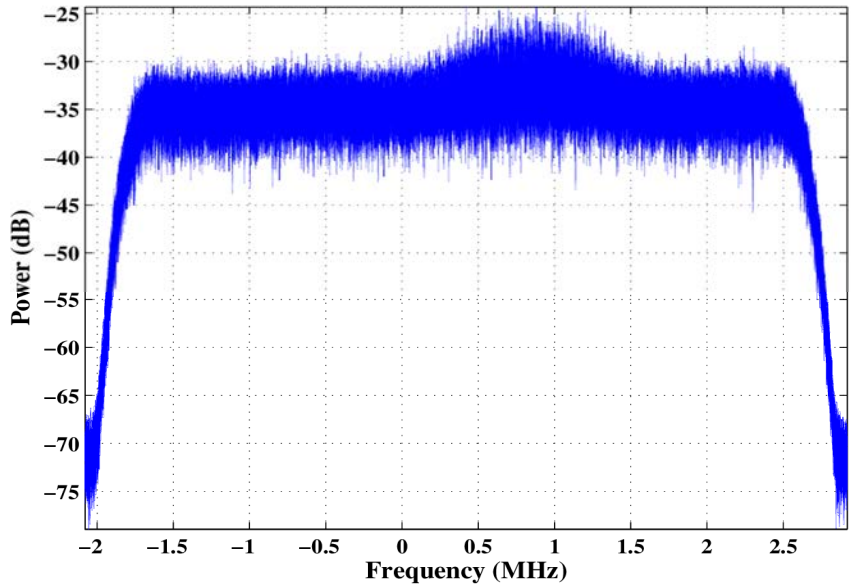

(a) Interference-free case

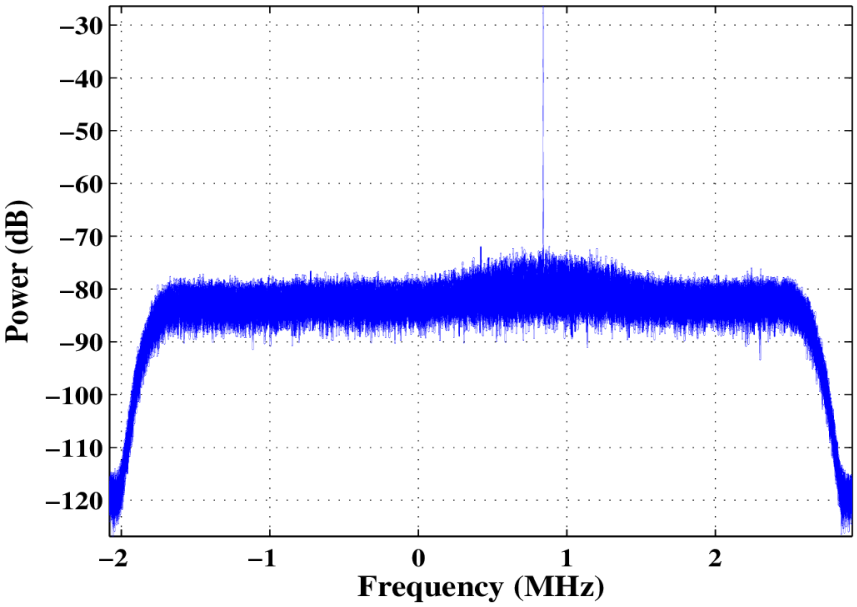

(b) Interference-corrupted case

Figure 2.11: Power spectrum for interference-free and interference-corrupted received signals

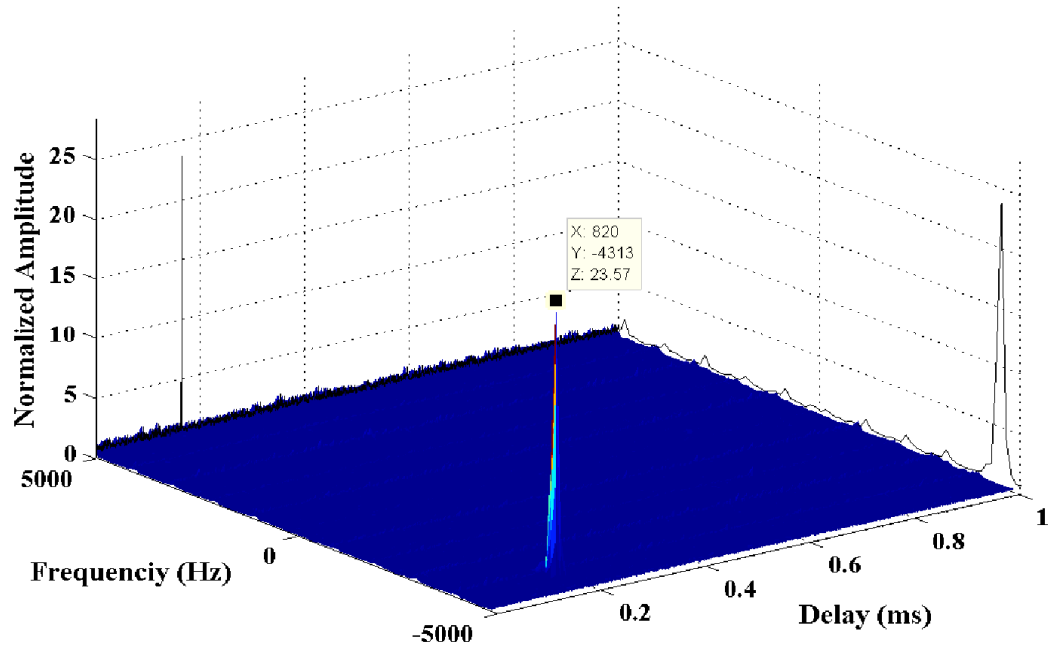

(a) Interference-free case

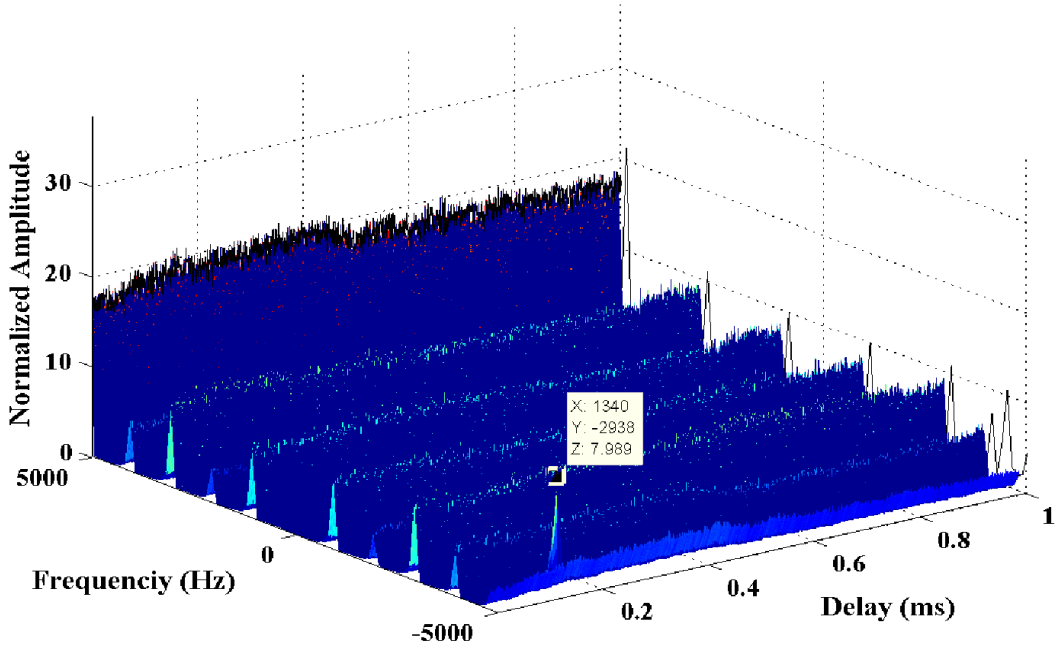

(b) Interference-corrupted case

Figure 2.12: Generic ROC for interference-free and interference-corrupted received signal

An example of histograms of the decision cell in the absence and presence of interference is shown in Figure 2.13. This figure shows the histogram of the bin for three different cases. In the first case (shown in red), the decision cell contains noise component only and there is neither interference nor GNSS signal present. For the second case shown in green, the cell contains noise and interference with the same level of noise as that of the first case. And at the end, the decision cell in the third case (shown in blue) contains the desired signal, noise and interference components with the same amount of noise and interference as case two. As it can be seen, the presence of the signal, depending on relative power of the interference the noise and the GNSS signal, may cause an increase in the average of the distribution even in the presence of interference. This might be employed to detect the correct cell.

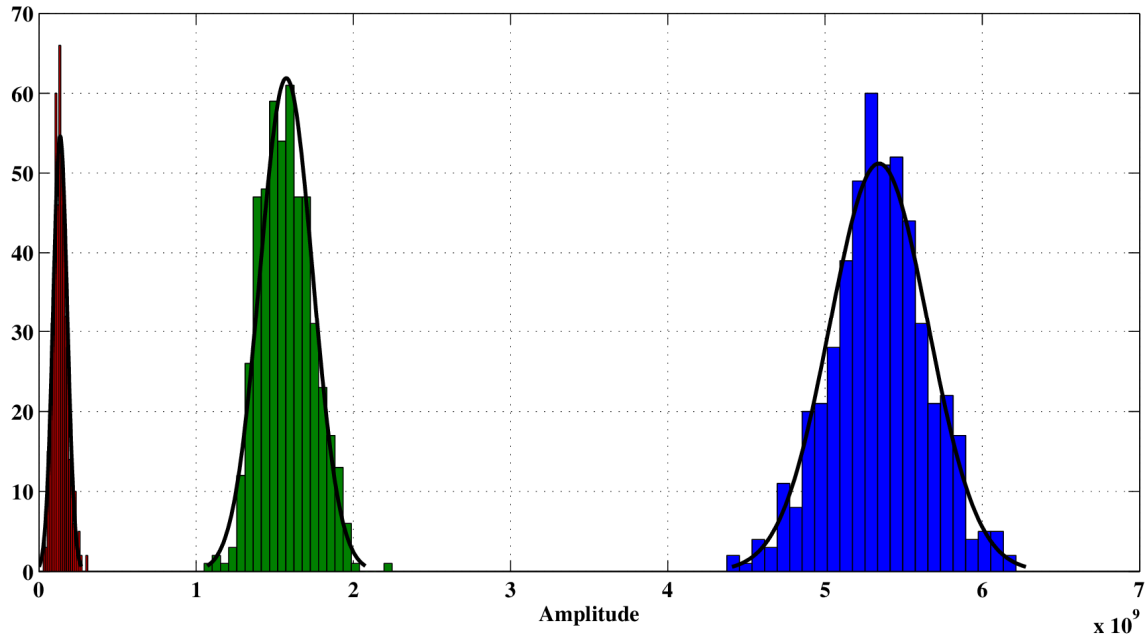

Figure 2.13: Histogram of CAF value for a cell for three cases: 1- The cell contains the noise only component (Black plot), 2- The cell contains the noise and interference (Green plot), and 3- The cell contains the GNSS signal, noise and interference components (Blue plot)

In this thesis, whenever the cell-level detection probability is of the interest, it will be assumed that the received signals code phase and carrier Doppler are completely known by the receiver. The cell-level detection probability of the acquisition process for a GNSS receiver is defined as the probability that squared magnitude of the decision variable $S(\tau, f_{\mathrm{D}})$ is higher than a constant threshold, β. The *decision metric*, T_0, for signal detection is presented as

$$T_0\colon\ |S(\tau, f_{\mathrm{D}})|^2 \underset{H_0}{\overset{H_1}{\gtrless}} \beta \tag{2.23}$$

where the null hypothesis, H_0, represents the GNSS signal absence and the alternative hypothesis, H_1, represents the situation that the desired GNSS signal is present. Thus, the cell-level detection probability is given by

$$\begin{aligned} P_{\mathrm{D}} &= \Pr(|S(\tau, f_{\mathrm{D}})|^2 \ > \ \beta \ : \ H_1) \\ &= \Pr(\ \ I_n^2 + Q_n^2 \ \ > \ \beta \ : \ H_1) \end{aligned} \tag{2.24}$$

The acquisition process will be discussed further in Chapter Five.

2.8 BER metric As an Alternative to C/N0 measurement

When designing the quantization configuration, the levels of the quantizer have to be adjusted so that the output signal-to-noise-ratio (*SNR*) is maximized (Kondoz 2004). For high values of signal to noise ratio and resolution quantization, this is equivalent to minimizing the signal distortion, i.e. quantization noise. That is, the minimum average distortion metric given by $(x - Q(x))^2$ is employed (Berger 1972, Widrow et al 1996, Widrow & Kollar 2008). This includes speech processing (sampling/coding), imaging, radar and digital filtering applications, wherein the desired signal is the dominant part of the received signal power. In this case, the best quantizer is the one minimizing the expected value of quantizer distortion. Moreover, the quantization process error can be approximated by "the additive noise" model. However, it is shown that this model is valid under the condition of high resolution quantization process (Bennett 1948, Marco & Neuhoff 2005).

On the other hand, in low *SNR* situations like GNSS applications where the desired signal is under the noise level, "average distortion metric" does not represents the *SNR* metric.

In this case, the exact *SNR* metric should be employed. In GNSS application, the post-correlated C/N_0 metric is employed as an estimate to *SNR*, which is defined as (Curran et al 2010, Borio 2008, Balaei et al 2008, Parkinson & Spilker 1996):

$$C/N_0 = \frac{\left(\mathrm{E}\left[\frac{1}{N}\sum_{n=0}^{N-1} r[n]h_c[n]\right]\right)^2}{\mathrm{Var}\left[\frac{1}{N}\sum_{n=0}^{N-1} r[n]h_c[n]\right]}. \tag{2.25}$$

As can be seen in Eq. (2.25), in the numerator the average of the post correlated received signal is considered as a measure of the signal power. Moreover, the variance of the post correlated received signal measures the noise variance.

The C/N_0 is one of the most important measurements in GNSS applications (Satyanarayana 2011). This estimate is necessary for the design and parameter setting of signal processing algorithms. The accuracy of the C/N_0 measurement depends upon the adopted estimation technique and the real conditions of the received signal (Pauluzzi & Beaulieu 2000).

In the presence of the interference signal, Eq. (2.25) is still used to estimate the SINR metric (Balaei et al 2008, Borio 2008, Sharawi 2007). In this case, a measure of the interference power appears at its denominator. That is, the denominator estimates noise plus interference power.

By examining Eq. (2.25), one can see that it is assumed that any undesired signal within the received signal has post-correlated zero mean in order to measure the desired signal power. That is, not only is the cross correlation between satellite codes ignored, but also the cross-correlation between desired code and interference signal is considered to be almost zero. However, in the presence of a strong interference signal, this assumption is

invalid (Cherniakov & Lo 1998). Thus, a residual bias might appear due to the presence of the interference signal (Groves 2005). To eliminate this bias, the definition of C/N_0 in Eq. (2.25) should be changed.

In this study, the BER metric is proposed as an alternative to the C/N_0 definition. Thus, an effective C/N_0, or equivalently *SNR* measurement, can be calculated using the results of computed BER (Abdizadeh et al 2012). Further information is given in Section 3.3.3. This new measurement approach is bias free for any interference signal shape and it provides the correct C/N_0 value. As it will be shown, this metric gives the same results given by Eq. (2.25) for low interference power (Section 3.5.1). In real applications, a one-to-one map can be defined between BER based C/N_0 and that of Eq. (2.25). This simple approach can be employed to estimate the *SNR* at a level closer to the RF part. Interestingly, any difference between these two C/N_0 estimates can be employed to detect the presence of interference signal.

In the presence of strong interference signal, not only can the metric be modified, but also the distribution of the quantizer levels can be carefully adjusted. That is, a non-uniform quantizer might provide less quantization loss compared to a uniform one based on the probability distribution function of the received signal. The focus of this study is limited to uniform quantization process.

2.9 Satellite Detection and Tracking

As mentioned earlier, each satellite uses a unique PRN. Thus, to detect a specific satellite, the receiver generates a corresponding local signal replica using that particular PRN

sequence, next correlates the received signal with that. If the signal is strong enough at the received signal, the CAF values show a significant peak in the search space.

After acquiring the satellite, the receiver starts to track the signal. The main idea of tracking is to maintain fine time, frequency and phase lock to the signal. A common metric to measure the received signal strength is C/N_0, which is typically between approximately 50 and 30 dB-Hz for good and poor conditions, respectively (Kaplan & Hegarty 2006).

2.10 Bit Demodulation and Position Estimation

By acquiring and tracking the satellite signals, the receiver can demodulate the navigation data bits. In this study, the GPS L1 C/A signal is taken as a case study for simulation. This signal is modulated by a binary phase shift keying (BPSK) data sequence with a bit period of 20 ms, denoted here by T_b. The data bits consist of all the required information to determine the satellite position and signal transmission time. For the GPS L1 C/A signal it takes approximately 30 seconds to demodulate this information (Parkinson & Spilker 1996, Kaplan & Hegarty 2006). When the receiver has this information for at least four satellites, it is possible to determine the distance to each of them simultaneously and afterwards, to compute the receiver position, velocity and time (PVT).

2.11 Summary and Conclusions

In this chapter, an overview of the GNSS signal structure was presented and will be used in the following chapters. In addition, the required steps to demodulate the received

signal were discussed. The signal quality loss due to employing a limited resolution quantizer was described. Moreover, a brief background of the detection problem of the GNSS signal was demonstrated. Finally, the GNSS acquisition process was discussed in detail.

In the following chapters, the performance of the different parts of the receiver is evaluated and presented. In Chapter Three, the quantization loss of the receiver in the presence of narrowband interference is discussed.

Chapter Three: Quantization Process in the presence of Narrowband Interference

Consumer-grade receivers, which utilize a low resolution quantizer for example 1- or 2-bit (Curran et al 2010), are likely the most vulnerable to interference. Such receivers are typically constructed with poor quality components and low resolution digitizers and, as a result, tend to exhibit a relatively small dynamic range. Thus, these receivers can be sensitive to AGC calibration and very susceptible to jamming. Employing such quantization degrades the received signal quality. This effect is compounded in the presence of interference. Hence, the configuration of the signal quantizer in a GNSS receiver implementation can have a significant effect on the performance of interference-suffering systems and, in order to provide reliable receiver performance under strong jamming/interference conditions, the design of the receiver's quantizer should be carefully considered.

3.1 Quantization Effects and Losses

Figure 3.1 shows the normalized power spectral density (PSD) of a CW interference assuming a sample rate of 8 MHz where both the IF and interference frequencies are equal to 0.5 MHz. This figure illustrates the spectrum for a no-quantizing receiver (infinite resolution) as well as that for 1-, 2-, and 3-bit quantizers. Here, the value of the AGC gain has been set to its optimal value in terms of BER performance, which will be discussed in the following sections. As can be seen, quantization introduces several harmonics in the spectrum. The frequency and amplitude of these harmonics depend on

the interference frequency, the sampling frequency and the particular quantizer configuration (Gray 1990). Under such conditions, low resolution quantizers, or those that are poorly configured, will induce more harmonics with higher relative powers.

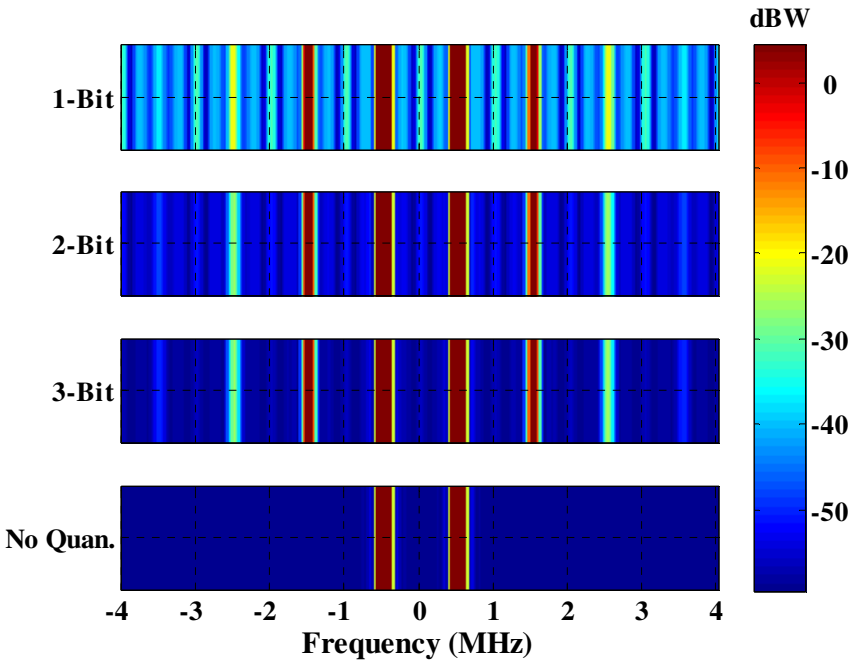

Figure 3.1: Normalized PSD of fixed frequency interference for no-quantizing and quantizing (1-, 2- and, 3-bit) receiver.

As the quantization process distorts and scales the received signal, the performance of subsequent receiver operations are often related to the characteristics of the signal immediately prior to quantization, specifically, $\square_{\mathrm{IF}}(t)$.

3.2 Coherent Signal-to-Interference-and-Noise-Ratio (SINR) and Effective C/N_0

In this section, the standard definition of C/N_0 and its application in the estimation of the quantization loss is presented. It will be shown that this figure of merit is not an

appropriate metric when measuring the received C/N_0 in the presence of interference. Due to the presence of interference, the C/N_0 metric becomes biased and it measures, not only the received signal, but also a portion of the interference power. For strong interference signals, this bias can become significant. As an alternative, a measure of bit error rate performance will be introduced.

To decode the signal, the receiver first demodulates the received signal using the estimate of the received signal code phase and carrier Doppler. Employing the conventional definition of the SINR as the squared mean of the correlation output, with correlation length of N, divided by its variance, the coherent SINR for a B-bit quantizer with a coherent integration period of $T_I = NT_s$ is given by (Kaplan & Hegarty 2006)

$$\rho_B = \frac{\left(\mathrm{E}\left[\frac{1}{N}\sum_{n=0}^{N-1} r_B[n]h_c[n]\right]\right)^2}{\mathrm{Var}\left[\frac{1}{N}\sum_{n=0}^{N-1} r_B[n]h_c[n]\right]}. \tag{3.1}$$

For the infinite resolution case, the expected value of the digital signal can be written as

$$\begin{aligned} \mathrm{E}[r_{\mathrm{IF}}[n]] &= \mathrm{E}[s_{\mathrm{IF}}[n]] + \mathrm{E}[i_{\mathrm{IF}}[n]] + \mathrm{E}[\eta_{\mathrm{IF}}[n]] \\ &= \mathrm{E}[s_{\mathrm{IF}}[n]] + \mathrm{E}[i_{\mathrm{IF}}[n]] \end{aligned} \tag{3.2}$$

and, the variance, after some simplification, can be expressed as

$$\begin{aligned} \mathrm{Var}[r_{\mathrm{IF}}[n]] &= \mathrm{E}[r_{\mathrm{IF}}^2[n]] - \mathrm{E}\left[r_{\mathrm{IF}}[n]\right]^2 \\ &= \mathrm{E}[(s_{\mathrm{IF}}[n] + i_{\mathrm{IF}}[n] + \eta_{\mathrm{IF}}[n])^2] - \mathrm{E}\left[s_{\mathrm{IF}}[n] + i_{\mathrm{IF}}[n]\right]^2 \end{aligned} \tag{3.3}$$

From Eq. (3.2), the numerator of Eq. (3.1) can be simplified to

$$
\begin{aligned}
&\mathrm{E}\left[\frac{1}{N}\sum_{n=0}^{N-1} r[n]h_c[n]\right] \\
&\quad \approx \frac{1}{N}\sum_{n=0}^{N-1} \mathrm{E}\left[s_{\mathrm{IF}}[n]c(nT_s-\tau)e^{-j(2\pi f_c nT_s+\theta)}\right] \\
&\quad + \frac{1}{N}\sum_{n=0}^{N-1} \mathrm{E}\left[i_{\mathrm{IF}}[n]c(nT_s-\tau)e^{-j(2\pi f_c nT_s+\theta)}\right] \\
&\quad = \frac{A_s}{2}R(0) + \frac{A_{\mathrm{int}}}{2}R_{c,x}\mathrm{sinc}(\pi f_\Delta T_I) \\
&\quad = \frac{A_s}{2} + \frac{A_{\mathrm{int}}}{2}R_{c,x}\mathrm{sinc}(\pi f_\Delta T_I)
\end{aligned}
\tag{3.4}
$$

where, $R_{c,x}$ represents the correlation between the interference and $c(t)$. The variance of the correlator output, which appears in the denominator of Eq. (3.1), can be approximated by

$$
\mathrm{Var}\left[\frac{1}{N}\sum_{n=0}^{N-1} r[n]h_c[n]\right] \approx \frac{\sigma_n^2}{2N} + \frac{A_{\mathrm{int}}^2}{8N}G_s(f_\Delta T_I) \tag{3.5}
$$

where, $G_s(f)$ represents the PSD of the GNSS signal.

The details of this calculation can be found in Appendix C. Hence, the coherent SINR for a no-quantizing receiver is given by

$$
\rho_\infty = \frac{\left(\frac{A_s}{2} + \frac{A_{\mathrm{int}}}{2}R_{c,x}\mathrm{sinc}(\pi f_\Delta T_I)\right)^2}{\frac{\sigma_n^2}{2N} + \frac{A_{\mathrm{int}}^2}{8N}G_s(f_\Delta T_I)}. \tag{3.6}
$$

The effective carrier-to-noise-floor-ratio of an interference and AWGN corrupted signal is defined as the C/N_0 of an AWGN corrupted signal, which exhibits an SINR equal to the SINR of the interference and AWGN corrupted signal, namely

$$\left(\frac{C}{N_0}\right)_{\text{eff}} = \frac{\rho_B}{2T_I} \tag{3.7}$$

The last term in Eq. (3.4) is proportional to the interference power and can be neglected for weak interference signals. In the presence of strong interfering signals, however, this term causes a significant effect. Ideally, the metric that is sought is the ratio of the desired signal power to that of the total power of the interference and noise and takes the form

$$\rho_\infty = \frac{\frac{A_s^2}{4}}{\frac{\sigma_n^2}{2N} + \frac{A_{\text{int}}^2}{8N} G_s(f_\Delta T_I)}. \tag{3.8}$$

Figure 3.2 shows the effective C/N_0 for $C_s/N_0 = 40$ dB-Hz for different values of the interference power. As can be seen, when interference has a power greater than 80 dBm, the C/N_0 metric begins to measure the interference power as well as that of the desired signal. It is clear, therefore, that this metric is not useful when the interference has a power greater than approximately 70 dBm. A trace of Eq. (3.8), labeled as "Expected C/N_0 Results", is shown in Figure 3.2 for comparison purposes.

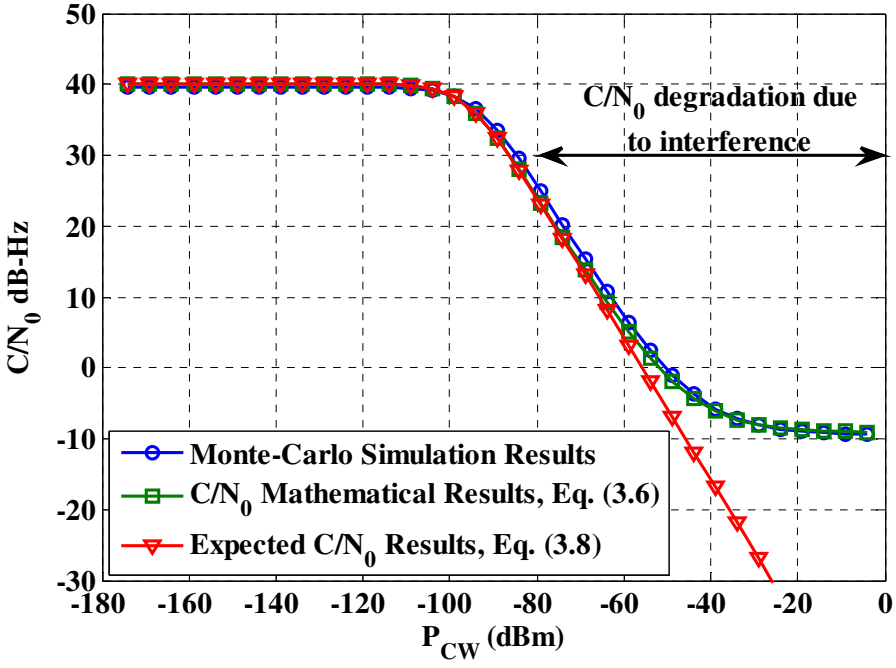

Figure 3.2: Theoretical effective C/N_0 for C_s/N_0 = 40 dB-Hz for different values of interference power ($f_\Delta \approx 0$ Hz) using Eq. (3.6) and Eq. (3.8) in conjunction with Eq. (3.7)

As shown in Figure 3.2, this figure of merit is not an appropriate metric when measuring the received C/N_0 in the presence of interference. In fact, in the presence of interference, the C/N_0 metric becomes biased and it measures, not only the received signal, but also a portion of the interference power. For strong interference signals, this bias can become significant. As an alternative, a measure of BER performance is introduced and utilized in this chapter (see Section 3.3.3) to alleviate this problem and measure the effect of interference on the quantizer and receiver performance.

3.3 Quantization Loss

This section presents an analysis of the loss induced by the use of a *B*-bit symmetric quantizer in a typical GNSS receiver. Specifically, the loss induced by a 1-bit quantizer is examined. The quantization loss for a *B*-bit quantizer is defined as (Borio 2008)

$$L_B = \frac{\rho_B}{\rho_\infty} \tag{3.9}$$

3.3.1 1-bit Quantization in the Presence of Interference

The 1-bit quantizer maps the continuous input signal to two discrete levels with the following associated probabilities:

$$\begin{aligned} p_{1,1} &= \Pr(r_1[n] = 1) = \Pr(r_{\mathrm{IF}}[n] > 0) \\ &= \Pr(s_{\mathrm{IF}}[n] + i_{\mathrm{IF}}[n] + \eta_{\mathrm{IF}}[n] > 0) \\ &= \Pr(\eta_{\mathrm{IF}}[n] > -s_{\mathrm{IF}}[n] - i_{\mathrm{IF}}[n]) \\ &= Q\left(-\frac{s_{\mathrm{IF}}[n] + i_{\mathrm{IF}}[n]}{\sigma_n}\right) \end{aligned} \tag{3.10}$$

$$\begin{aligned} p_{1,-1} &= \Pr(r_1[n] = -1) = \Pr(r_{\mathrm{IF}}[n] < 0) \\ &= \Pr(s_{\mathrm{IF}}[n] + i_{\mathrm{IF}}[n] + \eta_{\mathrm{IF}}[n] < 0) \\ &= \Pr(\eta_{\mathrm{IF}}[n] < -s_{\mathrm{IF}}[n] - i_{\mathrm{IF}}[n]) \\ &= Q\left(\frac{s_{\mathrm{IF}}[n] + i_{\mathrm{IF}}[n]}{\sigma_n}\right) \end{aligned} \tag{3.11}$$

where $Q(\cdot)$ represents the Q-function. From Eq. (3.1) and following the procedure described in Appendix C, the coherent SINR for a 1-bit quantizer can be approximated by

$$\rho_{\infty} = \frac{NA_s^2}{\pi\sigma_n^2} e^{-\frac{A_{\text{int}}^2}{2\sigma_n^2}} \mathcal{I}_0\left(\frac{A_{\text{int}}^2}{4\sigma_n^2}\right)^2. \tag{3.12}$$

It follows, therefore, that the associated quantization loss is given by

$$L_1 = \frac{\rho_1}{\rho_{\infty}} = \frac{\frac{NA_s^2}{\pi\sigma_n^2} e^{-\frac{A_{\text{int}}^2}{2\sigma_n^2}} \mathcal{I}_0\left(\frac{A_{\text{int}}^2}{4\sigma_n^2}\right)^2}{\frac{\frac{A_s^2}{4}}{\frac{\sigma_n^2}{2N} + \frac{A_{\text{int}}^2}{8N} G_s(f_\Delta T_I)}} \tag{3.13}$$

which simplifies to

$$L_1 = \left(\frac{2}{\pi} + \frac{A_{\text{int}}^2}{2\pi\sigma_n^2} \square_s(f_\Delta T_I)\right) e^{-\frac{A_{\text{int}}^2}{2\sigma_n^2}} \mathcal{I}_0\left(\frac{A_{\text{int}}^2}{4\sigma_n^2}\right)^2 \tag{3.14}$$

As can be seen, for the interference-free case, Eq. (3.14) reduces to the simple case of GNSS signal quantization only in the presence of noise as (Parkinson & Spilker 1996)

$$L_{1(\text{Interference-free case})} = \frac{2}{\pi} \approx -1.96 \text{ dB} \tag{3.15}$$

Figure 3.3 depicts the simulated quantization loss for 1-bit quantization for a signal containing interference, as a function of interference power. In this figure, the theoretical results of Eq. (3.14) as well as Monte-Carlo simulation results are shown. It can be seen in this figure that, for a low power interference situation, the C/N_0 loss performance is equal to that of the interference-free case, as given by Eq. (3.15). As the interference power increases, the C/N_0 loss increases to -10 dB loss. For an interference with power higher than -100 dBm the C/N_0 metric begins to measure the power of the interference. Thus, this C/N_0 loss metric is not reliable when high values of interference power are

present. Hence, the BER metric is considered as an alternative approach to measure the effect of interference on the quantizer and receiver performance.

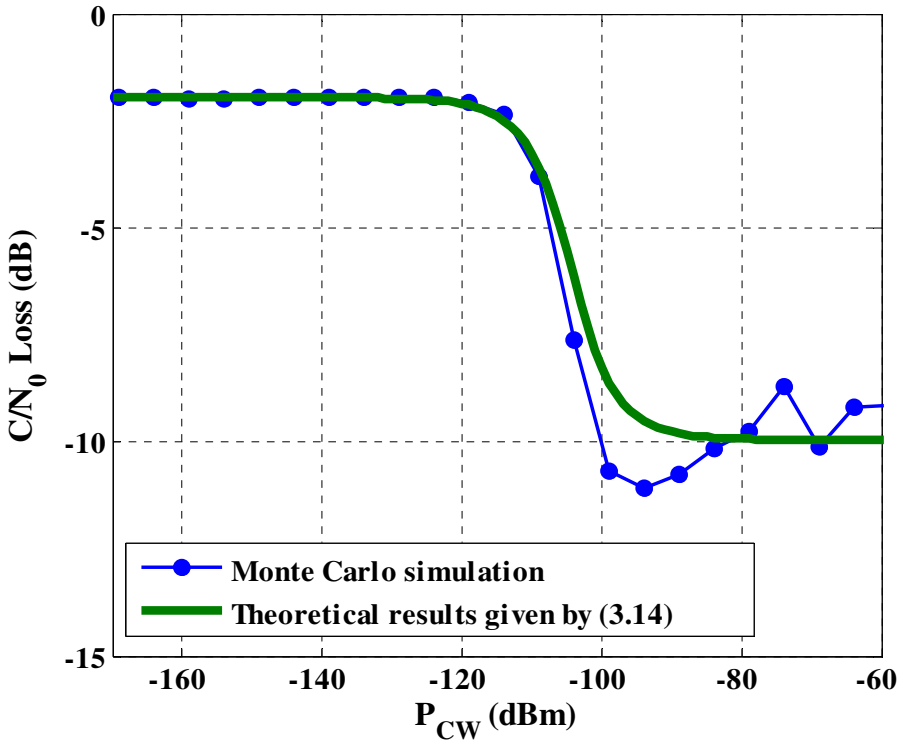

Figure 3.3: Simulated and theoretical C/N_0 loss results as a function of interference's power for 1-bit quantizer ($f_\Delta \approx 0$ Hz)

3.3.2 2- and 3-bit Quantization in the Presence of Interference

This section examines the performance of multi-bit quantizers in the presence of interference. The relationship between the quantizer gain tuning and the received signal are examined to gain an insight into how the loss induced by the quantizer can be minimized. This is explored via the use of Monte-Carlo simulations. In the following, it will be shown that, similar to the interference-free case, an optimal configuration exists for the quantizer gain.

In the presence of a high powered interference signal, the statistics of the received signal are no longer characterized by thermal noise alone. In fact, the received signal's statistics are dominated by the statistics of the interference signal. It is expected, therefore, that the quantizer gain, which provides optimal performance, will differ from that of the interference-free case.

3.3.3 Bit Error Rate

The GPS L1 C/A signal is taken here as a case study for simulation purposes. This signal is modulated by a data sequence with a bit period of 20 ms, denoted by T_b. If the phase synchronization between the reference signals and the received signal is performed perfectly before bit demodulation, the expected BER, P_e, is given by (Kaplan & Hegarty 2006, Proakis & Salehi 2007)

$$P_e = \frac{1}{2}\operatorname{erfc}\left(\sqrt{\frac{C}{N_0} \times T_b}\right) \tag{3.16}$$

where, $\operatorname{erfc}(\cdot)$ is the complementary error function. The effective C/N_0 for a given BER value can be calculated as

$$\left(\frac{C}{N_0}\right)_{\text{eff}} = \frac{1}{T_b}[\operatorname{erfc}^{-1}(2P_e)]^2 \tag{3.17}$$

and the C/N_0 loss in dB computed from the BER result is determined by

$$L_B = \left(\frac{C}{N_0}\right)_{\text{eff}} - \left(\frac{C}{N_0}\right). \tag{3.18}$$

3.4 AGC Adjustment in Real Conditions

In this section, AGC values adjusted by a NovAtel FireHose receiver (FireHose 2012) are presented to gain an insight of the AGC variation in actual interference-free reception scenarios. These results are shown for the static and dynamic reception mode of the GPS L1 C/A signal. The FireHose receiver employs an adaptive 8-bit analog to digital converter (ADC).

Figure 3.4 shows the AGC values in the stationary mode. In this case, GPS data was collected under good signal conditions from the rooftop of the CCIT building of The University of Calgary. The results of AGC values are shown for a full day, namely 20 February 2013. As it can be seen, AGC values are almost constant in the absence of interference.

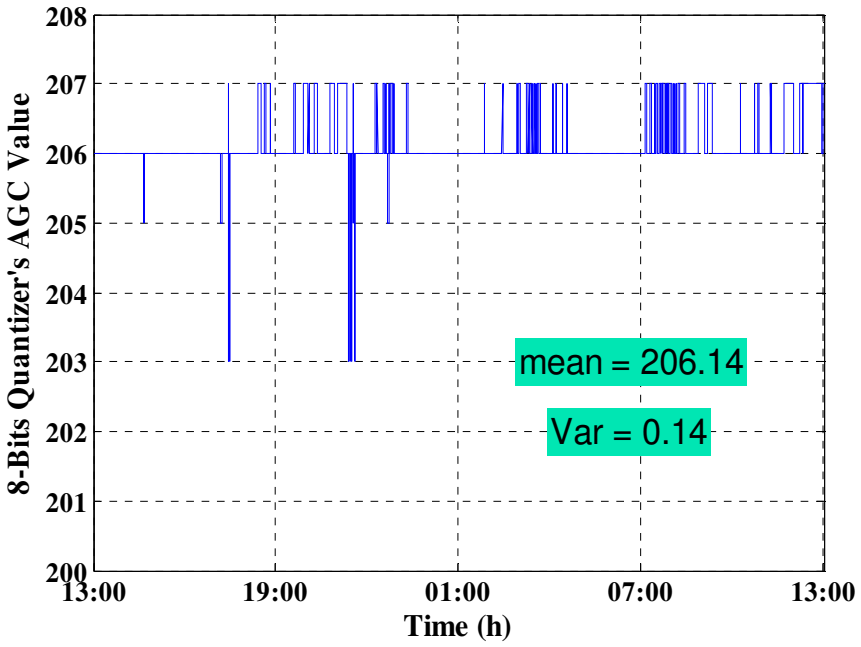

Figure 3.4: AGC values adjusted by the FireHose receiver in stationary mode

Figure 3.5 shows the adjusted AGC values by the Firehose receiver in a moving mode. The receiver trajectory is shown in Figure 3.6 for reference and includes two story buildings and the Calgary city core where buildings with 50 to 60 stories are present. The data collection duration was 1 h. As can be seen, although the AGC value changes are higher than when the receiver is stationary, the adjusted values are very close to their average value. That is, an AGC value can be calculated and adjusted based on noise variance by the GNSS receiver at the start and that value will be almost constant over a long period of reception time. Moreover, after the appearance of interference, the previous estimate of noise variance is still valid for some extent of reception time duration.

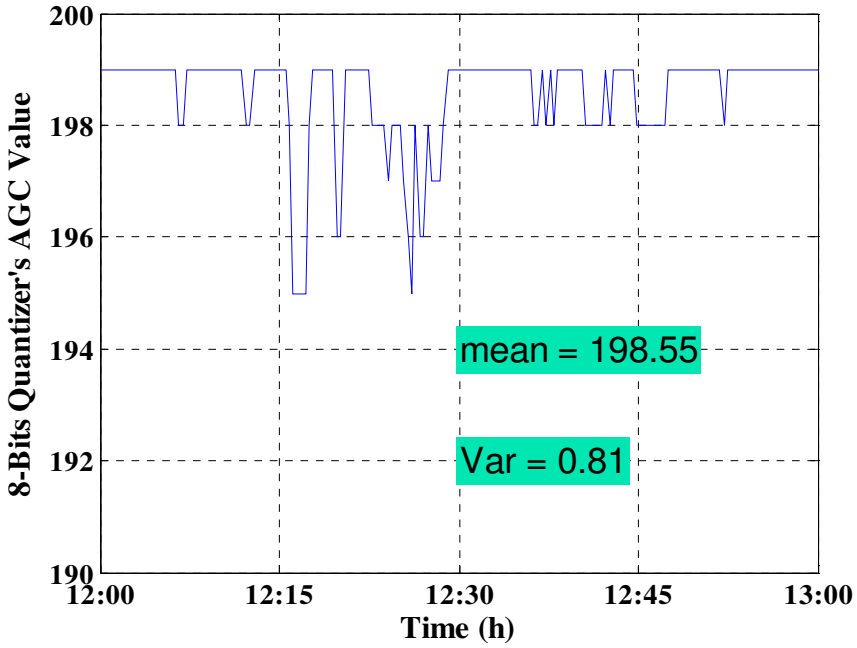

Figure 3.5: AGC values adjusted by the FireHose receiver in moving mode

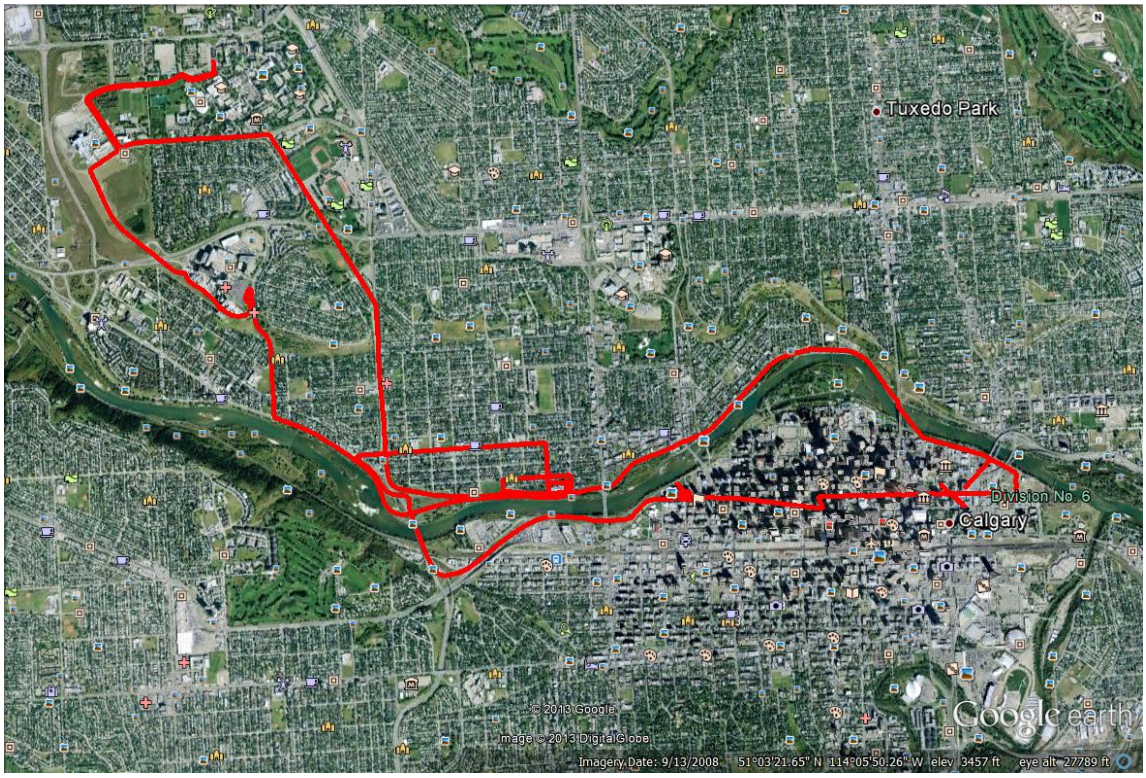

Figure 3.6: Calgary trajectory selected to collect FireHose AGC gains in moving mode

3.5 Analysis and Simulation

This section examines the performance of multi-bit quantizers in the presence of interference. The relationship between the quantizer tuning and the received signal quality are examined to gain an insight into how the loss induced by the quantizer can be minimized. The performance of the GPS L1 C/A signal is considered as a case study. To present the performance of the quantization process and detection probability results, MATLAB simulations are performed, simply assuming that the received signal has a C_s/N_0 of 45 dB-Hz in all of the subsequent experiments. Monte-Carlo simulations, the configuration of which is summarized in Table 3-1, are employed to evaluate the performance of various acquisition schemes. The receiver frequency plan and noise

figures are chosen to represent a typical consumer-grade receiver. The interference signal frequency is relatively close to that of the GPS signal carrier frequency, $f_\Delta \approx 0$ Hz.

Table 3-1: Simulation setup

Parameter	Value	Unit	Symbol
GPS C/A PRN number	1	-	
Noise floor	-174.0	dBm/Hz	N_0
Sampling frequency	8.0	MHz	F_s
Intermediate frequency	1.2	kHz	f_{IF}
Coherent integration time	1.0	ms	T_I
Non-coherent combinations	1	-	K

3.5.1 Quantization in the Presence of Interference

Figure 3.7 shows the BER performance of 1-bit quantization for interference-corrupted signals with C/N_0 values of 30, 35 and 40 dB-Hz, respectively. As can be seen, for low values of interference power, the interference has little effect and the BER performance is equivalent to that of the interference-free case. For an interference power approximately equal to -120 dBm, the BER begins to increase. It increases steadily until an interference power of approximately -90 dBm is reached when the BER reaches 0.5. Note that a BER of 0.5 is equivalent to blindly guessing the bit value and implies that no information can be recovered from the received signal.

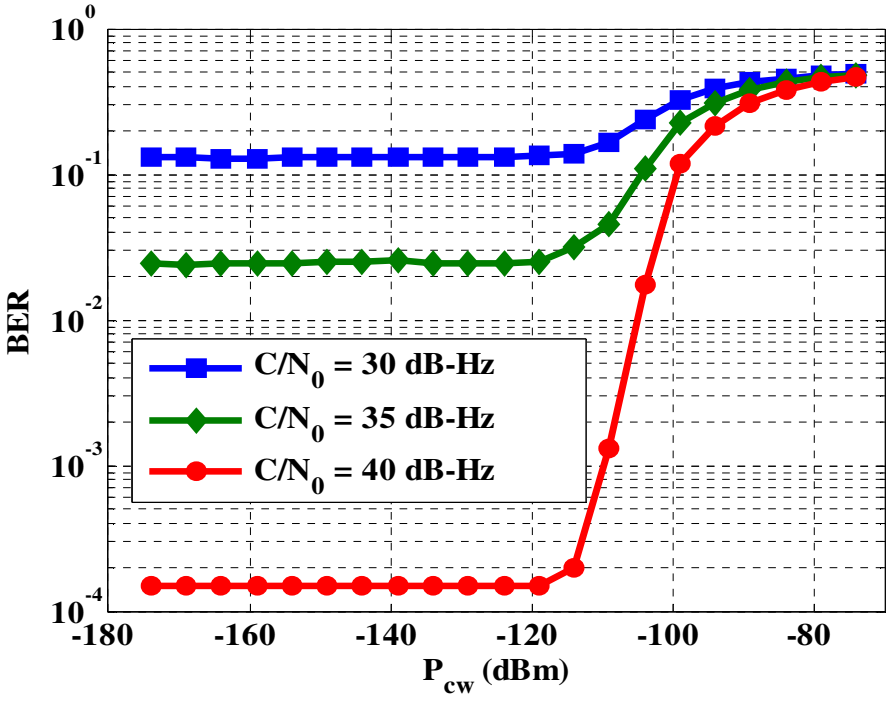

Figure 3.7: BER performance for 1-bit quantizer as a function of interference power ($f_{\Delta} \approx 0$ Hz)

The results of the calculated effective C/N_0 loss, calculated via the BER performance, for 1-bit quantization for a signal containing interference with a C_s/N_0 of 30, 35 and 40 dB-Hz are shown in Figure 3.8. Then, as the interference power increases beyond -110 dBm, the C/N_0 loss increases significantly. Furthermore, as can be seen, the signal quality loss induced by quantization and interference is dependent primarily on the interference power and quantizer configuration and is almost independent of the C_s/N_0. Thus, to simplify further analysis, the received signal is assumed to have a C_s/N_0 of 40 dB-Hz in all subsequent results.

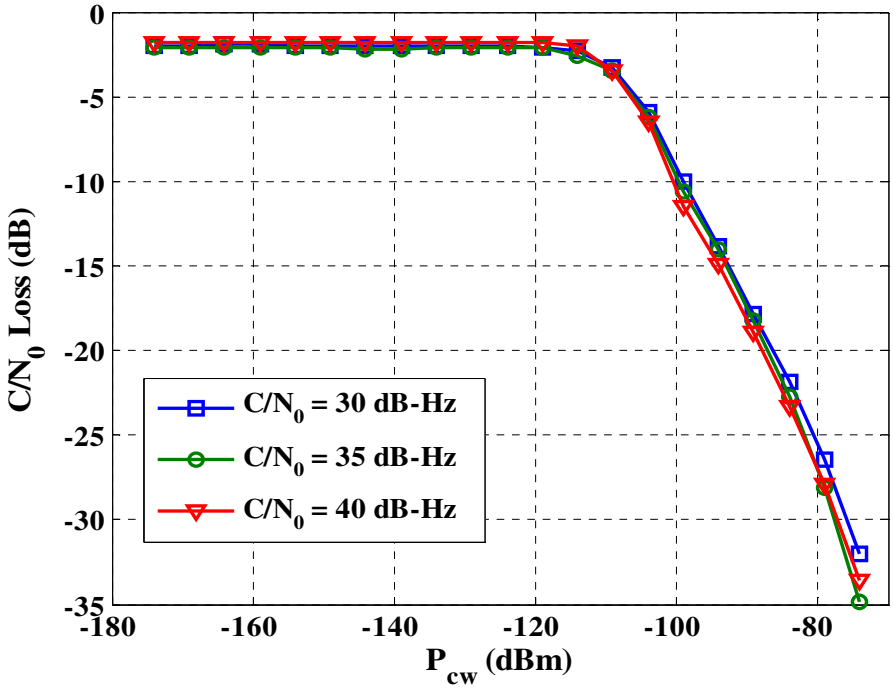

Figure 3.8: Quantization loss as a function of interference's power for 1-bit quantization ($f_{\Delta} \approx 0$ Hz)

In the presence of a high powered interference signal, the statistics of the received signal are no longer characterized by thermal noise alone. In fact, the statistics of the received signal are dominated by the statistics of the interference signal. It is expected, therefore, that the quantizer gain that provides optimal performance will differ from that of the interference-free case.

Figure 3.9 shows the BER for 2-bit quantization for a signal containing interference, as a function of $A_g\sigma_n$. The results are shown for interference power values in the range of -104 dBm to -79 dBm. As can be seen in the figure, the more interference power is present, the more BER performance degradation is experienced. In addition, there exists an optimum value for $A_g\sigma_n$ that results in a minimum BER. This value of $A_g\sigma_n$ decreases

as the value of P_{cw} increases. Meanwhile, the best achievable BER reduces as the power of interference increases. Another interesting observation that can be drawn from this plot is that the ability of the 2-bit quantizer to provide a given BER is limited by the interference power. For example, if a BER of less than 10^{-2} is required, then 2-bit quantization is not sufficient if the prevailing interference power is greater than -90 dBm. This observation may serve as a useful design principle, when choosing a quantizer configuration.

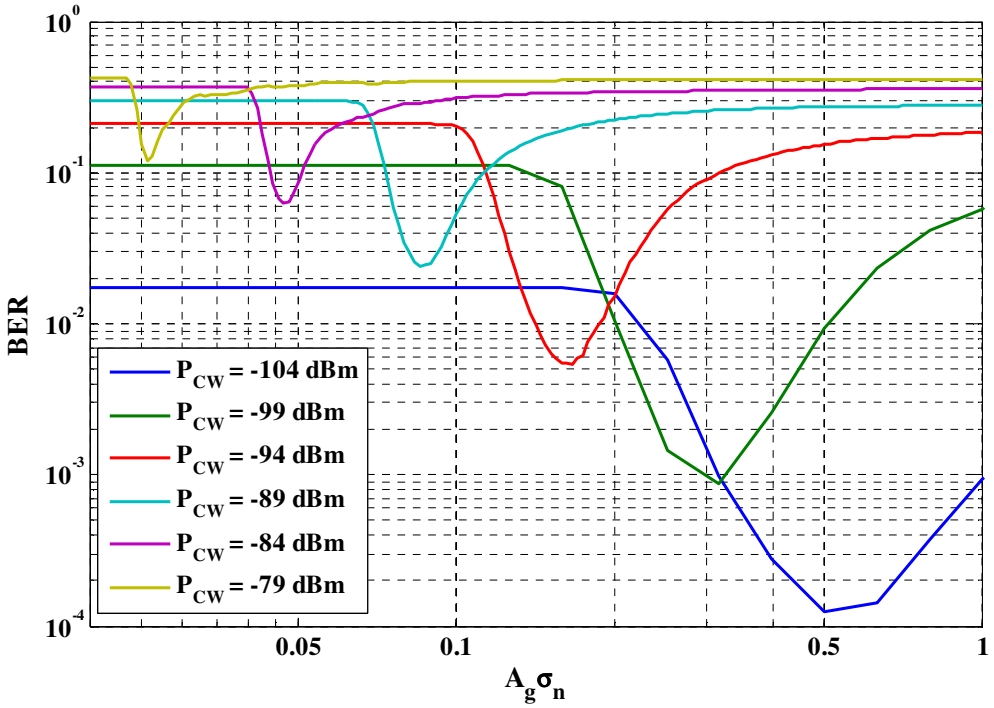

Figure 3.9: BER performance for a 2-bit quantizer as a function of interference power ($f_{\Delta} \approx 0$ Hz)

Figure 3.10 shows the BER results for the 3- and 4-bit quantization cases, as a function of $A_g\sigma_n$. The results are shown for P_{cw} in the range of -99 dBm to -79 dBm. As can be seen

in Figure 3.10, as the interference power increases, three and seven local minima appear in the BER results for 3- and 4-bit quantization, respectively. This is due to the fact that the statistics of the quantizer input signal are dominated by the interference signal (Abdizadeh et al 2012) and every $A_g\sigma_n$ value that aligns a PDF mode of the quantizer input and a quantizer threshold is a locally optimal value. Moreover, for 2-, 3-, and 4-bit quantizers, there is an optimum gain that results in a minimum bit error rate or, equivalently, to a maximum effective carrier-to-noise-ratio.

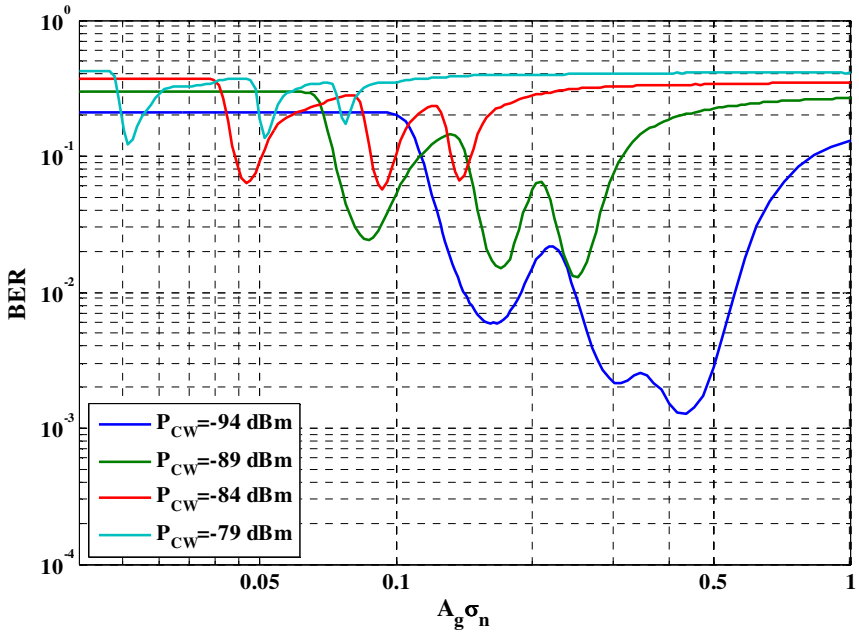

(a) 3-bit

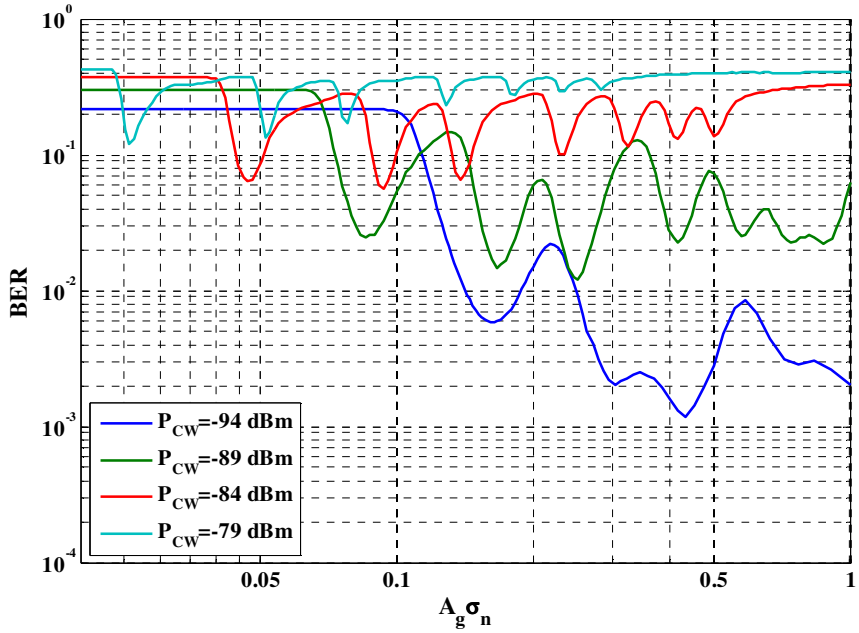

(b) 4-bit

Figure 3.10: BER performance for 3- and 4-bit quantizers as a function of interference power ($f_{\Delta} \approx 0$ Hz)

Figure 3.11 shows the effective C/N_0 loss as a function of $A_g\sigma_n$ for 2-, and 3-, and 4-bit quantizers calculated from the BER plots. These curves can be used to estimate the value of $A_g\sigma_n$ that minimizes the effective C/N_0 loss, for a given interference power. Note also that the loss curves are narrower for higher interference power. Thus, it is evident that the sensitivity of the loss to $A_g\sigma_n$ increases as the prevailing interference power increases. Moreover, as results show, setting the AGC gain to its optimal value can provide a significant improvement in effective C/N_0 performance. For example, in the presence of -99 dBm interference power and 2-bit quantization resolution, optimum AGC gain provides C/N_0 at levels more than 5 dB higher than a blind receiver setting $A_g\sigma_n$ to unity.

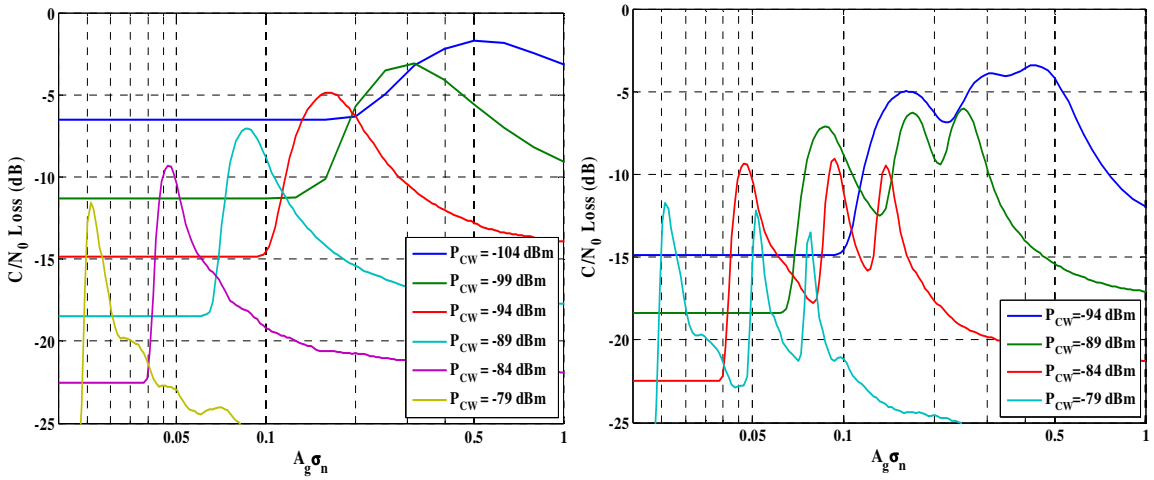

(a) 2-bit (b) 3-bit

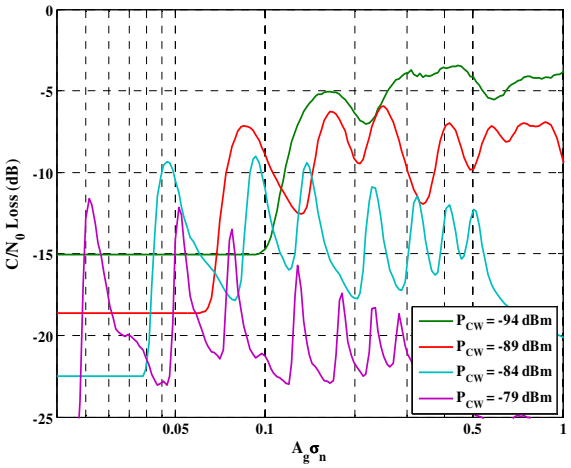

(c) 4-bit

Figure 3.11: Effective C/N_0 Loss for 2-, 3-, and 4-bit quantizers in the presence of interference calculated from the BER results

The results of minimum BER, minimum C/N_0 loss and corresponding $A_g\sigma_n$ for different interference power and quantization resolution, as shown in the previous figures, are summarized in Table 3-2. For each interference power case, the value of the AGC gain

can be automatically adjusted based on the last column of this table in order to achieve the tabulated minimum BER and C/N_0.

Table 3-2: Minimum BER and corresponding C/N_0 loss for different receiving scenarios

Number of bits	Interference power (dBm)	Minimum BER	C/N_0 loss (dB)	$A_g\sigma_n$
2	-104	1.2×10^{-4}	-1.71	0.501
	-99	9.8×10^{-4}	-3.19	0.316
	-94	5.0×10^{-3}	-4.79	0.166
	-89	2.4×10^{-2}	-7.09	0.086
	-84	6.3×10^{-2}	-9.32	0.047
	-79	1.2×10^{-1}	-11.61	0.026
3	-94	1.0×10^{-3}	-3.21	0.435
	-89	1.3×10^{-2}	-6.06	0.251
	-84	5.7×10^{-2}	-9.03	0.093
	-79	1.2×10^{-1}	-11.61	0.026

3.5.2 Histogram of the Quantized Signal

As can be seen in Figure 3.10, as the interference power increases, three local minima appear in the BER results in the 3-bit quantizer case. This is due to the fact that the statistics of the quantizer input signal are dominated by the interference signal. To better understand how the AGC works, the PDF of the quantizer input signal is shown in Figure 3.12, Figure 3.13 and Figure 3.14 for a selection of interference power levels.

For low interference power levels, for example $P_{\text{cw}} \approx$ -109 dBm, the quantizer input signal has a uni-modal PDF as shown in Figure 3.12. In this case, the value of $A_g\sigma_n$ that yields optimal performance is approximately equal to that of the interference-free case.

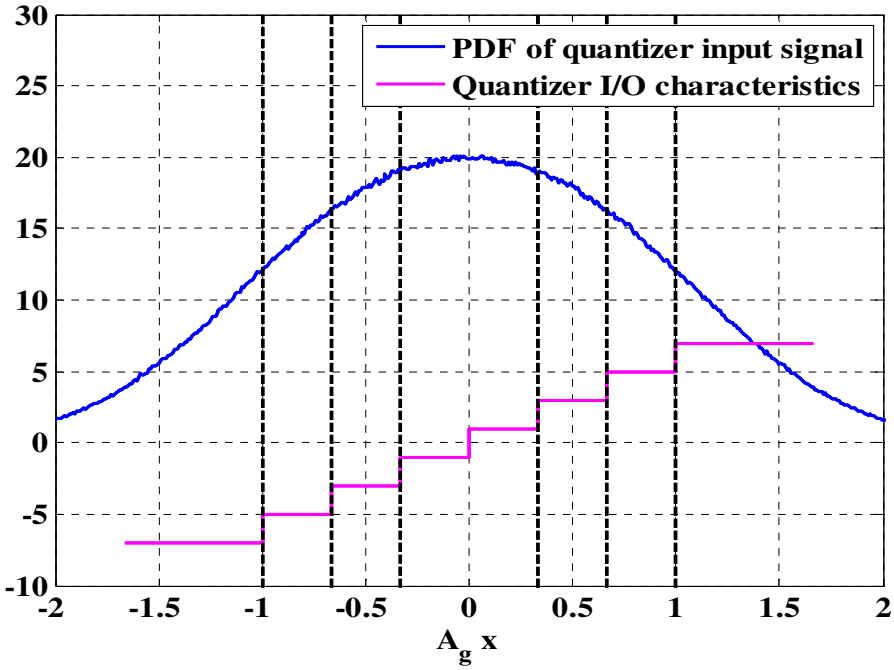

Figure 3.12: PDF and quantizer input-output characteristics for low power interference (P_{cw} = -109 dBm)

For medium levels of interference power (-100 dBm < P_{cw} < -80 dBm), the PDF of the input signal significantly deviates from that of a Gaussian PDF. An example of the PDF of the quantizer input is shown in Figure 3.13 for $P_{\text{cw}} =$ -84 dBm. Two distinct modes are evident in this PDF. As a result, the quantizer levels nearest these modes will be excited most frequently. As the value of $A_g\sigma_n$ is varied, the threshold nearest these modes will change and for every value of $A_g\sigma_n$ that places a mode directly at a quantizer

threshold, there is a corresponding trough in the BER curve (or peak in the effective C/N_0 curve). That is, every $A_g\sigma_n$ value that aligns a mode and a quantizer threshold is a locally optimal value.

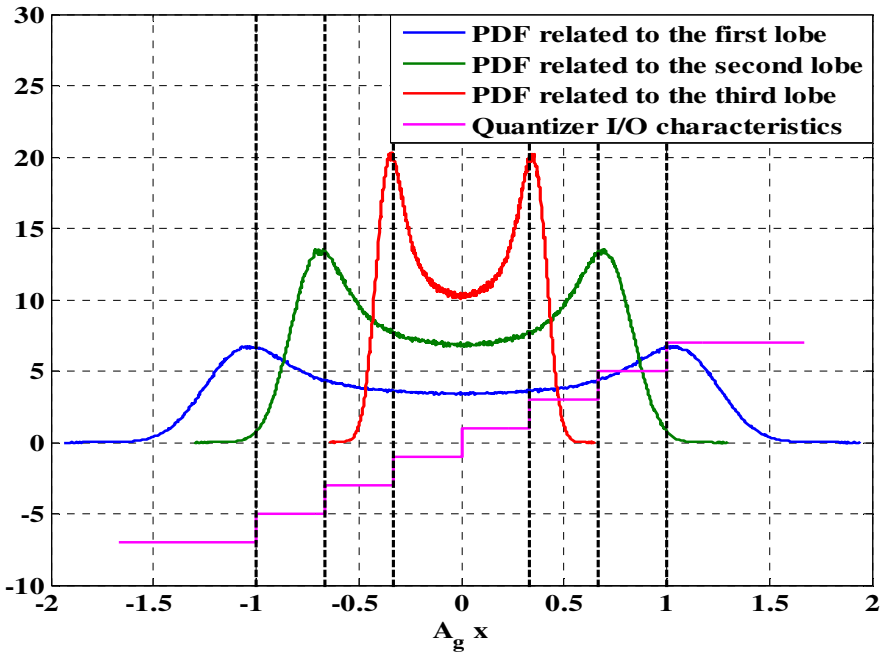

Figure 3.13: PDF and quantizer input-output characteristics for medium power interference (P_{cw} = -94 dBm)

For high interference power levels (P_{cw} > -79 dBm), the three locally optimal values of $A_g\sigma_n$ become more distinct, as shown in Figure 3.14 for P_{cw} > -79 dBm.

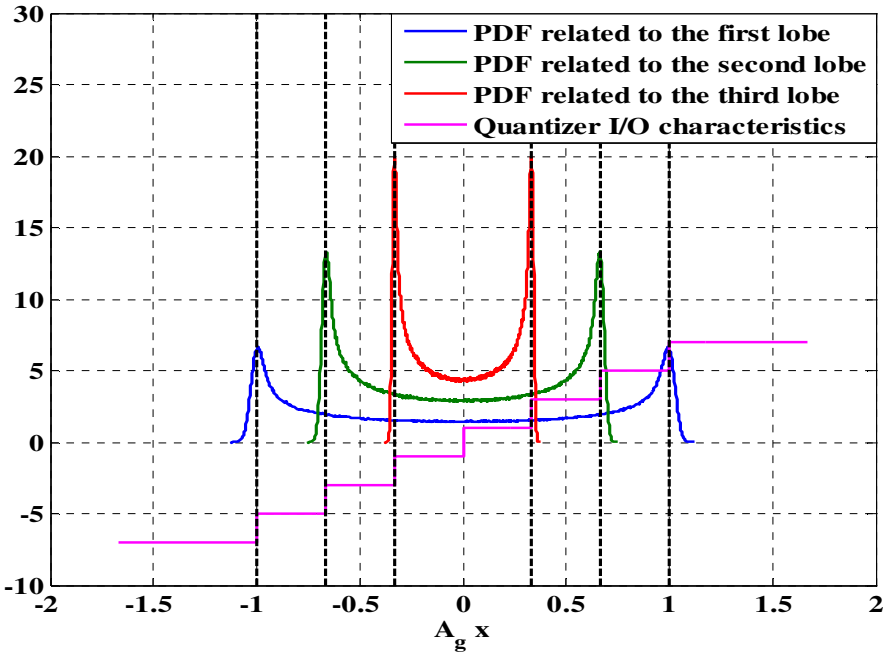

Figure 3.14: PDF and quantizer input-output characteristics for high power interference (P_{cw} = -79 dBm)

It is noteworthy that, depending on the interference power level, different locally optimal values of $A_g\sigma_n$ represent the global optimum. For high interference power levels, it is the highest locally optimal value of $A_g\sigma_n$. For medium power interference, it is the second highest value, and for low power interference, the lowest locally optimal value of $A_g\sigma_n$ corresponds to the global optimum, at which point the curve converges to the interference-free case.

In addition for a strong interference case, the k^{th} locally optimal value of $A_g\sigma_n$ is equal to k multiplied by a constant value, where k is 1, 2, …, $L = 2^{B-1} - 1$. This constant value is inversely proportional to the interference power.

3.5.3 Optimum Quantizer Configuration (AGC gain)

Similar to the interference-free case, which has been well documented (e.g. Curran 2010), there exists an optimal configuration for the quantizer gain. This optimal value is generally expressed in terms of $A_g\sigma_n$. Non optimal values of $A_g\sigma_n$ underutilize the quantizer resolution. When $A_g\sigma_n$ is too low, the higher quantization thresholds are not sufficiently employed while for $A_g\sigma_n$ values that are too high, the lower thresholds are rarely excited. In either case the quantizer loss converges to that of the 1-bit quantizer. In addition, for larger values of B, the range of $A_g\sigma_n$ that provides near optimal performance is widened. That is, an increased B not only provides superior performance, it also reduces the sensitivity to A_g tuning.

Figure 3.15 shows the values of $A_g\sigma_n$ that minimize the quantization loss of the signal as a function of P_{cw} for the 2-, 3-, and 4-bit quantizers. As expected, for low values of interference power, the optimum value of $A_g\sigma_n$ converges to that of the interference-free case as 1, 1.7, and 3 for 2-, 3-, and 4-bit quantizers, respectively (Curran 2010). As the interference power increases, this optimum value decreases rapidly. A measure of the benefit of increasing the number of quantizer bits is also evident in Figure 3.15. Increasing the resolution from 2- to 3-bit can yield a gain of up to 2 dB, in some cases. However, the gain appears to diminish rapidly as more bits are employed.

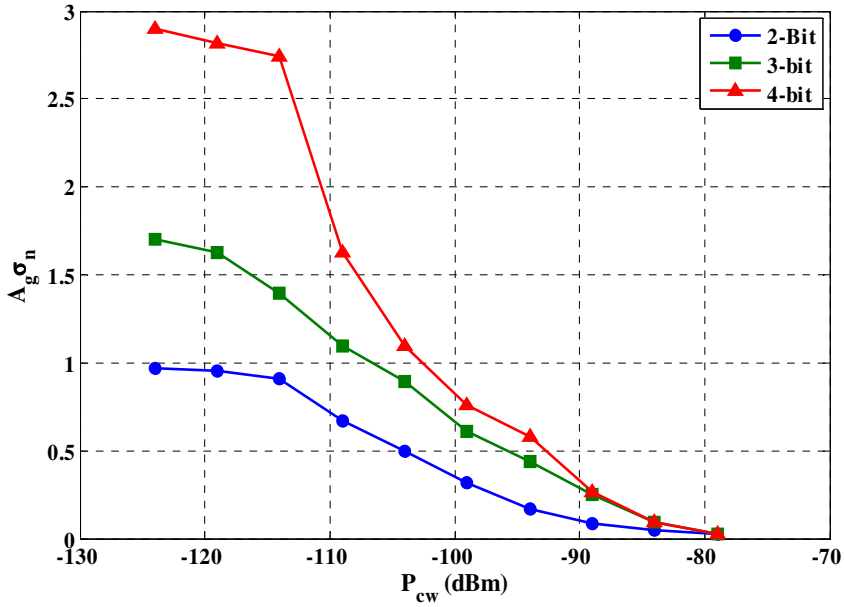

(a) $A_g\sigma_n$ for different values of interference power

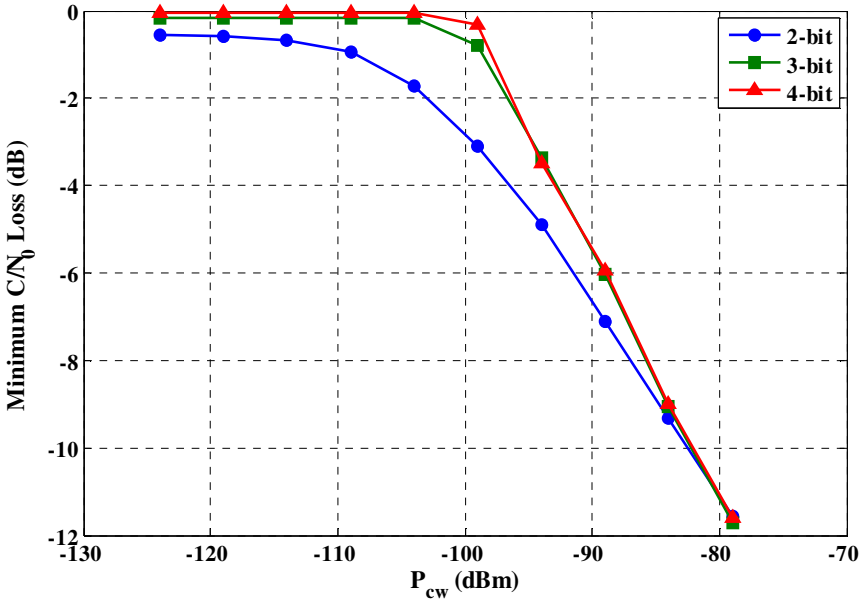

(b) Effective C/N_0 loss for different values of interference power

Figure 3.15: Optimum value of $A_g\sigma_n$ and minimum effective C/N_0 loss as a function of P_{cw}

3.6 Summary and Conclusions

The effect of interference is intensified due to quantization limitations. In this chapter, the performance of 1-, 2-, 3- and 4-bit quantizers was examined in the presence of interference. The limitations of traditional metrics for receiver performance estimation were explored and an alternative metric, namely the bit error rate, was examined. The effective C/N_0 loss experienced by a quantizing receiver in the presence of interference was calculated for a variety of quantizer configurations and interference power levels. For 2-, 3-, and 4-bit quantizers, the optimum gain that results in a minimum bit error rate or, equivalently, to a maximum effective carrier to noise ratio, was presented and discussed.

The result of this chapter enables a commercial GNSS receiver to optimally configure its quantization processor in order to achieve higher effective C/N_0 values and provide more robustness against narrowband interference.

Chapter Four: Interference Detection & mitigation Based on Notch Filtering

IIR filters are a widely employed class of notch filters because of their low computational complexity, efficient design and implementation, and low number of parameters to be adapted. However, the cost of this ease of implementation is stability problems and numerical errors (Haykin 2001). Due to the feedback structure used in IIR filters, every input and output sample should be considered to compute the future outputs. Hence, any error in the filter output will be fed back to the system to be used for the next output samples, which might cause stability problems.

In contrast, in terms of numerical errors, there is no feedback in FIR implementation and the errors do not leak to the next output samples. Moreover, from an implementation point of view, FIR filters can be implemented with fewer numbers of bits (precision) compared to IIR filters, which results in saving a large amount of calculation and computation load in filtering algorithms. For example, an FIR filter can be implemented with 8 bits, while an IIR filter requires 16 bits or even more to provide the same precision of the output samples (Haykin 2001, Diniz 2010). However, to implement a thin FIR notch filter, FIR notch filters require a relatively high number of taps.

In many measurement applications including GNSS systems, the timing between transmitter and receiver is of great importance. In general, the IIR filters have non-linear phase characteristics and the presence of such filters in GNSS receivers induces amplitude and phase distortions, which can lead to some biases in the pseudorange and carrier phase measurements. The phase distortion leads to a code delay bias in the pseudorange measurements as a function of the signal Doppler frequency. Despite phase

distortion, the amplitude distortion induced by the IIR notch filter can cause a distortion in the correlation function and induce an additional bias in the pseudorange measurements. In other words, the amplitude distortion induced by an IIR notch filter will make the correlation asymmetric with respect to the correlation peak and introduce a bias term in pseudorange measurements. Full details on the impact of notch filters on navigation measurements are provided by Giordanengo (2009), Montloin (2010) and Lin et al (2011). In this studies, it is shown that, since an IIR notch filter has a non-linear phase response, the amplitude distortion and the group and phase delays induced by an IIR notch filter are signal frequency dependent, and thus, cannot be automatically compensated by the clock bias state in the navigation solution. Therefore, employing additional bias compensation and calibration techniques is necessary. The navigation solution improvement due to this bias removal has been studied by Lin et al (2011).

Moreover, it is shown that because of the linear-phase property of a linear-phase FIR (LP-FIR) notch filter, the group and phase delays are signal frequency independent (Giordanengo 2009). In addition, it has been proven that linear-phase FIR notch filters will ensure that the correlation function remains symmetric (Oppenheim & Schafer 2009). Therefore, the bias terms in pseudorange and carrier phase measurements due to a linear-phase FIR notch filter are common for all satellite signals with different Doppler frequencies, and they can be fully absorbed by the clock bias term in the navigation solution. Therefore, an adaptive FIR notch filter (with or without the linear-phase property) is preferable in GNSS applications and its design is considered in this chapter.

A new class of adaptive FIR notch filters (FIR-ANF) is proposed and developed herein to efficiently detect and track CW interference and properly eliminate it with negligible side effects on the desired signal. First, a one-pole complex notch filter for the case of a single complex interference source is considered, which is initially an expansion of one-pole IIR notch filter. Here, a least mean squares (LMS) scheme is considered to adaptively modify the filter's zero location in order to track the interference signal. This adaptation is done by minimizing the filter output power that occurs when the notch frequency is placed on the corresponding interference frequency. That is, by minimizing the output power, the interference is cancelled automatically. Second, the developed FIR NF is extended to have a linear-phase response in order to satisfy the calibration needed in the pseudorange measurements. Third, to mitigate multiple CW interference, i.e. multi-pole notch filter, cascading two or more one-pole complex notch filters can be employed. This kind of structure was originally introduced by Soderstrand et al (1997), Wang & Milstein (1988), Nishimura & Jiang (1998) and Borio (2008). However, the addition of a notch filter results in removing more frequency components of the desired GNSS signal. Fourth, the performance of complex adaptive IIR and FIR notch filters is investigated in a GNSS software receiver by processing simulated GNSS signals with fixed and swept interference generated from a hardware simulator. Finally, the BER performance of the NF in the presence of quantization loss is presented. Interestingly, it will be shown that the optimum AGC configuration, discussed in Chapter Three, results in an optimum BER performance provided by notch filtering.

4.1 Designing The Notch Filter

After detecting the interference presence by means of an interference detection unit, notch filtering techniques might be employed to attenuate a certain frequency in the received bandwidth which contains the CW interference (Soderstrand et al 1997). It is important to note that NF schemes can also be employed in detecting the presence of CW interference. Generally, notch filters, either FIR or IIR, can be divided into the following two different classes: 1- Fixed Notch Filter, 2- Adaptive Notch Filter. In the following, characteristics and properties of each filter are discussed. In addition, for the sake of simplicity, complex forms of notch filters are considered.

4.1.1 Complex IIR Notch Filter

The IIR notch filter is the most widely employed notch filtering scheme because of its low computational complexity and efficient implementation. The transfer function of an one-pole complex IIR notch filter is given by (Borio 2008, Oppenheim & Schafer 2009)

$$H_{\mathrm{IIR}}(z) = \frac{1 - z_0 z^{-1}}{1 - \rho z_0 z^{-1}} \tag{4.1}$$

where z_0 is the notch filer zero corresponding to the interference frequency and $0 \ll \rho < 1$ is the pole contraction factor. This factor controls the bandwidth and mitigation level of the notch filter and therefore implicitly there is a trade-off between interference mitigation level and the side effect on the desired signal. An increase in the pole contraction factor results in a lower notch bandwidth and interference mitigation level.

IIR notch filters can be generalized to have higher orders, their mathematical steps being presented in Appendix E. Interestingly, it can be shown that increasing the order of a

notch filter provides extra redundancy to have a narrower NF for a given interference mitigation level.

4.1.2 Complex FIR Notch Filter

The transfer function of an FIR complex notch filter can be derived by keeping the first *N* terms in the expansion series of the complex IIR notch filter and is presented as (Carusone & Johns 1999):

$$H_{\mathrm{FIR}}(z) = 1 + \sum_{k=1}^{N-1} z_0^k[\rho^k - \rho^{k-1}]z^{-k} - \rho^{N-1}z_0^N z^{-N} \tag{4.2}$$

The transfer function of FIR notch filter can be written as

$$H_{\mathrm{FIR}}(z) = \sum_{k=0}^{N} \alpha_k z_0^k z^{-k} \tag{4.3}$$

where the coefficients, α_n, are given by

$$\alpha_k = \begin{cases} 1, & k = 0 \\ \rho^k - \rho^{k-1} & 1 \le k < N \\ -\rho^{N-1} & k = N \end{cases} \tag{4.4}$$

The notch filter output or the error signal of the filter can be expressed as

$$e[k] = x[k] \bigstar h[k] \tag{4.5}$$

where the NF input signal, i.e. $x[n]$, is assumed to contain a sinusoid interference signal buried in noise, $\eta[n]$, and given by

$$x[k] = A_{\mathrm{int}} e^{j(2\pi f_{\mathrm{int}} k T_S + \theta_{\mathrm{int}})} + \eta[k] \tag{4.6}$$

4.1.3 Proposed Algorithm: Linear-Phase Adaptive FIR Notch Filter

In the previous discussed FIR filter design, there was no constraint on the phase response of the FIR filter. However, as mentioned before, a linear-phase FIR filter is preferable in GNSS applications. Linear-phase FIR filters can be derived by using back-forward filtering. That is, a linear-phase notch filter impulse response can be implemented as follows (Smith 2002):

$$h_{\mathrm{FIR-LP}}[k] = h_{\mathrm{FIR}}[k] \bigstar h_{\mathrm{FIR}}^{*}[N-k] \tag{4.7}$$

where $*$ denotes the conjugate operator and N is the order of FIR notch filter. This transfer function can be written as (See Appendix G)

$$H_{\mathrm{LP-FIR}}(z) = \sum_{n=0}^{N}\sum_{m=0}^{N} \alpha_n \alpha_m^{*} z_0^{n} z_0^{*m} z^{-N-n+m} \tag{4.8}$$

The order of this linear-phase FIR notch filter is $2N$ and its group delay is given by

$$\tau_g(\omega) = \frac{N}{F_s} \tag{4.9}$$

As it can be seen, the phase response of a linear-phase FIR notch filter is not only linear but also independent of the NF's contraction factor.

Figure 4.1 shows the amplitude and phase responses of complex IIR and linear-phase FIR notch filters for two different pole contraction factor values, i.e. 0.90 and 0.98, and $N = 300$. As indicated in this figure, IIR notch filters have non-linear phase characteristics, where the phase of a linear-phase FIR notch filter is linear. The notch level of linear-phase FIR filter is half of that of the IIR NF, due to the convolution operation in Eq. (4.7). The z-transform of Eq. (4.7) can be presented as

$$H_{\mathrm{LP-FIR}}(z) = H_{\mathrm{FIR}}(z)(H_{\mathrm{FIR}}(z^{*-1})z^{*-N})^{*}. \tag{4.10}$$

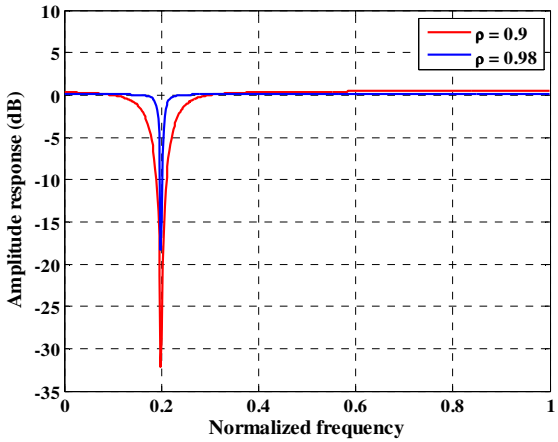

(a) Amplitude response of a complex IIR notch filter

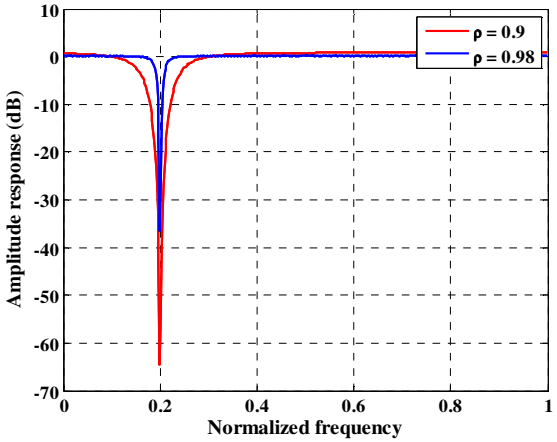

(b) Amplitude response of a complex linear-phase FIR notch filter

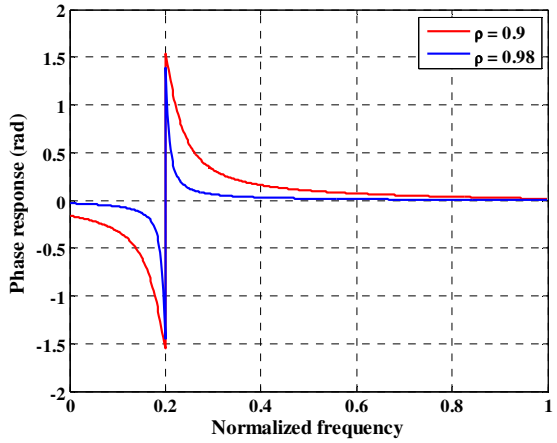

(c) Phase response of a complex IIR notch filter

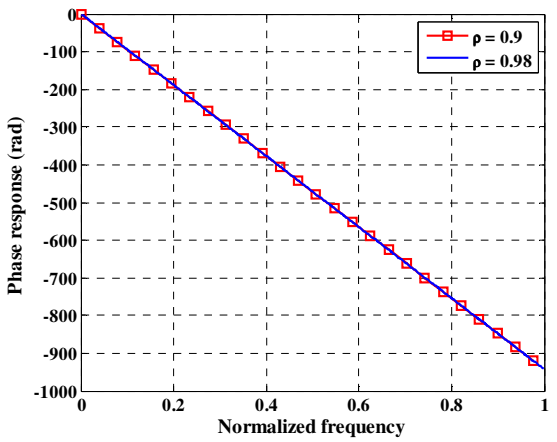

(d) Phase response of a complex linear-phase FIR notch filter

Figure 4.1: Amplitude and phase responses of complex IIR and linear-phase FIR notch filters for two different pole contraction factors and $N = 300$

4.2 Adaptation Mechanism

Fixed Notch filters are appropriate to eliminate fixed frequency band of the received signal. However, some interference signals, e.g. chirp and swept interference, have time varying frequency, which makes them resistant against fixed frequency notch filter based interference mitigation algorithms. To overcome this limitation, adaptive notch filters can be employed. Whenever the interference signal, such as CW interference, has predictable statistics, adaptive filtering predicts these values and removes the interference from the received signal. Moreover, adaptive notch filters try to minimize the NF output signal's power. That is, in adaptive notch filtering, the notch frequency of the filter is modified along with the center frequency variation of the interference signal. In the following, adaptive FIR notch filter is discussed in more details.

The core of the proposed adaptive notch filter is represented by the adaptive block that tracks the fixed and swept CW interference frequency and adjusts the filter coefficients in order to minimize the desired cost function. In this thesis, the normalized LMS criterion descried in Haykin (2001) is employed. The cost function is defined as

$$J[\mathrm{k}] = \mathrm{E}[|e[k]|^2] \tag{4.11}$$

and, the adaptation equation or zero update is given by

$$\hat{z}_0[k+1] = \hat{z}_0[k] - \mu[k]\nabla_{z_0}[|e[k]|^2] \tag{4.12}$$

where $\hat{z}_0[k]$ is the complex parameter that represent the zero estimate of the CW frequency. ∇ is the gradient operator and $\mu[k] = \frac{\mu_0}{\mathrm{E}[|x[k]|^2]}$ is the normalized LMS step size where μ_0 is a constant value.

By employing Eq. (4.5), Eq. (4.12) can be rewritten as

$$\hat{z}_0[k+1] = \hat{z}_0[k] - \mu[k](x[k]\bigstar h[k])(x[k]\bigstar g[k])^* \tag{4.13}$$

where $g[k]$ is the impulse response of the gradient system function given by

$$g[n] = \frac{\partial h[n]}{\partial z_0} \tag{4.14}$$

For adaptive linear-phase FIR-ANF, the update and adaptation expression can be written as (see Appendix G)

$$\begin{aligned}\hat{z}_0[k+1] = \hat{z}_0[k] - \mu[k]e[k] \\ \times \sum_{n=0}^{N}\sum_{m=0}^{N} n\alpha_n^*\alpha_m z_0^{*n-1} z_0^m x^*[k-N+n-m]\end{aligned} \tag{4.15}$$

where the α coefficients are given by Eq. (4.4).

In this thesis, a straightforward plain gradient (PG) scheme is employed to update the zero of the NF. Extensive studies on the PG scheme have shown that this method is inherently a biased estimator. To reduce its bias, either the pole radius should be set close to unity or some modified PG methods should be employed (Punchalard 2012). In Appendix J and Appendix K, the steady state solution and mean square error (MSE) of a general adaptive FIR NF are proposed and developed.

4.2.1 Convergence Analysis and Wiener Solution

The Wiener solution is the value of $\hat{z}_0$ that results in the minimum value of the cost function, i.e. *J*. It was shown that the LMS solution converges towards the Wiener solution in the steady state condition (Haykin 2001, Borio 2008). The Wiener solution for z_0 is obtained by setting the gradient value of the cost function to zero as follows:

$$\nabla J[k] = \mathrm{E}[\mathrm{grad}(J[\mathrm{k}])] = 0 \tag{4.16}$$

The Wiener solution for FIR notch filter is given by (See Appendix H)

$$z_{0,\ \mathrm{Wiener}}^{\mathrm{FIR}} = \frac{(1+4\gamma) - \sqrt{(1+4\gamma)^2 - 16\rho\gamma}}{2\rho} e^{j2\pi f_{\mathrm{int}}} \tag{4.17}$$

where γ is given by

$$\gamma = \frac{A_{\mathrm{int}}^2}{\sigma_n^2(1-\rho)} \tag{4.18}$$

The Wiener solution for a linear-phase FIR-ANF notch filter is given by (See Appendix I)

$$z_{0,\ \mathrm{Wiener}}^{\mathrm{LP-FIR}} = \frac{\sqrt[3]{4\gamma} - 1}{\sqrt[3]{4\gamma} - \rho} e^{j2\pi f_{\mathrm{int}}} \tag{4.19}$$

And, the Wiener solution for IIR notch filter is reported in Borio (2008) as follows

$$z_{0,\ \mathrm{Wiener}}^{\mathrm{IIR}} = \frac{-\gamma(1-\rho) - 1 + \sqrt{(\gamma(1-\rho)+1)^2 + 4\rho\gamma(\gamma-1)}}{2\rho(\gamma-1)} e^{j2\pi f_{\mathrm{int}}} \tag{4.20}$$

It is important to note that, since the linear-phase FIR filter has a magnitude response equal to that of the second order IIR notch filter, in order to fairly compare the Wiener results, the results are evaluated for the same notch bandwidth by means of the mathematical formulas given in Appendix J. Figure 4.2 shows the magnitude of the Wiener results of these notch filters for ρ = 0.9. In this case, the pole contraction factor of the linear-phase FIR-ANF is 0.93. This figure shows that the Wiener solution for the FIR filter has a higher magnitude, and consequently, a lower zero-estimate bias error compared to those of the other solutions. Moreover, when the Wiener solution is closer to unity in the steady state, the filter presents a narrower bandwidth and higher notch

frequency attenuation. However, the IIR notch filter has the lowest computational burden of zero update equations. As mentioned before, for better zero estimation, some bias removing methods need to be employed (Punchalard 2009, 2012).

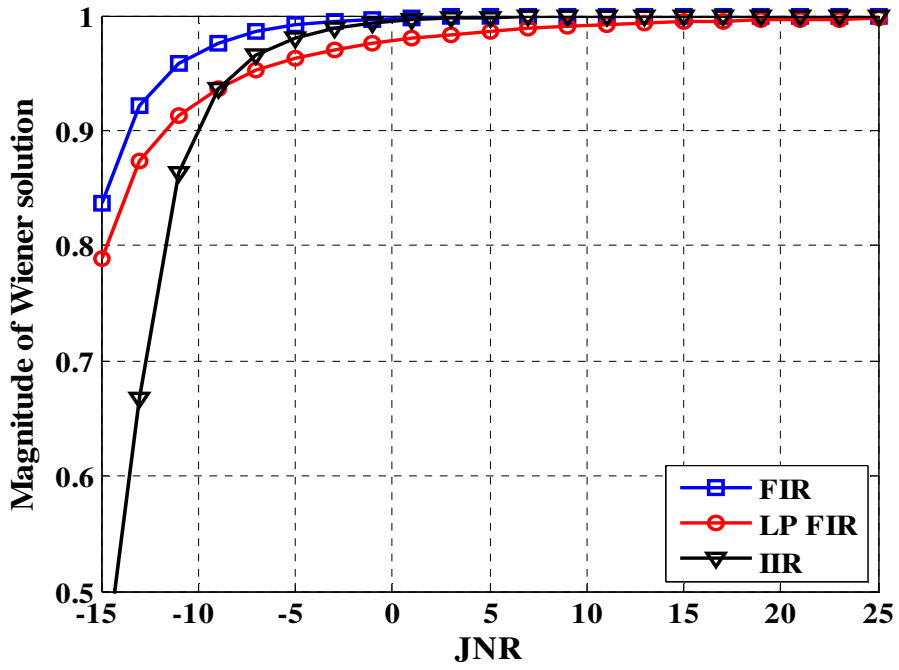

Figure 4.2: Wiener solution for different notch filters for IIR pole contraction factor of $\rho = 0.9$

4.3 Detection Mechanism

In real GNSS applications, the receiver is not only required to estimate the CW frequency but also needs to detect the presence of the interference. Adaptive notch filtering can make it possible for GNSS receivers to detect the presence of the narrowband interference. Specifically, the magnitude of the estimate $\hat{z}_0$ of the adaptive notch filter can be used to determine the presence and the absence of the narrowband interference. To study the detection mechanism of the NF, three CW interference signals with *JNR* of 5,

15 and 15 dB were generated and modulated by an on-off scheme. These interference signals were then input to a linear-phase FIR-ANF. Figure 4.3 shows the magnitude of the estimated zero. It indicates that the magnitude of the estimated zero is close to one in the presence of interference, and otherwise takes a small value. Thus, comparison of the magnitude of the estimated zero to a threshold indicates the presence and absence of interference signals. However, it is important to note that this threshold is a function of notch filter parameters and should be adjusted based on the reception scenario.

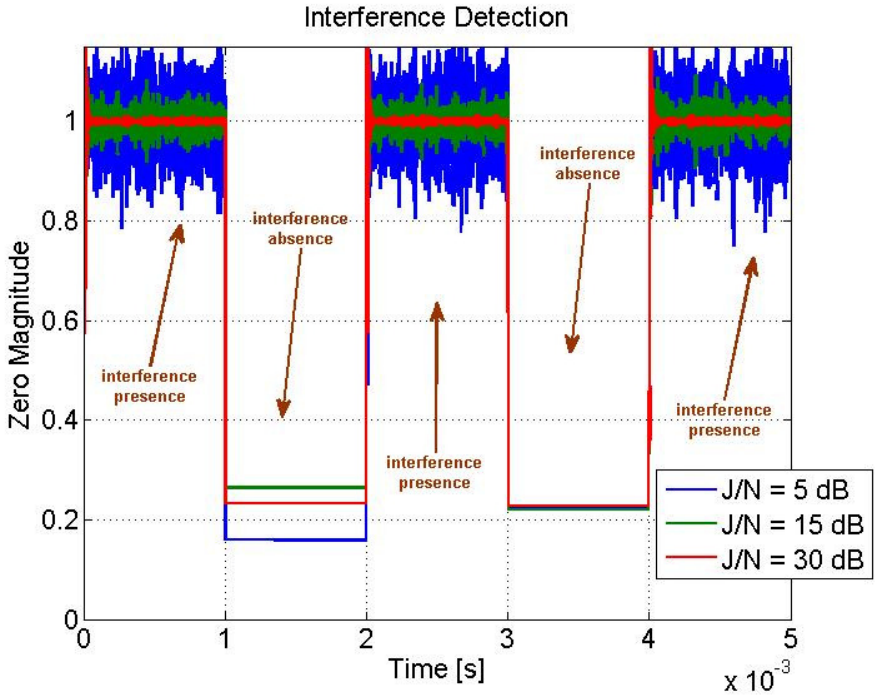

Figure 4.3: Detection scheme based on NF

4.4 Multiple-Interference Removal

Previously studied notch filters can only eliminate a single frequency of the receiver bandwidth. However, in real applications, the presence of multiple narrowband

interference in GNSS band is possible. Considering this, the number of active CW interference, either fixed or swept, is not known by the receiver. To mitigate multiple-interference signals, a cascade scheme of one-pole NFs can be utilized by the receiver (Kwan & Martin 1989, Soderstrand et al 1997, Wang & Milstein 1988, Nishimura & Jiang 1998, Borio 2008). Although quite simple and not optimal in terms of minimizing the output signal power, this scheme provides an effective suboptimal multiple-interference mitigation technique in GNSS applications. Figure 4.4 shows the block diagram of the cascaded NF scheme.

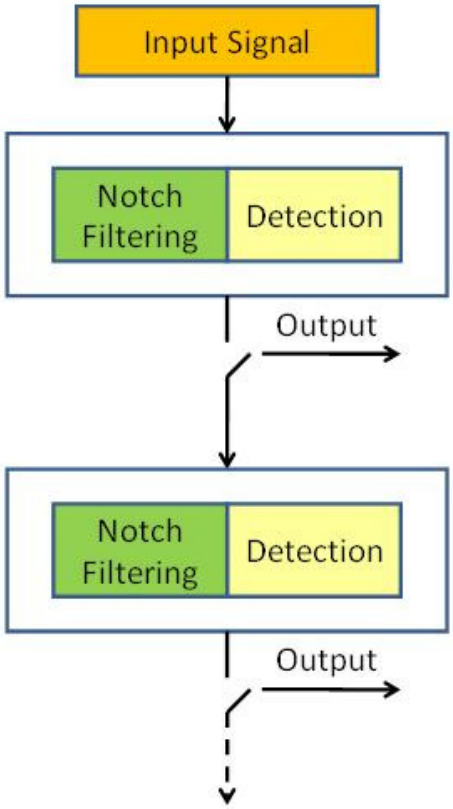

Figure 4.4: Cascaded multi-pole notch filtering scheme

4.5 Performance Evaluation of Proposed Architecture

In order to study the performance of the notch filter based interference mitigation, the proposed multi-pole adaptive linear-phase FIR and IIR notch filters are implemented in the software navigation receiver GSNRx-int, a version of the standard GSNRx (Petovello et al 2008) developed at the University of Calgary. Figure 4.5 depicts the structure of the modified software receiver. As it is shown, since the NF-based interference mitigation scheme is GNSS signal dependent and is the same for all satellite signals, an interference mitigation block in the pre-correlation domain is added to the receiver. A Spirent GSS 7700 simulator (Spirent 2008) was employed to generate a jammed GPL L1 C/A signal. The hardware setup, which collects the generated data by National Instrument RF front-end (National Instruments 2013), is shown in Figure 4.6. The simulated data was amplified through a low noise amplifier (LNA) and was then down-converted and recorded by a 14-bit NI front-end (see Figure 4.6). The receiver configuration is summarized in Table 4-1.

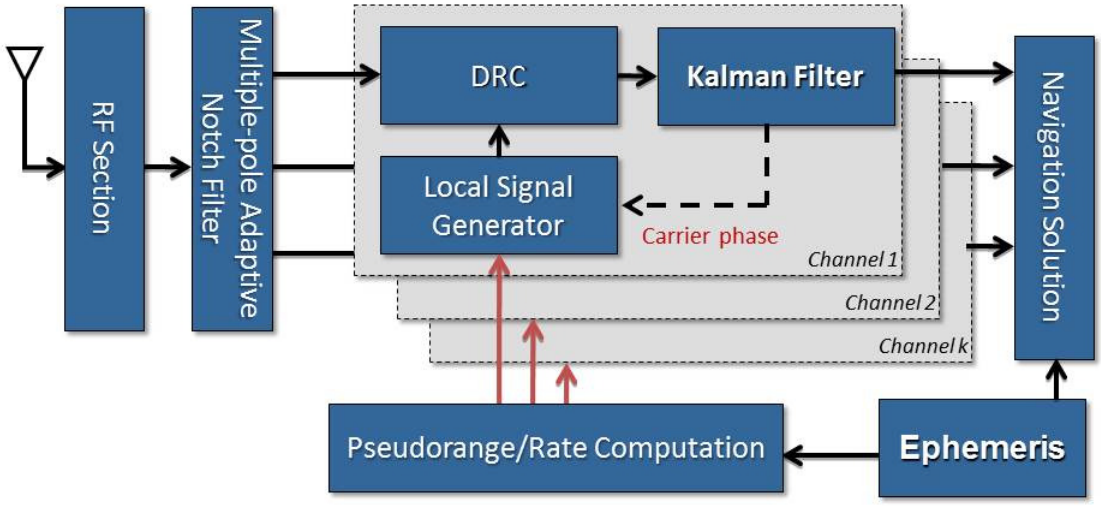

Figure 4.5: GSNRx-int architecture

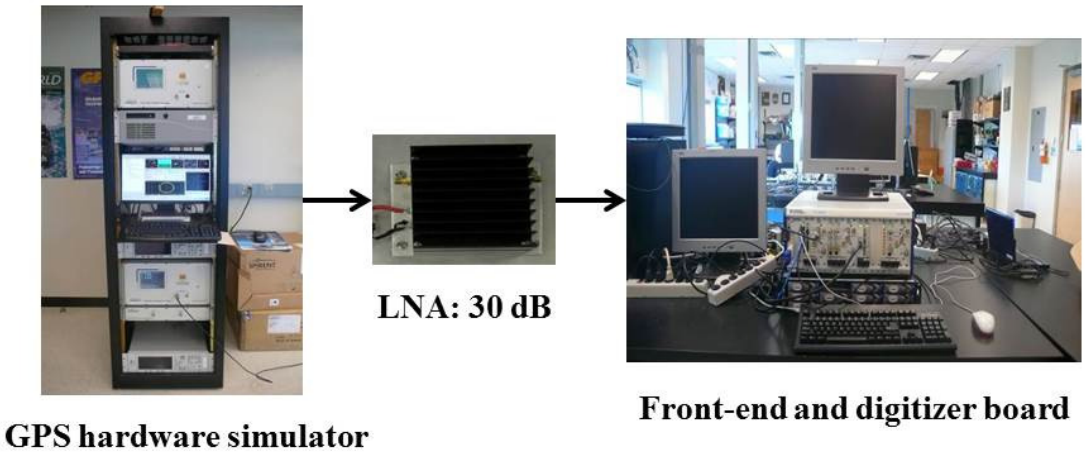

Figure 4.6: Data collection hardware setup

Table 4-1: Receiver configuration

Parameter	Value	Unit	Symbol
GPS C/A PRN number	1	-	
C/N_0	40	dB-Hz	-
Noise floor	-130.0	dBm/Hz	N_0
Sampling frequency	10.0	MHz	F_s
Intermediate frequency	420.0	kHz	f_{IF}
RF front-end bandwidth	5	MHz	-
Coherent integration time	10.0	ms	T_I
DLL bandwidth	2	Hz	-
PLL bandwidth	15	Hz	-
FLL bandwidth	8	Hz	-

Two reception scenarios are considered. The signal specifications of these scenarios are given in Table 4-2. In the first scenario, it is assumed that the received signal is corrupted by a swept-like CW interference. The frequency range and swept time of the swept-like interference are [1574.92 to 1575.92] MHz and 16 s, respectively. To investigate the performance of the multiple-interference mitigation scheme in the second scenario, the received signal consists of a swept-like and a fixed interference source.

Table 4-2: Interference signal specifications

Scenario	Interference type	Frequency (MHz)	Power (dBm)
1	Swept-like	[1574.92 to 1575.92]	-90
2	Fixed + Swept-like	Fixed: 1575.42 Swept: [1574.42 to 1575.42]	-90 -90

Figure 4.7 illustrates the interference frequency estimate based on NF's zero phase (for the first scenario) and also the true interference frequency. The results given in Figure 4.7 reveal that the NF-based frequency estimation scheme is precise enough to successfully track the interference and mitigate its effect.

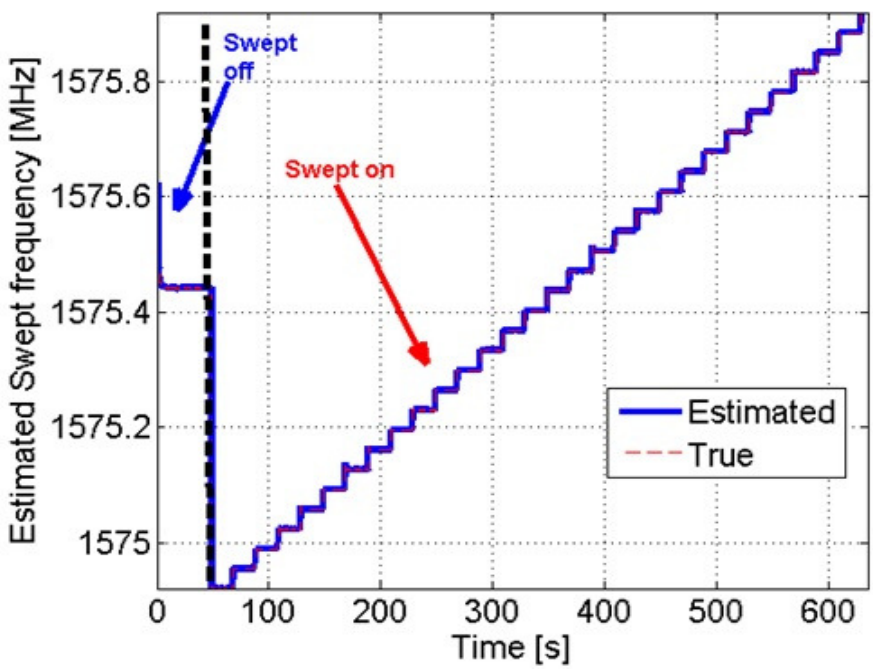

Figure 4.7: Interference frequency estimate for the first scenario

The estimated fixed and swept-like interference frequencies of the second scenario (which are shown in Figure 4.8) indicate that after interference activation, NF starts to track both interference signals. This shows that the cascade interference mitigation scheme tracks jamming signals and mitigates their effect on the desired GNSS signal.

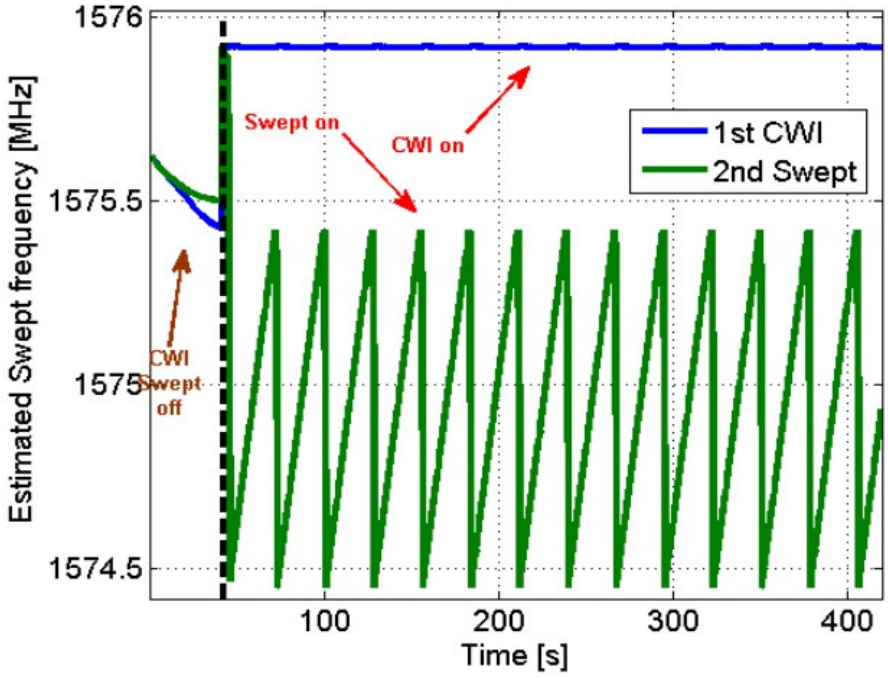

Figure 4.8: Interference frequency estimate for the second scenario

4.6 Notch Filtering Performance in The Presence of Quantization Loss

Figure 4.9 shows the BER results of 2-, 3- and, 4-bit quantization in the presence of -94 dBm interference. This value of interference power is adopted from Figure 3.15 where the optimum value of $A_g\sigma_n$ is 0.166, 0.435, and 0.435 for 2-, 3-, and 4-bit quantization, respectively. The results are shown for two different cases. In the first case, the receiver is not equipped with NF schemes to mitigate the interference. In the second case, the receiver employs an NF to remove the interference effect. Since the BER

performance of the IIR NF is almost the same as that of the FIR NF, the IIR NF is employed to demonstrate BER performance.

As it is indicated, the BER performance of a receiver equipped with NF shows a similar trend to that of a receiver without any interference mitigation scheme. Moreover, the optimum AGC gains of these two cases are almost equal. This is due to the fact that BER performance is generally a function of the effective C/N_0 and optimum AGC gain. It increases effective C/N_0 and would not change irrespective of using NF or not.

In summary, for a receiver employing an NF-based interference mitigation scheme to reach the optimum BER results, the quantization configuration should be carefully adjusted (as discussed in Chapter Three).

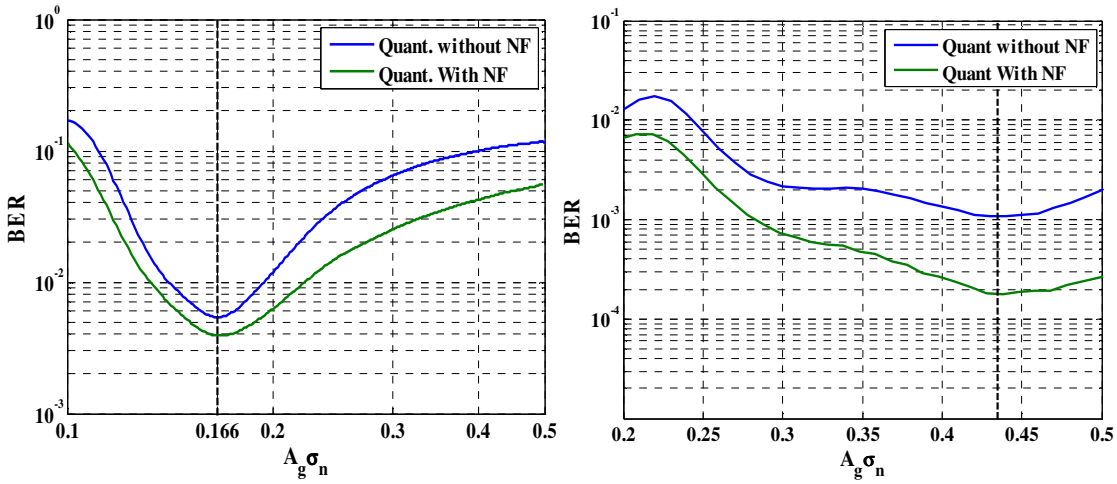

(a) 2-bit quantization (b) 3-bit quantization

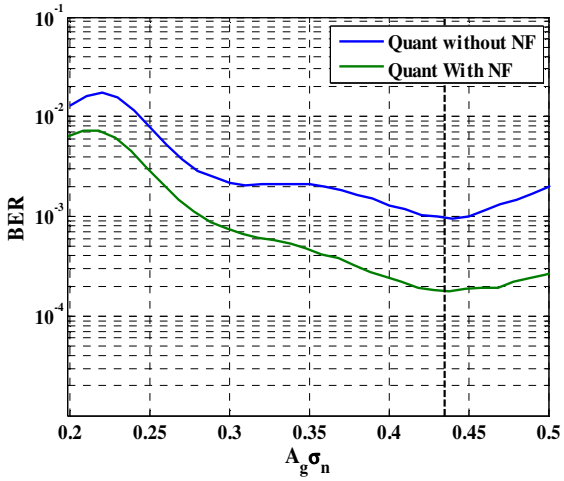

(c) 4-bit quantization

Figure 4.9: BER results in the presence of -94 dBm interference and NF-based interference mitigation

4.7 Summary and Conclusions

Although the FIR notch filtering has a higher computation load, it provides more stability and less numerical error. Moreover, linear-phase FIR filters do not distort the sharpness of the autocorrelation and induce frequency independent biases in measurements that are automatically absorbed in the clock bias.

The study of the effect of quantization on the NF-based interference mitigation performance shows that there exists an optimum AGC gain that results in a maximum BER performance. Moreover, it is shown that the optimum AGC gain in the presence of NF matches that of a receiver without applying NF. Moreover, although employing a notch filter increases the interference resistance of the GNSS receiver, for high interference power (and especially in the presence of low resolution quantization process), this level of immunity is not enough and more considerations, particularly for signal acquisition, should be taken into account.

Chapter Five: GNSS Signal Acquisition in The Presence of Interference

The ROC performance of the acquisition process is degraded due to distortion caused by employing a low sampling rate and low resolution quantizers. Interference increases this degradation, resulting in reduced carrier-to-noise-floor-ratio values. Acquisition is the initial stage in the GNSS receiver and has the lowest sensitivity of the entire receiver operation (e.g. Deshpande 2004). The acquisition scheme is a two dimensional search, determining Doppler frequency and code phase. The acquisition process can be examined either for a given Doppler frequency and code phase (cell-level) or entire possible values of Doppler frequency and code phase (system-level). Cell-level statistics, however, do not describe the entire problem and, unfortunately, the system-level acquisition performance has not yet received sufficient attention. The main goal of this chapter is to identify and quantify the search space properties in the presence of narrowband interference to develop new strategies based on these properties to achieve enhanced system-level acquisition performance. Moreover, the effect of the quantization process on the GNSS signal acquisition will be considered, paying attention to the cell-level as well as to the system-level detection performance. The results of the probability of detection and false-alarm, determining the ROC, for the most commonly used 1-, 2- and 3-bit quantizers will be computed to identify and quantify the benefits of increasing quantizer resolution.

5.1 Cell-Level Acquisition Performance

For coherent bit demodulation where the phase and the frequency of the incoming signal is estimated and removed by using a phase lock loop (PLL) (Kaplan & Hegarty 2006), I_n samples are coherently accumulated for one bit interval and the data bit is determined based on the phase of the complex result value. Thus, the bit demodulation decision metric can be presented by (Kaplan & Hegarty 2006, Proakis & Salehi 2007)

$$T_1 : I_n \underset{D_0}{\overset{D_1}{\gtrless}} 0 \tag{5.1}$$

where D_0 is the null hypothesis that the data bit "zero" is transmitted and D_1 represents the data bit "one" transmission hypothesis.

The decision variables T_0 given by Eq. (2.23) and T_1 are all functions of effective *C/N₀* values. Intuitively, a higher received signal quality provides higher T_0 and T_1 values in order to better detect either the signal present or the transmitted bit. To better understand the effect of AGC gain on the BER and detection probability, these parameters are shown in Figure 5.1 for a 2-bit quantizer, different values of the AGC gain and interference power, P_{cw}, of -89 dBm, and $P_{\mathrm{fa}} = 10^{-2}$. In this plot, the effective *C/N₀* is also shown. Here, f_{Δ} is assumed to be 1 kHz to reduce the effect of interference on the calculated *C/N₀*. In this figure, BER and detection probability results are observed to have similar trend as that of the calculated *C/N₀*. Specifically, BER and detection probability take their maximum at the same $A_g\sigma_n$ point which results in the highest calculated *C/N₀*. Thus, it is expected that adjusting the AGC gain to its optimal value in terms of BER also results in the best cell-level acquisition performance. The effect of AGC gain on both of these

detection problems is studied in Section 5.2. It will be also shown that the value of the AGC gain that minimizes BER and maximizes detection probability follows a similar trend for different interference frequencies.

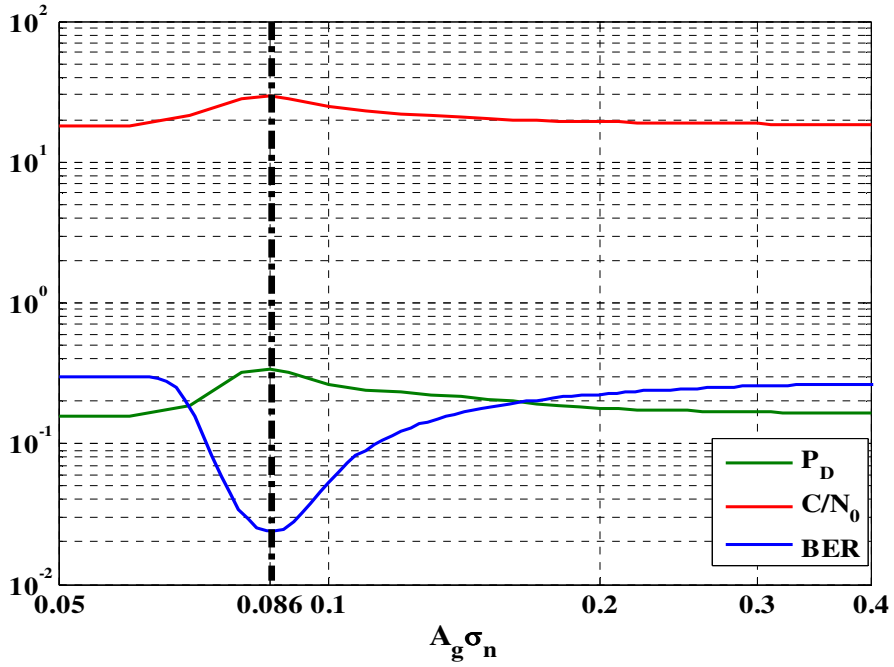

Figure 5.1: BER performance and cell-level probability of detection for 2-bit quantizer and different values of $A_g\sigma_n$, P_{cw} = -89 dBm, f_Δ = 1 kHz ($P_{\text{fa}} = 10^{-2}$)

5.2 Effect of Interference Frequency on Optimum AGC Gain

Here, the effect of interference frequency on the value of the optimum AGC gain is studied. Figure 5.2 depicts the BER and detection probability of a 2-bit quantizer for different values of interference frequency, with false-alarm probability, $P_{\text{fa}} = 10^{-3}$ and P_{cw} = -89 dBm. As it can be seen, since the decorrelation process attenuation on narrowband interference depends on the interference frequency (Poisel 2011), the levels of BER and detection probability vary. Nevertheless for different interference

frequencies, the values of the optimum AGC gain stays approximately constant. This is because the ratio of the histogram bins of quantizer output depends mostly on the interference power rather than its frequencies. That is, the optimum AGC gain is independent of interference frequency. For the sake of simplicity, in the followings, the interference signal is assumed to have a frequency relatively close to that of the GPS signal carrier frequency, i.e. $f_{\Delta} \approx 0$ Hz.

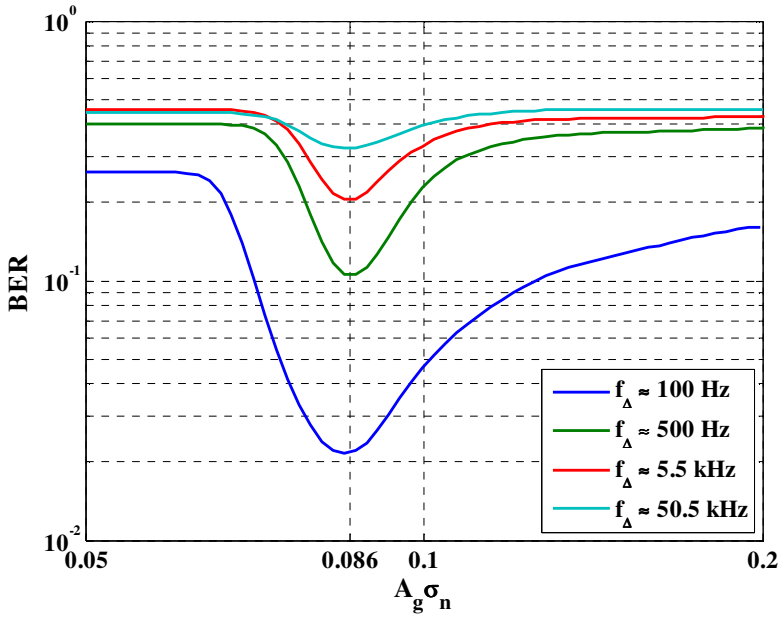

(a) BER performance

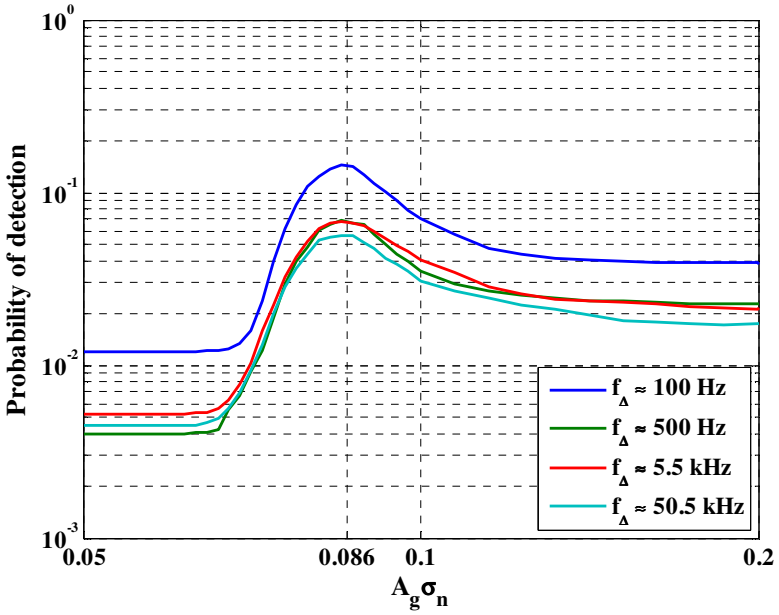

(b) Probability of detection

Figure 5.2: Interference frequency effect on BER and cell-level detection probability for a 2-bit quantizer for different values of $A_g\sigma_n$ and interference frequency P_{cw} = -89 dBm

5.3 Effect of optimum AGC gain on detection probability

Figure 5.3 demonstrates the BER performance and cell-level probability of detection, P_{D}, for 2- and 3-bit quantizers, different values of the AGC gain, and given probabilities of false-alarm, i.e. $P_{\mathrm{FA}} = 10^{-2}$ and 10^{-1}. The interference has power of P_{cw} = -89 dBm. In this case, the detection threshold, β, is carefully adjusted in order to have the desired P_{fa}. As it can be seen, the BER results are consistent with detection probability results. That is, the BER and detection probability reach their peaks for almost the same value of $A_g\sigma_n$, in this case 0.086. Thus, a receiver with an adjusted AGC gain to its optimal value in the sense of BER performance also provides the best cell-level acquisition performance.

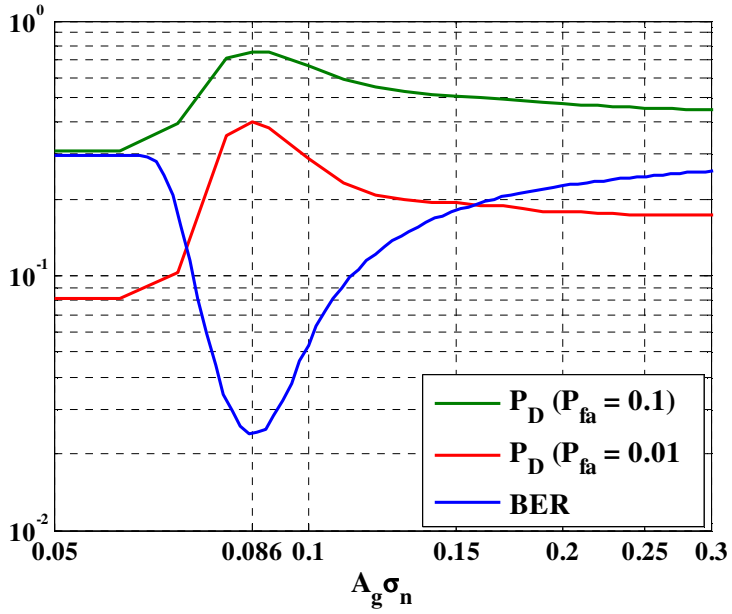

(a) 2-Bit quantizer

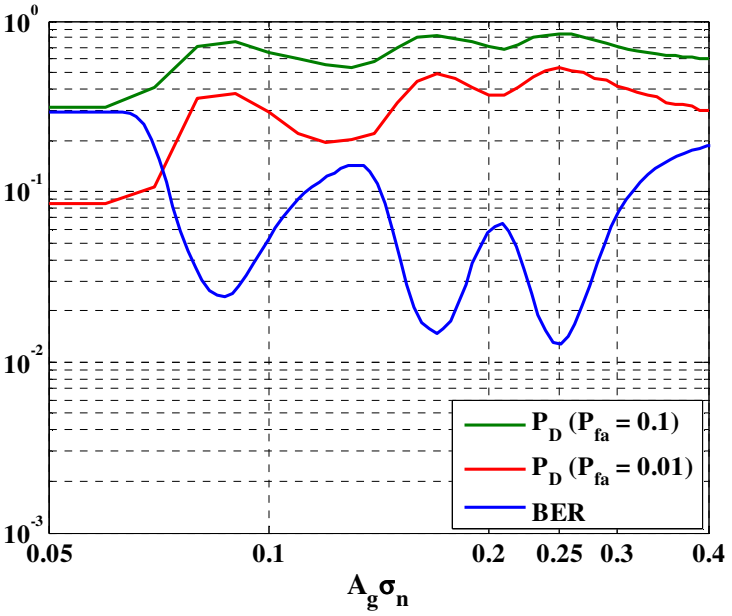

(b) 3-Bit quantizer

Figure 5.3: BER performance and cell-level detection probability for limited resolution quantizers for different values of $A_g\sigma_n$ and interference frequency P_{cw} = -89 dBm

5.4 AGC effect on Cell-level ROC performance

Figure 5.4 shows the cell-level ROC performance of 1-bit quantization for different values of interference power. As can be seen, the ROC performance decreases as the interference power increases. Figure 5.5 illustrates the ROC performance at the cell-level for 2-, 3-, and 4-bit quantization for different values of the AGC gain and P_{cw} = -89 dBm. Each simulation configuration was repeated 10^6 times. As it can be seen, the ROC performance improves as $A_g\sigma_n$ reaches its optimal value of 0.086, 0.25, and 0.25 for 2-, 3- and 4-bit quantizer, respectively. For example, for 2-bit quantization and a false-alarm probability of 0.01, by modifying $A_g\sigma_n$ from 0.1 to 0.086, the detection probability increases from 0.28 to 0.40. This is the case where the receiver already knows the presence and the power of the interfering signal in order to set the optimal AGC gain value.

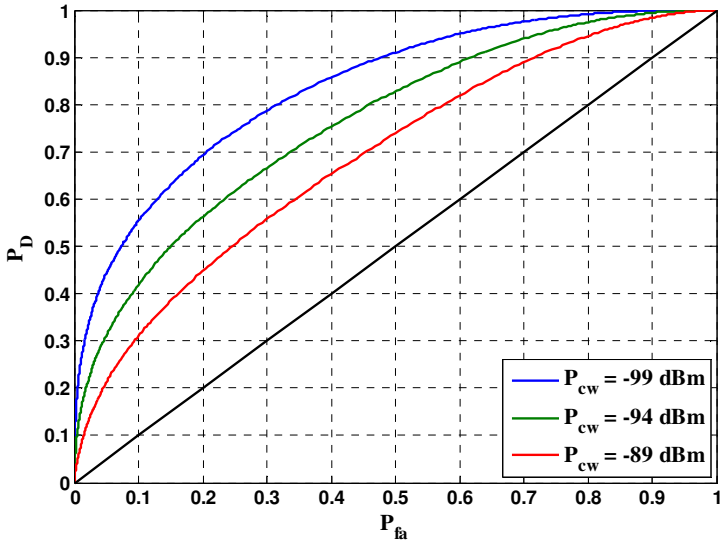

Figure 5.4: ROC performances in cell-level for 1-bit quantization for different values of interference power

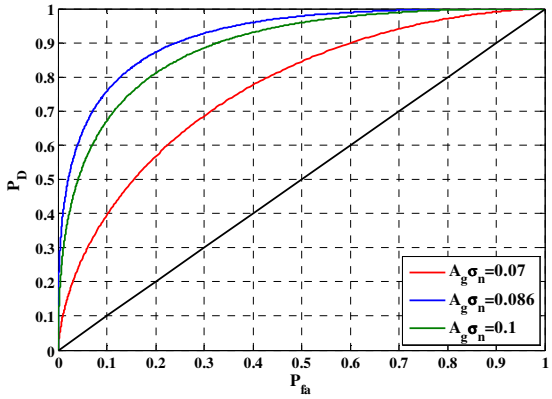

(a) 2-bit quantizer

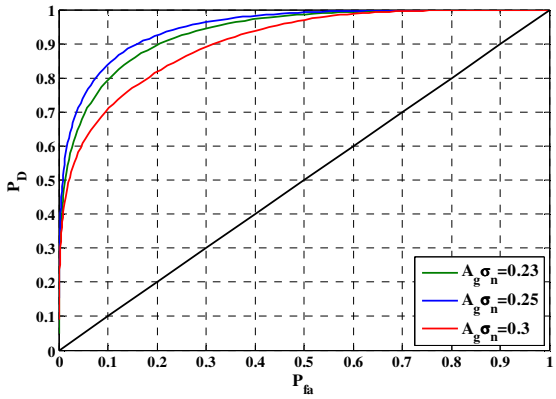

(b) 3-bit quantizer

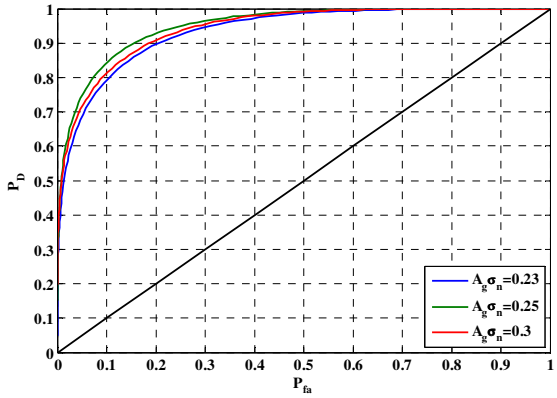

(c) 4-bit quantizer

Figure 5.5: ROC performances in cell-level for different values of $A_g\sigma_n$

Considering that signal sampling and quantization should be done prior to any digital interference mitigation schemes, the above results demonstrate a significant performance improvement for a GNSS receiver in terms of effective C/N_0, BER and detection probability. These results show the limitation for the considered quantizer configuration and present the best performance that can be achieved by each quantizer. Moreover as it shown, adjusting the AGC gain to its optimal value not only increases the receiver performance in terms of BER, but also results in better cell-level detection statistics of

the desired signal. However, applying the optimal AGC gain by the receiver requires knowledge of noise variance and interference power. That is, the receiver should be equipped with an interference detection and characteristics estimation block in order to provide an estimate of these values. These estimates can then be employed to calculate the optimal value of AGC gain for a given quantizer structure (see Chapter Three).

5.5 Real Data Collection and Monte-Carlo Simulation

In the following, the system-level acquisition of the GPS L1 C/A signal is studied. In order to generate a simulated interfered GNSS signal, a Spirent GSS 7700 simulator controlled by the SimGEN software was employed (Spirent 2008). The simulator was used to generate variety of interference powers and frequencies. A static antenna mode is considered here and the simulated noise floor is set to -130 dBm. The resulting signal is first amplified by an LNA and then down converted and digitalized through a National Instrument RF front-end (National Instruments 2013) resulting in 16-bit complex raw IF samples with F_s = 5 MHz.

To present the ROC level results at the system-level, MATLAB simulations were performed, simplify assuming that the received signal has a C/N_0 of 45 dB-Hz in all of the subsequent experiments. Monte-Carlo simulations, the configuration of which is summarized in Table 5-1, were employed to evaluate the performance of various acquisition schemes. The frequency plan and noise figure are chosen to represent a typical consumer-grade receiver.

A coherent integration period commensurate with the harsh environment under consideration is chosen, specifically $T_I = 7.0$ ms is used as it represents a suitable trade-off between correlation gain and data-modulation related losses (Diggelen 2009). To minimize losses due to residual Doppler and code delay error, the acquisition search space was configured to have a code bin width, $\Delta\tau$, of 0.5 chips and a Doppler bind width, ΔF, of 125.0 Hz.

Table 5-1: Simulation setup

Parameter	Value	Unit	Symbol
GPS C/A PRN number	1	-	
Noise floor	-174.0	dBm/Hz	N_0
Sampling frequency	2.0	MHz	F_s
Intermediate frequency	420.0	kHz	f_{IF}
Coherent integration time	7.0	Ms	T_I
Non-coherent combinations	5	-	K
Doppler bin width	125.0	Hz	ΔF
Code bin width	0.5	Chip	$\Delta\tau$

5.6 System-Level Acquisition

In the presence of interference, the statistics of the CAF across the search space vary depending upon the interference characteristics. Figure 5.6 shows a CAF for a received signal corrupted by CW interference, with $JNR = 50$ dB and $f_\Delta \approx 100$ Hz. For the interference-free case, the CAF values exhibit a maximum value located at the correct

code delay and carrier Doppler and, therefore, conventional methods based on comparing the CAF level to a threshold can be employed. However, as it can be seen for CAF values in the presence of any appreciable interference, the correct code delay and carrier Doppler no longer correspond to the CAF global maximum. As a result, a traditional threshold comparison is no longer effective. In this section, the properties of the CAF in the presence of interference are examined.

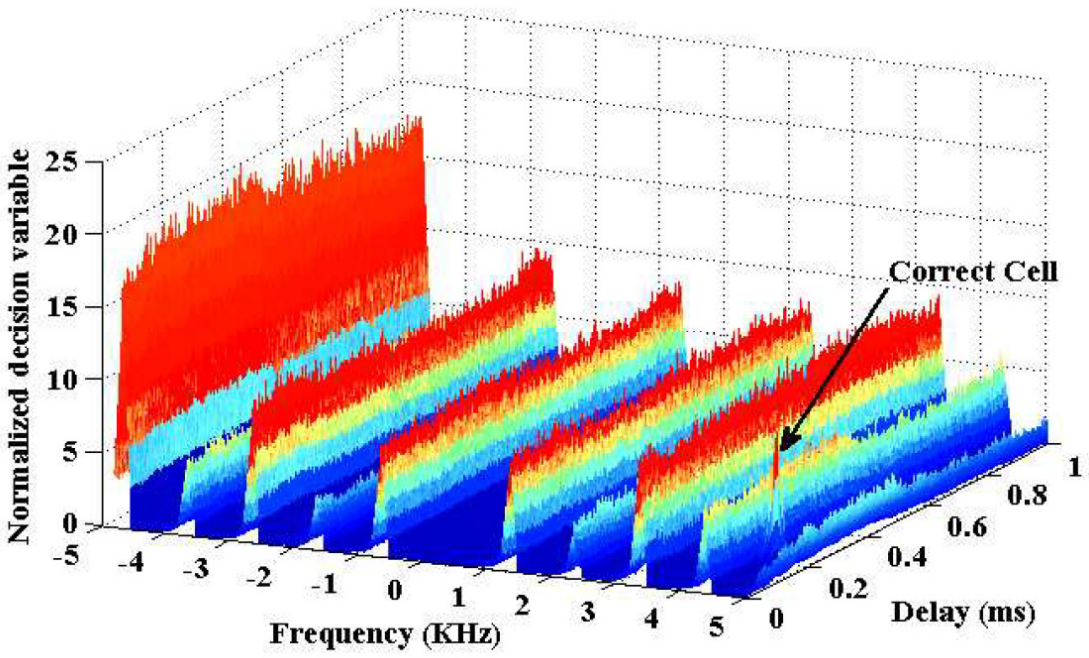

Figure 5.6: Generic *decision variable* values, i.e. $D(\tau, f_D)$, in the presence of interference

Acquiring the correct cell inside search space is generally a pattern recognition problem. In the interference-free case, however, this problem can be reduced to that of a simple detection or detection-and-verification scheme (O'Driscoll 2007). Generally, a *decision variable* is computed as some function of one or more conservative samples of the CAF.

For example, a widely used *decision variable*, denoted here by D, considers the non-coherent combinations of the K conservative samples:

$$D(\tau, f_D) = \sum_{k=0}^{K-1} |S_k(\tau, f_D)|^2 \tag{5.2}$$

where the subscript k denotes the interval, $kT_I \leq t < (k+1)T_I$, over which the CAF, given by Eq. (2.18), is calculated. To identify the presence of the desired signal, this variable is compared to some threshold, V_T, which is generally tuned to provide a desired false-alarm probability (Kaplan & Hegarty 2006, Parkinson & Spilker 1996). In the presence of interference, as can be seen in Figure 5.6, however, it is clear that this simple detection scheme will perform poorly. Nonetheless, the signal is clearly distinguishable and, while it does not represent the global maximum, it does represent a local maximum in the decision space.

Provided $\Delta\tau$ and ΔF are not too small relative to T_I, the desired signal represents not only a local maximum, but also a sharp peak in the search space. It is useful, therefore, to examine the second partial derivative of D in both the τ and f_D dimensions. The signal may then be identified amongst the noise and interference by choosing a *decision variable* that represents a large change in curvature of D across the search space. One suitable candidate is the Laplacian of D, denoted here by D^{Lap}, which, for a discrete function such as the acquisition search space, can be approximated by the four-neighbor Laplacian, given by (Gonzalez & Woods 2006):

$$D^{\mathrm{Lap}}(\tau, f_D) = |\nabla^2 D(\tau, f_D)|$$
$$= |4D(\tau, f_D) - D(\tau - \Delta\tau, f_D) + D(\tau + \Delta\tau, f_D) \quad (5.3)$$
$$- D(\tau, f_D - \Delta F) + D(\tau, f_D + \Delta F)|.$$

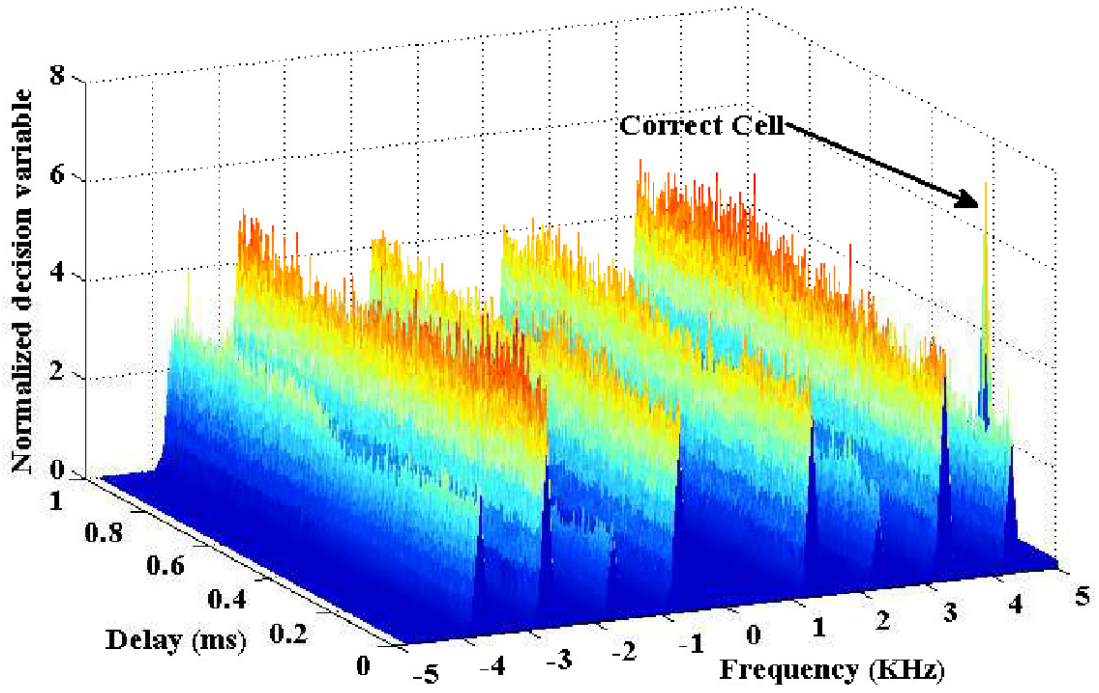

Figure 5.7: Laplacian, i.e. $D^{\mathrm{Lap}}(\tau, f_D)$, of the acquisition search space

Note that the factors $\frac{1}{\Delta\tau}$ and $\frac{1}{\Delta F}$ are intentionally omitted from the partial derivatives in an effort to render the metric insensitive to code and Doppler bin width. Figure 5.7 depicts the D^{Lap} for the search space depicted in Figure 5.6. The peak in this new *decision variable*, corresponding to the GNSS signal, has two contributing factors: 1- The curvature in the τ dimension and the curvature in the f_D dimension, both of which are proportional to the received GNSS signal power, 2- Peaks in the *decision variable* results

which correspond to the interference only, are dominated by the curvature in the f_D dimension and are proportional to the received interference power. As can be seen both by examination of Figure 5.7 or by evaluation of Eq. (2.21) {see Borio (2010)}, the curvature of D in the τ dimension is quite small, even for high interference power levels. As the interference power may be significantly higher than the GNSS signal power, D^{Lap} may still be dominated by the interfering signal.

These observations suggest another possible *decision variable*, which considers only the curvature in the τ dimension. Denoted D^{τ}, it is given by

$$D^{\tau}(\tau, f_D) = |2D(\tau, f_D) - D(\tau - \Delta\tau, f_D) + D(\tau + \Delta\tau, f_D)|. \tag{5.4}$$

An example of D^{τ} corresponding, once again, to Figure 5.6, is presented in Figure 5.8. In this case the GNSS signal is clearly identifiable within the search space, confirming that in the presence of strong interference, the signal is best characterized by a large curvature along the τ dimension. Indeed, use of this new *decision variable* has implications for the calculation of a suitable detection threshold and will have a corresponding effect on the achievable detection and false-alarm probabilities. These and other issues will be discussed further in Section 5.7 and Section 5.8 wherein insights gained here will be employed to develop a more robust acquisition *decision variable*.

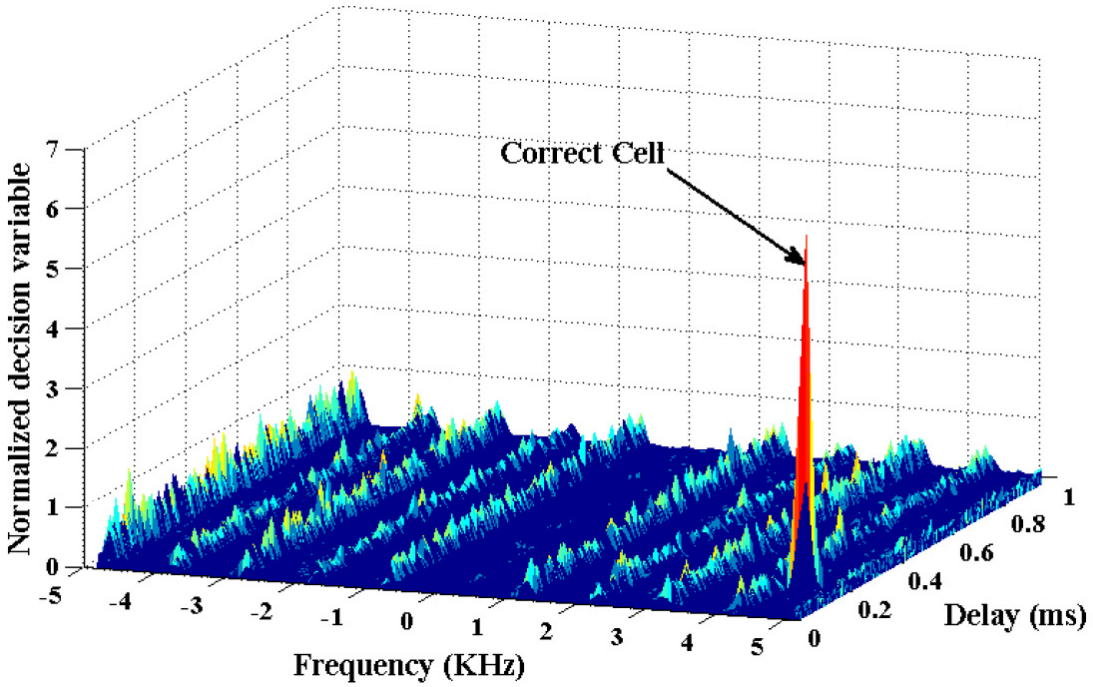

Figure 5.8: Curvature along the $\boldsymbol{\tau}$ dimension of D, denoted D^{τ}

Another useful property of the interference-corrupted CAF is that the *decision variable* is somewhat symmetrical. This is shown in Figure 5.9 wherein the search space has been extended significantly for illustrative purposes. In this case, the interference frequency is 5 kHz below the intermediate frequency and, the square magnitude of the value of the interference component, $S_{\text{int}}(\tau, f_D)$, is bilateral-symmetric around the plane[1] $f_D = f_\Delta = f_{\text{int}} - f_{\text{IF}}$, which in this case is -5 kHz. In contrast, neither the GNSS signal nor the additive noise exhibits any such symmetry. If the frequency of the interfering signal is known, therefore, these facts might be exploited for the signal detection. Specifically, the receiver can mitigate the effects of the interfering signal by examining

[1] For interested readers, this property can be derived by expansion and evaluation of Eq. (2.21), see Borio (2010), for details.

the difference between a given point in the search space and the point given by a projection through the plane of symmetry. This property and the development of a related *decision variable* will be discussed further in Section 5.7.

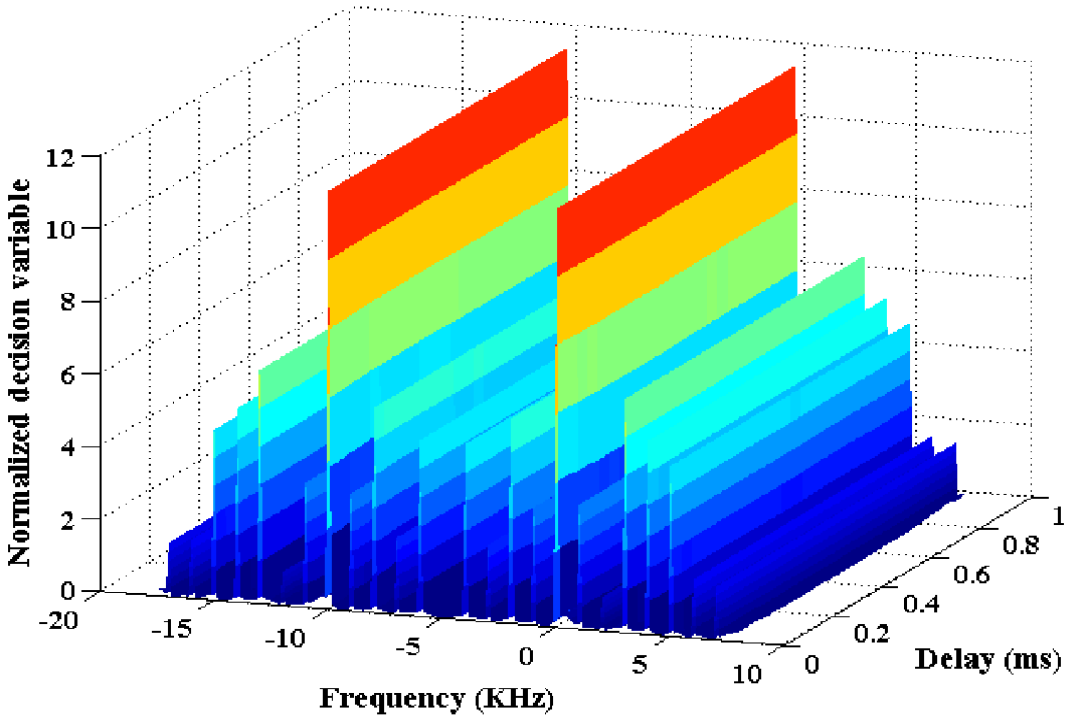

Figure 5.9: S_{int} evaluated over an extended search space, illustrating the line symmetry across $f_{\Delta} = f_{\text{int}} - f_{\text{IF}}$ (around f_{D} = -5 kHz in this case)

Finally, it is worth mentioning that S_{int} is highly predictable. Given the non-coherent nature of D and, therefore, any derived *decision variable*, only the interference frequency and amplitude need to be known by the receiver to estimate the value of S_{int} across the search space. Exploitation of this property for the purposes of acquisition is discussed further in Section 5.7.3. As an example, however, Figure 5.10 illustrates the search space for a GNSS signal corrupted by a CW interference with a *JNR* of 75 dB. In this case, the

amplitude and frequency of the interference are perfectly known to the receiver and, using Eq. (2.21) and Eq. (5.2), the interference has been removed. Interestingly, the GNSS signal represents the global maximum over the search space. Further details of this procedure will be discussed further in Section 5.7.3.

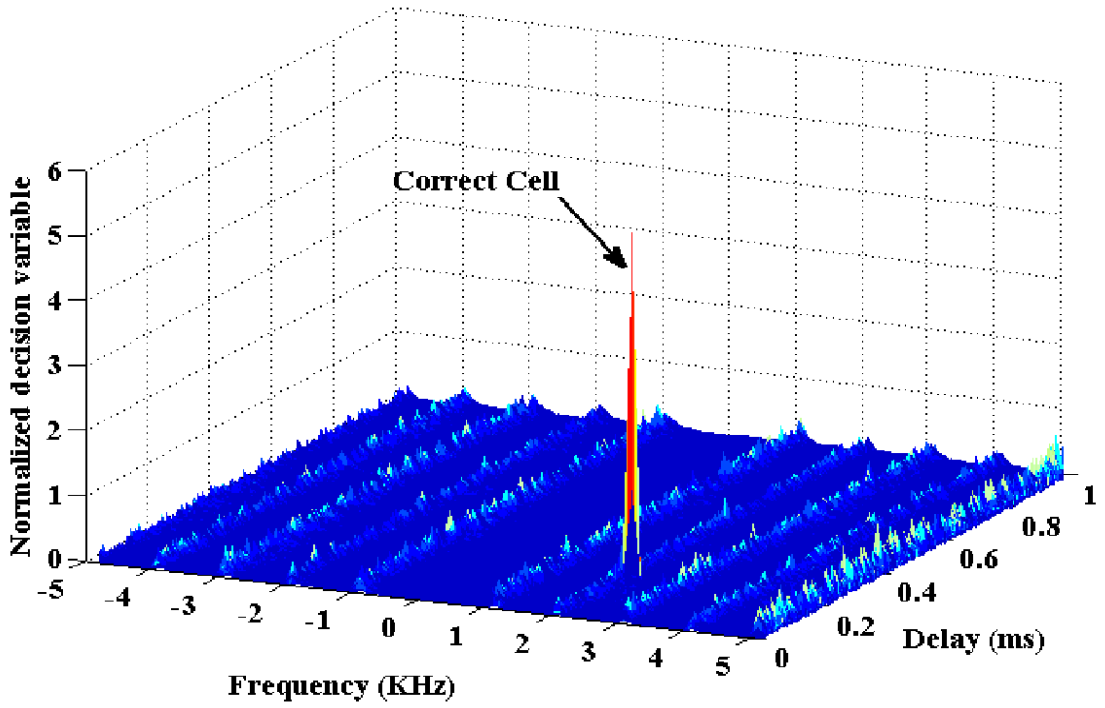

Figure 5.10: Subtracted decision variable values, D^{IntR}, for the generated interference and received signal

5.7 Cell-Level Performance of Proposed Methods

This section examines the cell-level acquisition performance of the receiver experiencing strong CW interference. The insights gained from Section 2.7 and Section 5.4 are leveraged to develop new *decision variables* which provide a degree of interference resilience. Environments wherein the receiver has either no prior knowledge of the interference, knowledge of the interference frequency, or both knowledge of the

interference frequency and its amplitude, are considered, in Section 5.7.1, 5.7.2 and Section 5.7.3, respectively.

In the absence of interference, the traditional *decision variable*, *D*, is compared to a threshold, V_T. The value of V_T depends, amongst other things, on the desired false-alarm probability, and can be readily calculated given an estimate of the receiver's noise-floor (Ziemer et al 1995, Kaplan & Hegarty 2006, Parkinson & Spilker 1996, O'Driscoll 2007). The most practical technique to estimate the noise variance is to correlate the received signal with a local replica of an unused PRN code. This method is reliable as the noise floor is effectively uniform over the entire acquisition search space and does not vary noticeably from one PRN to another. As has been shown in Section 2.7, however, the same is not true in the presence of CW interference.

Although the relationship between probability of false-alarm and detection threshold in the presence of interference can be described (Borio 2010), the expression is rarely useful for receiver tuning. This reason is that both the interference power and frequency must first be known by the receiver. Therefore in the more likely event that the receiver does not know these interference properties, V_T cannot be set for the traditional *decision variable* based on the desired probability of false-alarm.

A number of problems become apparent at this point, including the choice of an appropriate value for V_T becomes difficult and, moreover, it is likely that the resultant acquisition performance is unsatisfactory. Figure 5.11 illustrates this problem, wherein a *JNR* of 75 dB is assumed and the ROC is assessed for a no-quantizing and 1-, 2- and 3-bit receiver. It is clear that, for any reasonably low P_{fa} value, regardless of the quantizer

configuration, the best attainable detection probability is still effectively unusable. It seems that tuning the traditional acquisition scheme will not suffice. To address this problem, this section presents a selection of novel *decision variable*, based upon the observations made in Section 2.7.

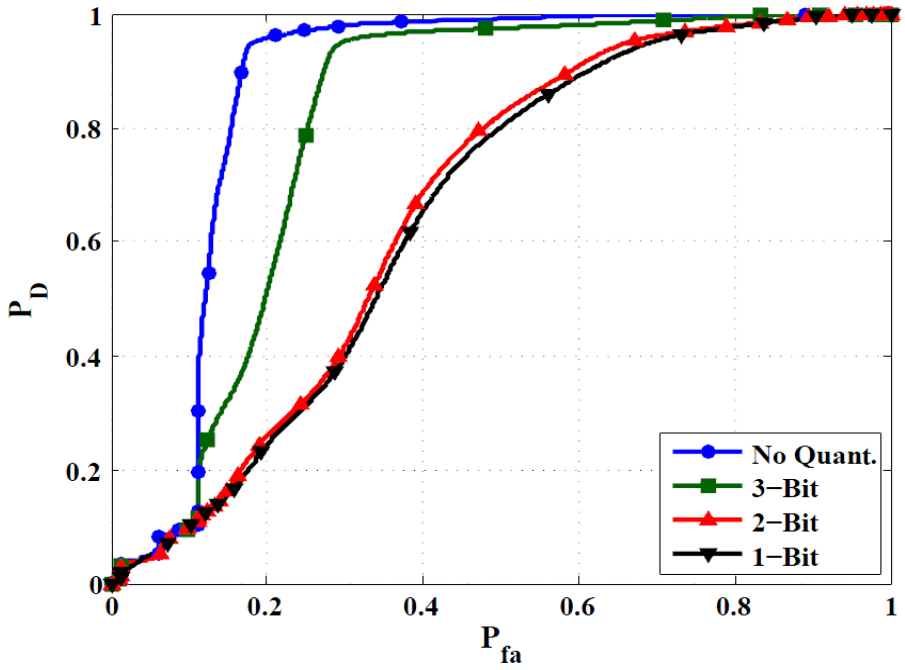

Figure 5.11: Cell-level ROC performance of *D* for a selection of quantizer configurations with JNR = 75 dB

Similar to traditional schemes, the detection quality of the proposed decision variables is dependent primarily on the C/N_0, interference power and quantizer configuration. To have an insight into the effect of GNSS signal power, the results of the cell-level ROC performance for 2-bit quantization for a signal containing interference with C_s/N_0 values of 40, 45 and 50 dB-Hz are shown in Figure 5.12. As can be seen, the signal detection probability reduces as the C/N_0 decreases. An increase in C/N_0 value always improves the

acquisition performance to some extent; however, in the case where CW interference is present, the acquisition performance is dependent primarily on interference rather than thermal noise. In the following, to simplify further analysis, the received signal is assumed to have a C/N_0 of 45 dB-Hz in all of the subsequent results.

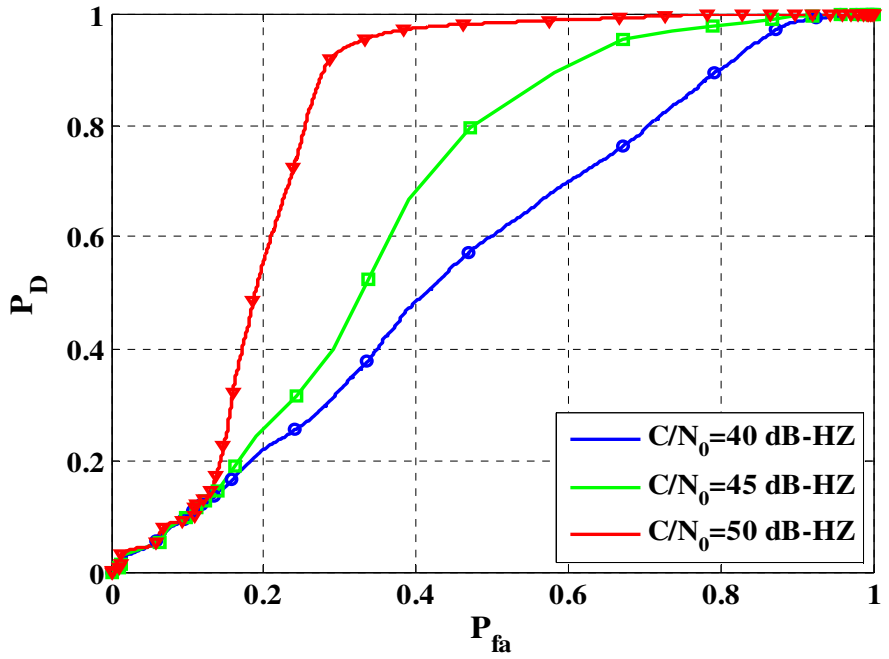

Figure 5.12: Cell-level ROC performance of D for a selection of GNSS signal power values and 2-bit quantizer configurations with a JNR = 75 dB

5.7.1 Window-Based Acquisition Scheme

When a receiver lacks *a priori* information regarding the presence or properties of the interfering signals, modifying the traditional search space can prove useful with the modified space, D^{τ}, showing particular promise. The ROC performance of this *decision variable* and some of its variations are considered here. It is noted that, although the differencing with adjacent cells provides insensitivity to interference, it also increases the

noise component of the *decision variable*. To alleviate this effect, the D^{τ} function can be generalized to consider not only the immediately adjacent cells, but a *window* surrounding the cell under test. This window-based *decision variable* can be expressed as

$$D^{\mathrm{Wind}}(\tau, f_D) = |D(\tau, f_D) - \langle D(\tau, f_D)\rangle_W|. \tag{5.5}$$

where the operator $\langle\cdot\rangle_W$ represents the average of the *decision variable* values in τ dimensions calculated across a window of *W* cells centered on the cell under test. As can be seen in Eq. (5.5), the average of *decision variable* values over the code delay space is subtracted from the conventional *decision variable*, *D*, in Eq. (5.2). The second term in Eq. (5.5) can be estimated by considering a small window centered at the cell under test, and, when this window extends one cell in either direction, it is equivalent to D^{τ}. The ROC performance of this *decision variable* is presented in Figure 5.13 for both the no-quantizing and the 2-bit quantizing receiver assuming a *JNR* of 75 dB. Although not immediately obvious in the no-quantizing case, the curves representing the 2-bit quantizing receiver illustrate that increasing the window length increases detection performance. This is particularly useful for receivers employing a fast Fourier transform (FFT)-based acquisition scheme and, therefore, the full range of code-bins available simultaneously. Also, for receivers performing conventional correlation, it is useful to note that as few as nine bins yield a significant performance improvement.

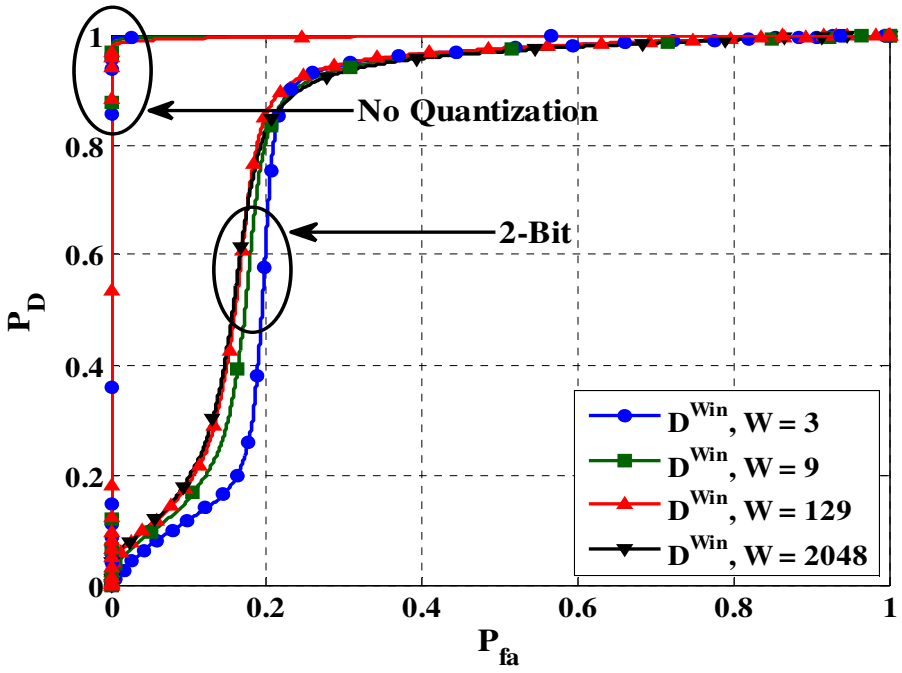

Figure 5.13: Effect of window length on ROC performance for a receiver equipped with no-quantizing and 2-bit receiver

Figure 5.14 illustrates the ROC performance of 1-, 2-, 3-bit and no-quantizing receiver for the D^{Wind} *decision variable* using all available code bins for a *JNR* of 75 dB. The results show that D^{Wind} can provide a significant improvement over the traditional *decision variable*, a result that will become even more evident in the system-level analysis in Section 5.8. A noticeable dependence on the quantizer resolution is still apparent however and stems from the unavoidable signal-strength losses incurred by jamming effects in the quantizer (Abdizadeh et al 2012).

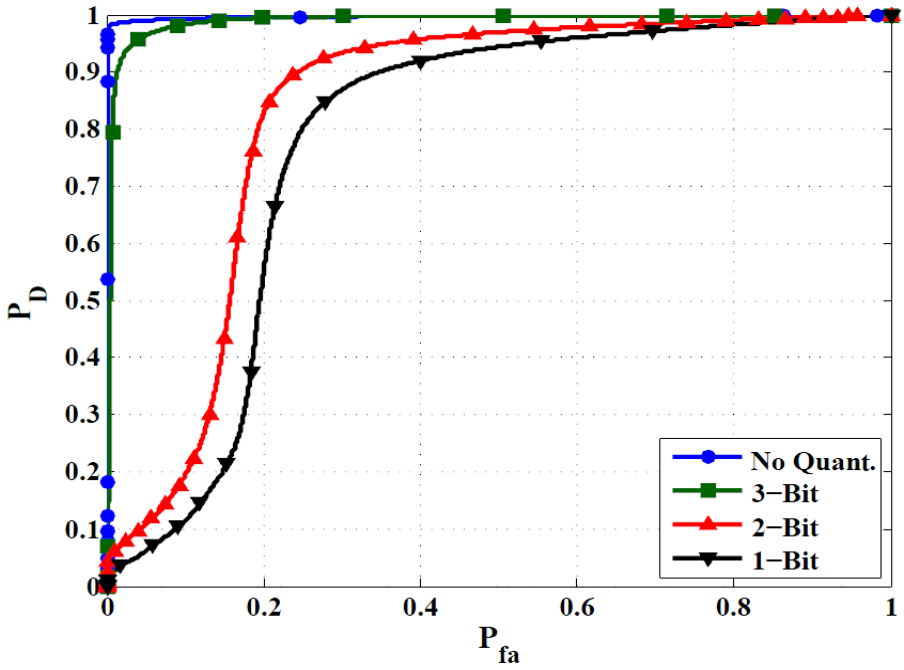

Figure 5.14: Cell-level ROC performance of D^{Wind} for a selection of quantizer configurations with a *JNR* = 75 dB

5.7.2 Frequency-Pair Acquisition scheme

If a receiver has some *a priori* information regarding the prevailing interference frequency, a modified *decision variable* can be employed. As illustrated in Section 2.7, the interference component of D exhibits bilateral-symmetry around the plane $f_D = f_{\text{int}} - f_{\text{IF}}$. Thus, a *decision variable* based on this property can be defined as

$$D^{\text{Pair}}(\tau, f_D) = \left|D\left(\tau, f_{D,}\right) - D\left(\tau, f_{D,\text{Pair}}\right)\right|$$
$$f_{D,\text{Pair}} = 2f_{\text{int}} - 2f_{\text{IF}} - f_D \tag{5.6}$$

The interference component of D for a given cell under test will be approximately equal to that of the cell centered at the *pair* frequency. Differencing these two cells will leave only the signal if it is present, the thermal noise and perhaps some residual interference power. If the interference frequency is sufficiently well known, this decision variable can

significantly improve detection performance, albeit at the cost of increasing both the computational load and *decision variable* noise. This scheme is completely insensitive to the true interference amplitude, frequency and to errors in the receiver estimate of the interference amplitude. It is however sensitive to errors in the receiver's estimate of the interference frequency as they will result in the incorrect pairing of cells.

Figure 5.15 shows the cell-level ROC performance of the frequency-pair method for 1-, 2-, 3-bit and no-quantizing receiver for a *JNR* of 75 dB. It is clear that the performance of this *decision variable* significantly degrades with reducing quantization resolution. This is due to the introduction of harmonics in the interfering signal by the quantizer, as depicted earlier in Figure 3.1. Unlike the fundamental interference frequency, the harmonics are likely to fall outside the Nyquist band and, thus, experience spectral folding and appear elsewhere within the pass-band. These folded harmonics no longer exhibit symmetry in the search space and cannot be so readily canceled.

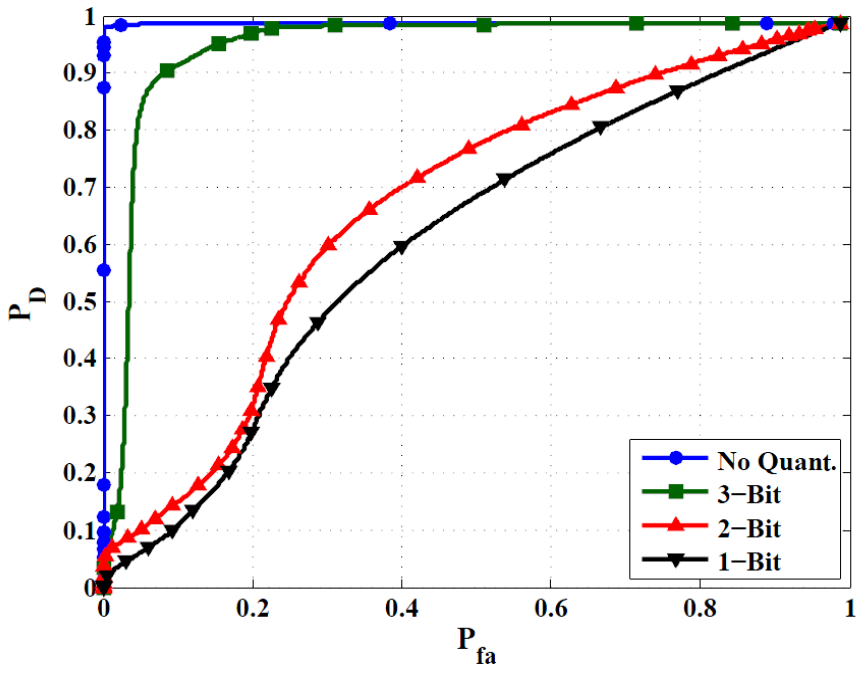

Figure 5.15: Cell-level ROC performance of the frequency-pair method (using D^{Pair}) for different quantization processes with a *JNR* = 75 dB

5.7.3 Direct Interference Removal

As discussed in Section 2.7, the interference component of D is highly predictable. Therefore, in the event that the receiver has some *a priori* information about the interference frequency and its amplitude, its contribution to D can be directly removed. Being a non-coherent metric, D is insensitive to both the phase of the interference and the relative phases of the interference and the GNSS signal. Given knowledge of the quantizer configuration, the AGC gain and the sample rate, the interference contribution, S_{int}, can be evaluated. Alternatively, a synthesized interference can be computed, quantized and correlated with the local replica signal. Subtracting the predicted interference from the traditional *decision variable*, D, produces a new

pseudo-interference-free search space, denoted here by D^{IntR}. Figure 5.16 shows the ROC performance for a receiver employing this scheme.

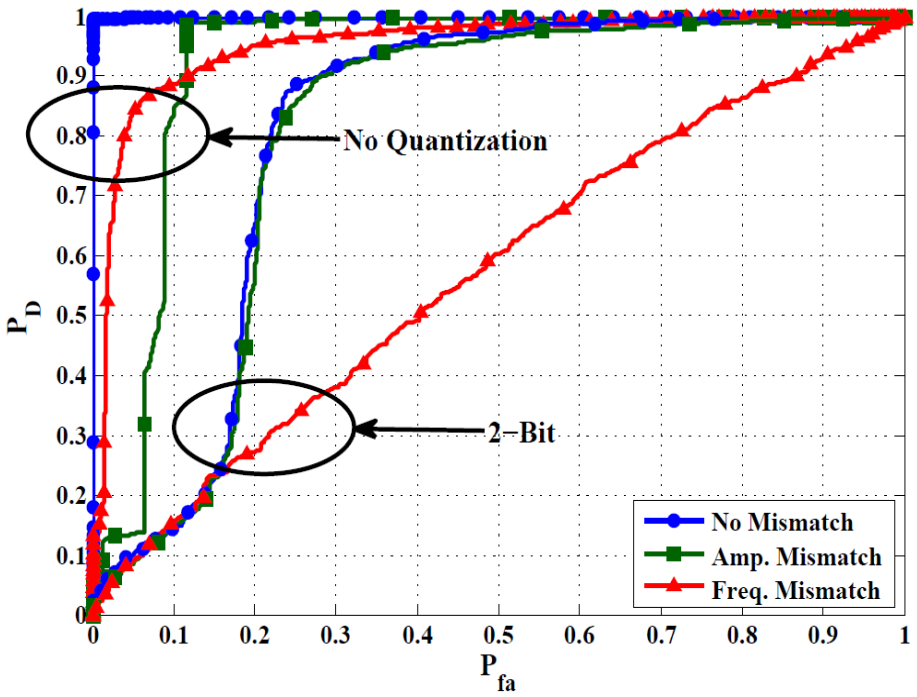

Figure 5.16: ROC performance of D^{IntR} for a *JNR* of 75 dB for both the no-quantizing and 2-bit receiver (amplitude estimate error = 0.2 dB and frequency estimate error is 10 Hz)

Although this procedure does significantly increase detection performance and is relatively insensitive to quantization effects, it is quite sensitive to the accuracy of the *a priori* interference amplitude and frequency estimates. Studies have shown that, via the use of notch filters, FFT or subspace algorithms (Host-Madsen & Handel 2000, Mahata & Soderstrom 2004, Pantazis et al 2010), these parameters can be estimated to an accuracy of -10 dB and 5 Hz, respectively. As an interference transmitter is generally within a small range of the receiver, under even benign dynamics, the amplitude and

frequency uncertainties can grow considerably. Illustrated also in Figure 5.16 is the ROC performance when the amplitude and frequency estimates are in error by 0.2 dB and 10 Hz, respectively. It is clear that the scheme is quite sensitive and, unless the receiver has highly accurate estimates of the interference parameters, may be relatively unusable.

5.8 System-Level Performance of Proposed Methods

This section discusses the performance of the traditional and new *decision variables* presented in Section 5.4. Although many different search, detection and verification strategies exist, this work considers only the parallel search scheme (Ziemer et al 1995, Kaplan & Hegarty 2006, Borio 2010, O'Driscoll 2007) for simplicity. This scheme computes the *decision variable* of choice over the entire search space and, should it be larger than some predefined threshold, declares the corresponding cell as containing the GNSS signal. Here, the performance of this system-level scheme is evaluated for each of the four *decision variables* discussed in 5.6, namely the traditional, window-based, frequency-pair and direct interference removal decision variables.

Monte-Carlo simulation analysis was used to evaluate the acquisition performance for each of the four *decision variables* and for each of the no-quantizing, 1-, 2- and 3-bit receivers. The interference frequency was fixed such that $f_{\text{int}} - f_{\text{IF}} = 125$ Hz and a range of interference power levels were considered, corresponding to *JNR* values in the range of 10 to 90 dB. For each of these scenarios, the acquisition performance was evaluated by considering a selection of received signal configurations, corresponding Doppler values in the range ± 5.0 kHz and all code phase values. Each simulation configuration was then repeated 1,000 times. The results of these simulations are

presented in Figure 5.17 in terms of detection probability versus interference *JNR*, where in all cases the detection threshold has been numerically optimized to yield a system-level (or global) false-alarm probability of 10^{-2}. This false alarm probability represents a typical level for a typical medium strength GNSS signal (Grewal et al 2007).

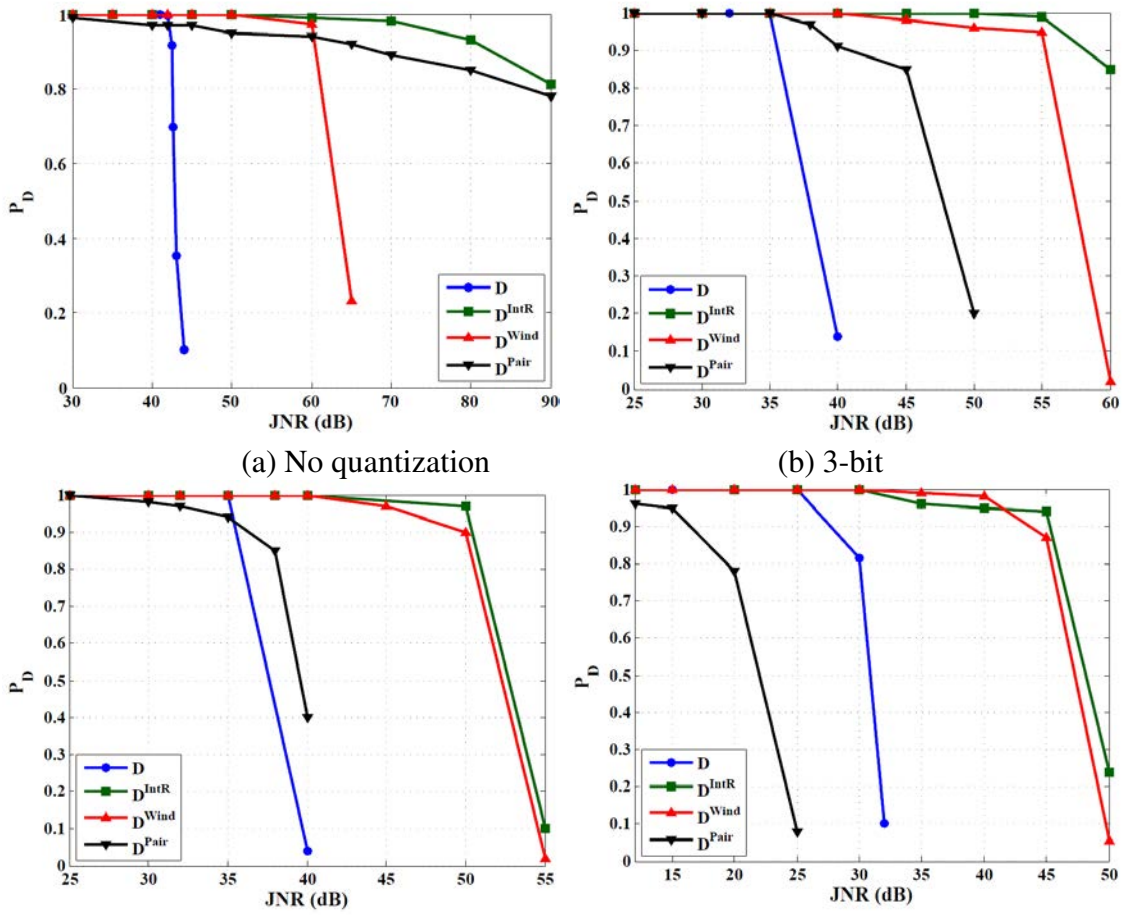

(a) No quantization (b) 3-bit

(c) 2-bit (d) 1-bit

Figure 5.17: System-level ROC performance of different *decision variables* for a range of *JNR* values and f_{int} - f_{IF} = 125 Hz.

The results presented illustrate a stark performance improvement for some of the modified *decision variable*, relative to the traditional approach; however, it appears that

some are more suited to certain receiver configurations than others. In particular, some *decision variables* appear to be particularly sensitive to quantization effects.

Rather unsurprisingly, it is clear that the scheme that utilizes the most *a priori* information provides the best performance. Examining Figure 5.17 (a), it can be seen that the interference removal scheme, D^{IntR}, can sustain CW interference with a *JNR* of the order of 70 dB without significantly degrading the detection performance. The effects of quantization however are significant, resulting in a reduction in the performance at a significantly lower *JNR*. For example, the use of a 3-bit quantizer reduces the tolerable *JNR* by 15 dB and each of the 1- and 2-bit quantizers incurs a further reduction of approximately 5 dB, as evidenced in Figure 5.17 (b), (c) and (d).

While relaxing the requirements for *a priori* information, the frequency-pair acquisition scheme can provide quite impressive performance in the presence of interference. In the case of the no-quantizing receiver, it provides almost as good a detection performance as in the interference removal scheme. Unfortunately, it suffers significantly from the effects of quantization, as can be seen by the dramatic drop of over 30 dB in tolerable *JNR* from Figure 5.17 (a) to (b). This trend continues with reducing quantizer resolution, resulting in a detection performance for the 1-bit receiver that is significantly worse than the traditional *decision variable*.

Considering now the most likely receiver operating scenario, where it has no *a priori* information whatsoever, the window-based detection scheme appears to provide quite a significant resilience to interference. Although in the no-quantizing receiver scenario, it fails to match the performance of the frequency-pair and direct interference removal

schemes, for all quantizing receiver cases, it compares well. In comparison to the traditional acquisition scheme, it provides from a 15 to 20 dB improvement in the tolerable *JNR* and, even for the 1-bit quantizing receiver, can provide a probability of detection in excess of 0.9 in the presence of a CW interference signal with a *JNR* of 40 dB. Moreover, in the case that the receiver performs FFT-based correlation, this performance enhancement is delivered at no extra correlation cost to the receiver and without the need for any *a priori* information.

5.9 Summary and Conclusions

The performance of the acquisition process for a typical consumer GNSS receiver in the presence of continuous wave interference was examined in this chapter. The limitation of the blind acquisition processor was shown and three new alternative approaches were examined.

Through an analysis of the effects of interference on the observed acquisition search space, a selection of novel *decision variables*, which provide robustness against this interference, was developed considering both the operation of a blind-receiver and one which may have knowledge of the interference characteristics such as amplitude and frequency. These new strategies were developed by leveraging search space properties to achieve enhanced system-level acquisition performance. It was shown that, depending on how much information a receiver has, it can exploit a different range of schemes to achieve higher acquisition performance.

The resultant acquisition performance enhancement was examined at both the cell-level and system-level for a variety of receiver configurations differing in their quantizer configuration. Results show that these novel *decision variables* can provide a significant improvement in system-level detection performance. In particular, the window-based scheme emerges as a particularly effective, robust and efficient method and can provide acceptable detection performance in the presence of higher CW level than that can be tolerated by traditional acquisition schemes.

Chapter Six: Overall GNSS System Performance Analysis

This chapter presents the overall consumer-grade GNSS receiver performance in the presence of narrowband interference. Specifically, the BER and acquisition performance of consumer-grade GNSS receivers is investigated. The approach considered is to combine the proposed quantization and acquisition methods of previous chapters to improve performance. In this chapter, acquisition optimization and real signal tests are conducted as well.

6.1 Simulation Setup for Real Jamming Scenario

In this section, three real interference scenarios are considered for evaluation. In these scenarios, a target vehicle is employing a consumer-grade GPS receiver. Moreover, it is assumed that a vehicle equipped with an interference generating device passes the target vehicle for each case. Figure 6.1 shows the physical configuration of these scenarios. In the first case, two vehicles are travelling in the same direction with relative velocity of 20 km/h. Variable x denotes the relative along-track location of the interferer device. Moreover, variable y represents the cross-track distance between the two vehicles. In the second case, two vehicles are on the opposite sides of a street with a relative velocity of 120 km/h. In the third case, the target vehicle is assumed to be static and the interferer vehicle passes with a velocity of 70 km/h. The simulation setup is given in Table 6-1. In all of the cases, the cross-track distance of the interferer and target vehicles is assumed to be 3 m.

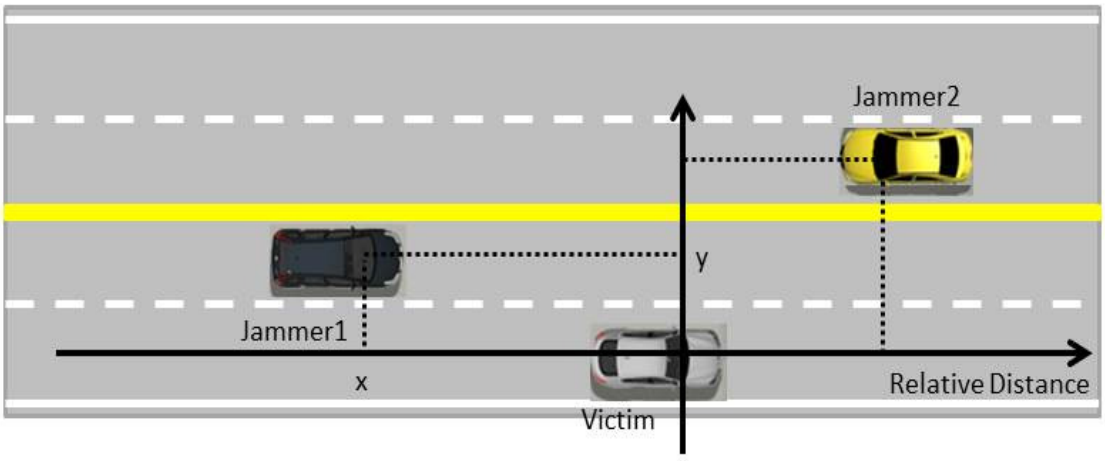

Figure 6.1: Relative location of interferer: (a) Jammer1, both vehicles are on the same side of the street, (b) Jammer2, vehicles are on the different sides of the street

Table 6-1: Simulation setup for real jamming scenario

Parameter	Value	Meaning
y	3 m	Cross-track distance
x	-10 m to 10 m	Along-track distance
Cs/N_0	40 dB-Hz	Received signal power
V_{rel}	20 km/h, 70 km/h, 120 km/h	Relative velocity
c	299 792 458	Speed of light
f_c	$1575.42e^6$	L1 frequency
λ	$\frac{c}{f_c}$	L1 Wavelength
$f_{\text{D,jammer}}$	$-\frac{V_{\text{rel}}}{c} \times f_c \times \frac{x}{\sqrt{x^2+y^2}}$	Doppler frequency of jammer
P_j	100 mW	Transmitted jammer power
G_t	3 dB	Jammer antenna gain
G_r	-4 dB	Receiver antenna gain for jammer
P_{jammer}	$P_j G_t G_r \left(\frac{\lambda}{4\pi\sqrt{x^2+y^2}}\right)^2$	Received jammer power

Figure 6.2 shows the received signal power versus the relative location of the interference source. As it can be seen, the received interference power is in the range of -100 to -80 dBm. All the considered reception scenarios experience the same amount of received interference power and due to the dynamic nature of the scenarios, the interference appears with different Doppler frequency at the receiver.

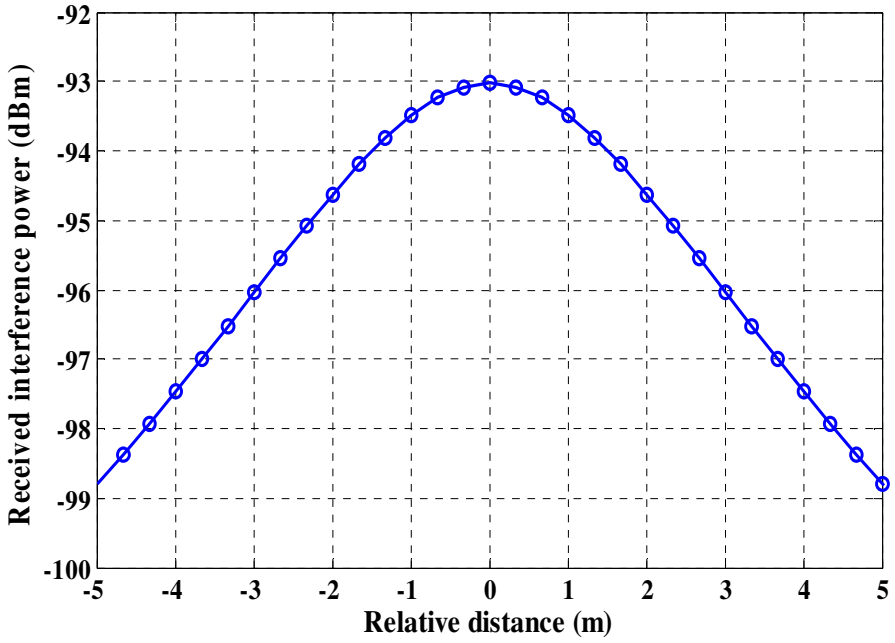

Figure 6.2: Received interference power

Figure 6.3 shows the received interference Doppler frequency as a function of relative interferer location. As it can be seen, the higher the relative velocity, the higher is the experienced Doppler frequency. The highest Doppler frequency is in the range of -150 to 150 Hz for the 120 km/h case.

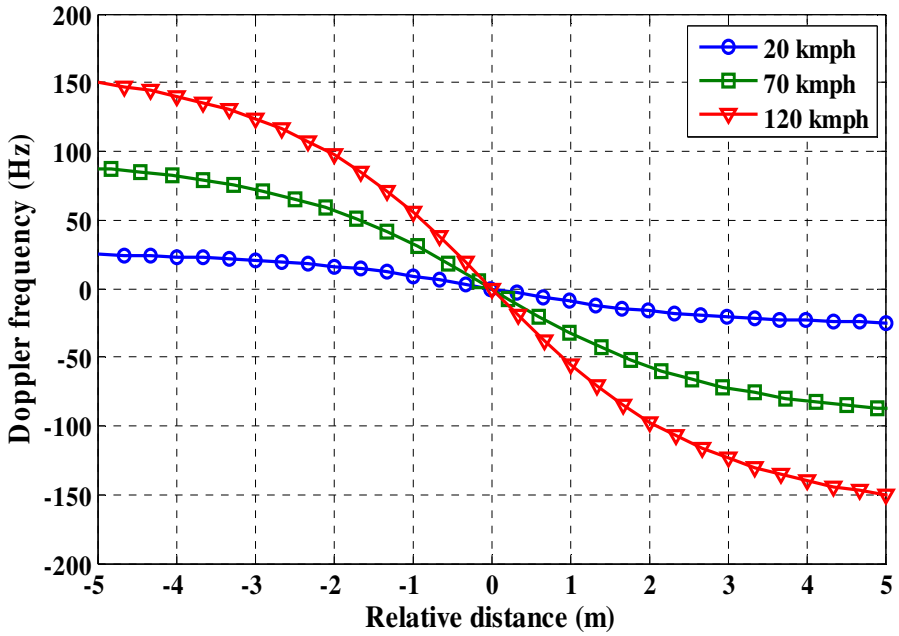

Figure 6.3: Received interference Doppler frequency

6.2 Simulation Results for Real Jamming Scenario

In this part, the effect of the quantization process and notch filtering on the received signal is evaluated for the considered scenarios. Here, an adaptive IIR notch filter is considered with μ = 1e-6 and ρ = 0.98. Figure 6.4 shows the effect of NF on the received signal PSD for the 70 km/h relative velocity case using the peiodogram PSD spectrum estimate command in MATLAB (MATLAB 2013). It is assumed that the receiver automatically adjusts the AGC gain to its optimum value (see Chapter Three). As it can be seen, PSD results contain several undesired harmonics due to interference and the non-linear quantization process. Although the fundamental frequency is removed by the NF, the harmonics degrade signal quality.

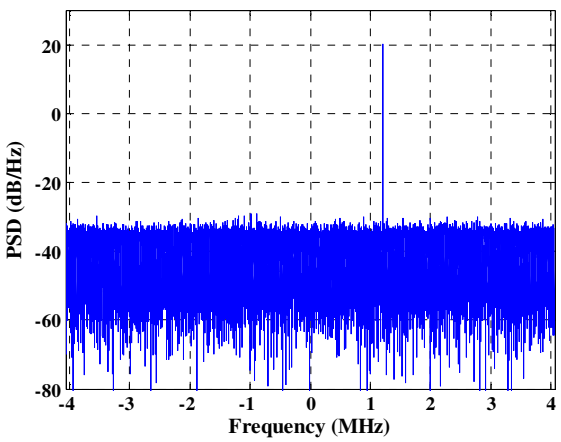

(a) Received signal PSD

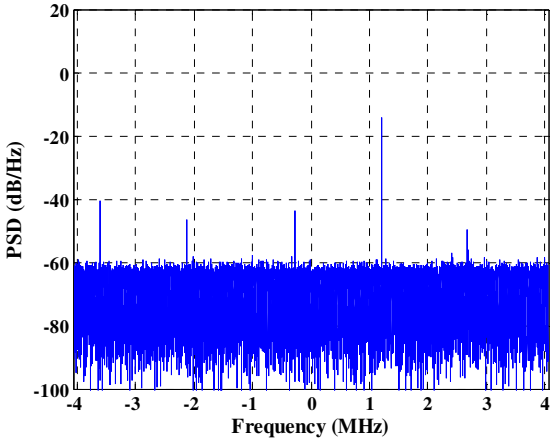

(b) Signal PSD after 2-bit quantization

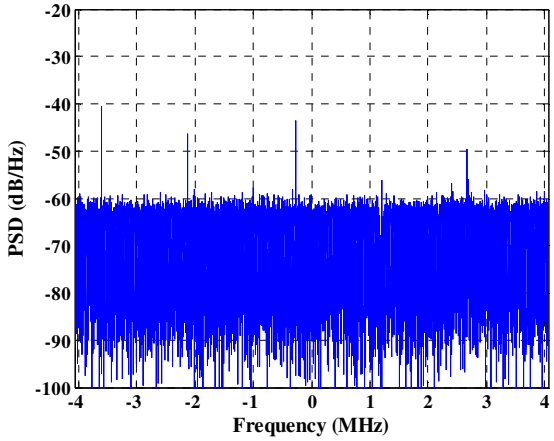

(c) PSD of interference removed 2-bit quantized signal using single Notch Filter

Figure 6.4: Effect of quantization process and notch filtering on received signal

The frequency estimate and frequency estimation error based on NF for 2-bit quantization and second scenario are shown in Figure 6.5. The performance of NF of the other scenarios is almost similar to this figure. Generally, when the relative distance is close to zero, the estimation scheme provides better results due to higher interference power. Table 6-2 summarizes the average error and variance of the estimation. As it can be seen, the variance of the estimate frequency slightly increases as the relative velocity increases.

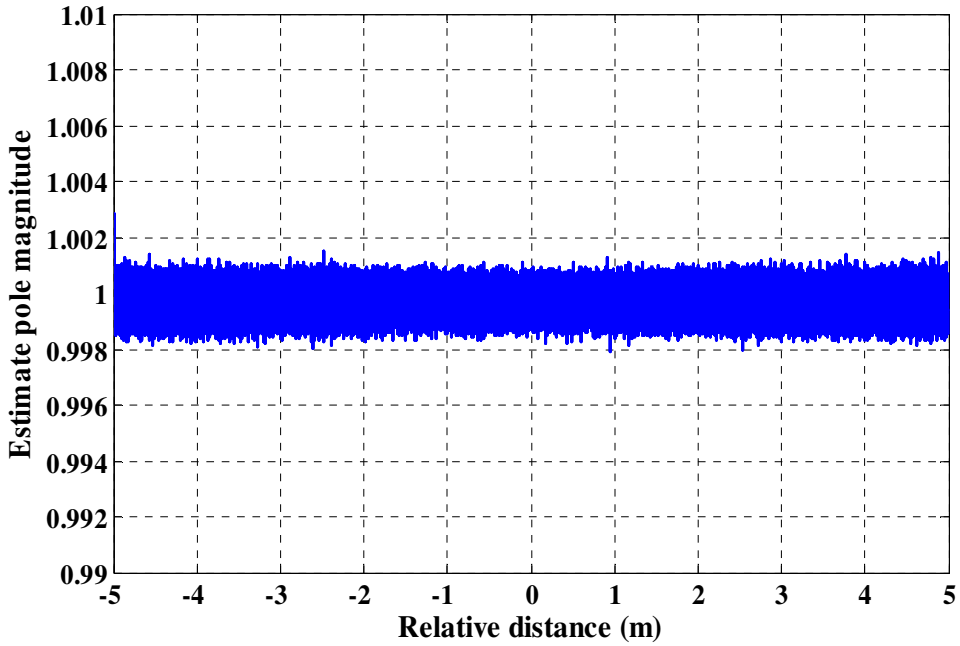

(a) Estimate zero magnitude

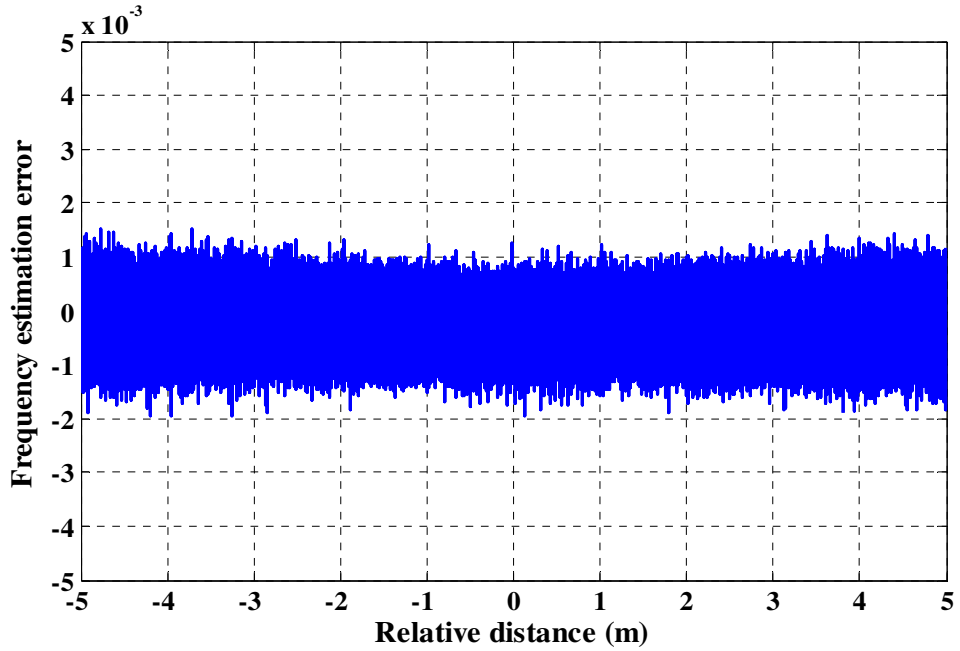

(b) Frequency estimation error

Figure 6.5: Frequency estimate and frequency estimation error based on NF for 2-bit quantization and second scenario (70 km/h)

Table 6-2: Frequency estimate and frequency estimation error for different scenarios

Velocity (km/h)	Zero magnitude		Relative estimate frequency	
	Average	Variance	Average	Variance
20	0.9997	1.28×10^{-7}	-1.90×10^{-4}	1.26×10^{-7}
70	0.9997	1.29×10^{-7}	-2.43×10^{-4}	1.28×10^{-7}
120	0.9997	1.29×10^{-7}	-2.95×10^{-4}	1.33×10^{-7}

6.2.1 BER Performance

Here, BER results are shown for different quantization configurations. For each case, three scenarios are considered. The results are associated with a receiver without any interference mitigation algorithm as well as a receiver employing an NF scheme.

Figure 6.6 illustrates the BER results for the 2-bit quantization case. The effective C/N_0 values can be easily calculated using these plots and Eq. (3.18). BER increases as the interferer vehicle approaches the target receiver, where for the worst case, BER is about 1×10^{-2} by an NF-free receiver. Using an NF, BER value goes to 4×10^{-3}. For the higher quantization resolution, the performance improvement due to NF increases because the interference fundamental frequency (which is removed by NF) includes a higher portion of the distorted interference power. Comparison shows that BER performance is almost the same for different relative velocity scenarios.

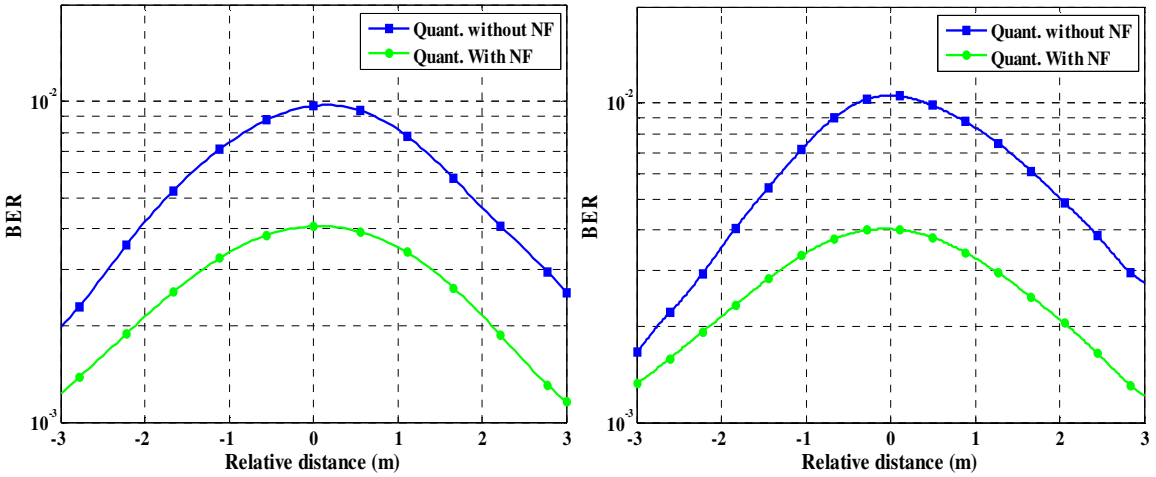

(a) 20 km/h relative velocity (b) 70 km/h relative velocity

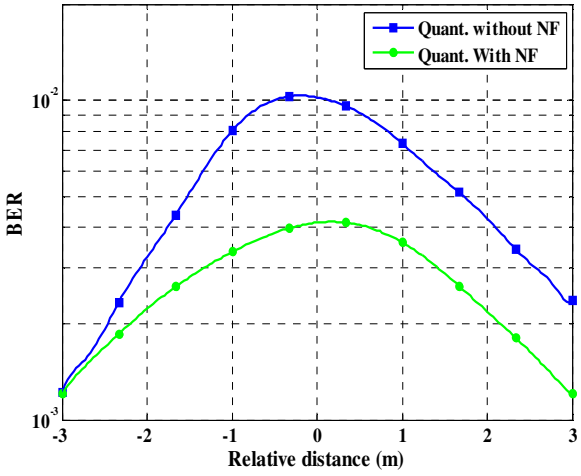

(c) 120 km/h relative velocity

Figure 6.6: BER results for 2-bit quantization

Generally, as the quantization resolution increases, the power of interference harmonics decreases. These harmonics are not removed by NF and are embedded in the post-correlation signal. Moreover, the effect of Doppler frequency due to relative interferer and interfered vehicles movement is negligible. That is, the BER results have almost a similar trend for different scenarios. The results of BER performance for 1-, 3- and 4-bit receivers are presented in Appendix L.

6.3 Data Collection Scenario

In this section, acquisition results for simulated interfered GNSS signal (generated by a hardware simulator and collected using the NI) are presented. The data collection setup is summarized in Table 6-3. In this data collection setup, five snapshots (i.e. a constant along-track distances) of reception scenarios associated with Figure 6.1 are considered. The amplitude and Doppler frequency of these snapshots are tabulated in Table 6-3. As shown, for each relative velocity scenario, five snapshots associated with relative distance of -5, -3, 0, 3 and 5 m are considered.

Table 6-3: Power and Doppler frequency setups for considered snapshots of jamming scenario

Relative velocity	Relative along-track distance	*JNR*	P_{cw} (dBm)	f_D
20 km/h	-5	75.20	-98.8	25.03
	-3	77.96	-96.04	20.64
	0	80.98	-93.02	0
	3	77.96	-96.04	-20.64
	5	75.20	-98.8	-25.03
70 km/h	-5	75.20	-98.8	87.57
	-3	77.96	-96.04	72.32
	0	80.98	-93.02	0
	3	77.96	-96.04	-72.32
	5	75.20	-98.8	-87.57
120 km/h	-5	75.20	-98.8	150.2
	-3	77.96	-96.04	123.9
	0	80.98	-93.02	0
	3	77.96	-96.04	-123.9
	5	75.20	-98.8	-150.2

Table 6-4 shows the data collection parameters and the visible satellite PRNs. In the following, Satellite PRN 21 is considered because of its high elevation of 80^o and the

correct cell is not close to zero Doppler frequency. This is a necessary condition to employ frequency-pair acquisition scheme.

Table 6-4: Data collection setup

Parameter	Value	Unit
GPS C/A PRN numbers	8, 16, 21, 29, 30, 18, 19, 26	-
C/N_0	40	dB-Hz
Noise floor	-130.0	dBm
Sampling frequency	8.0	MHz
Intermediate frequency	420.0	kHz

Figure 6.7 shows the power spectrum of the collected data as well as re-quantized values for a 20 km/h relative velocity and -5 m relative distance scenario. The collected data is in 16-bit complex form and is converted to 1-, 2-, 3-, and 4-bit precision data values in MATLAB using optimum AGC configuration (see Chapter Three).

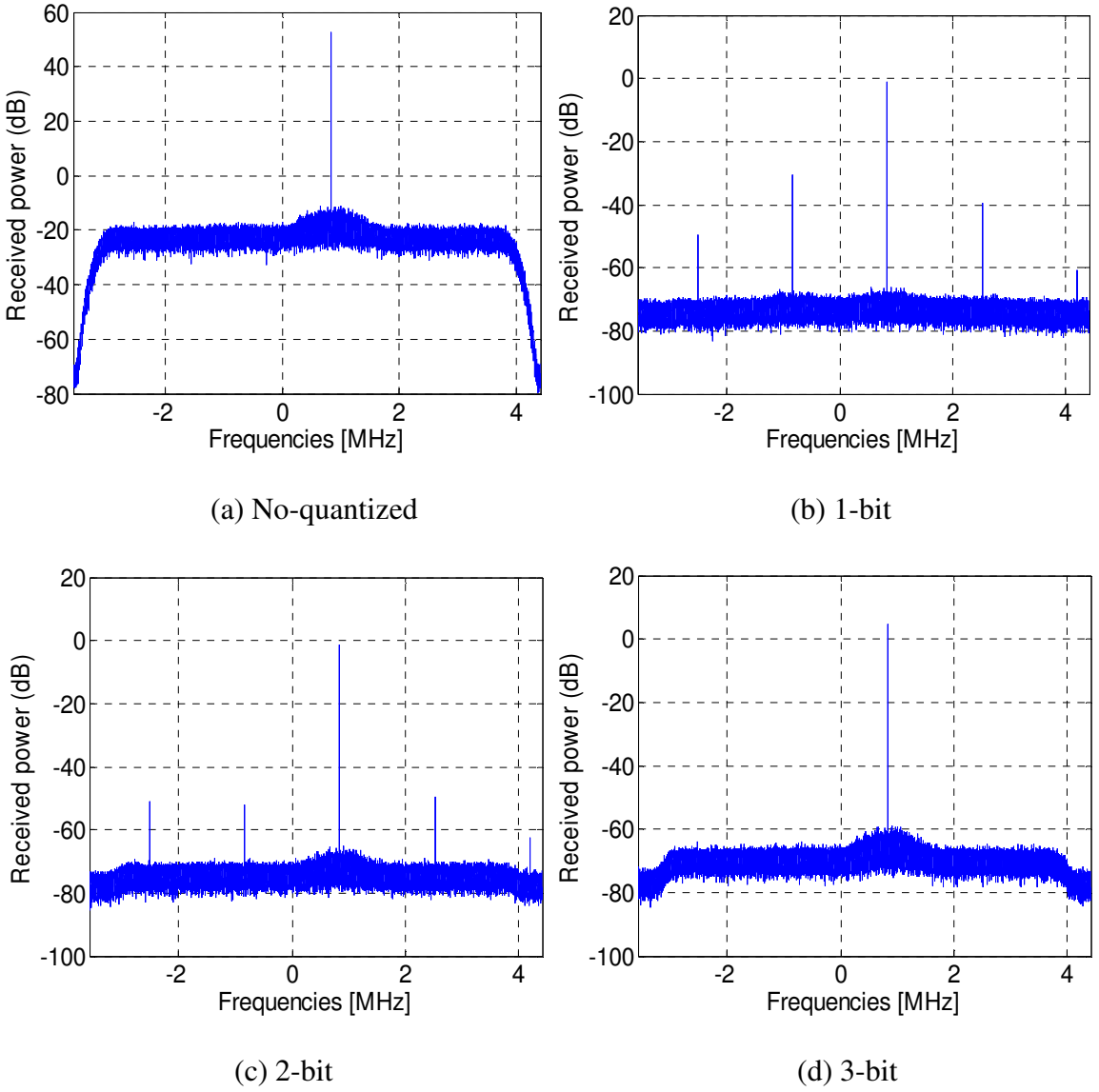

Figure 6.7: Power spectrum of collected data

6.4 Notch Filtering Effect

A generic result of zero magnitude estimated by an adaptive FIR notch filter is presented in Figure 6.8. These results are shown for the 2-bit quantization case and the first collected data scenario, where the relative velocity is 20 km/h and the relative distance is -5 m. Generally, the zero magnitude of the other scenarios shows a similar trend. Here,

since the power of the received signal varies for each scenario, the normalize LMS scheme is applied to update NF's zero.

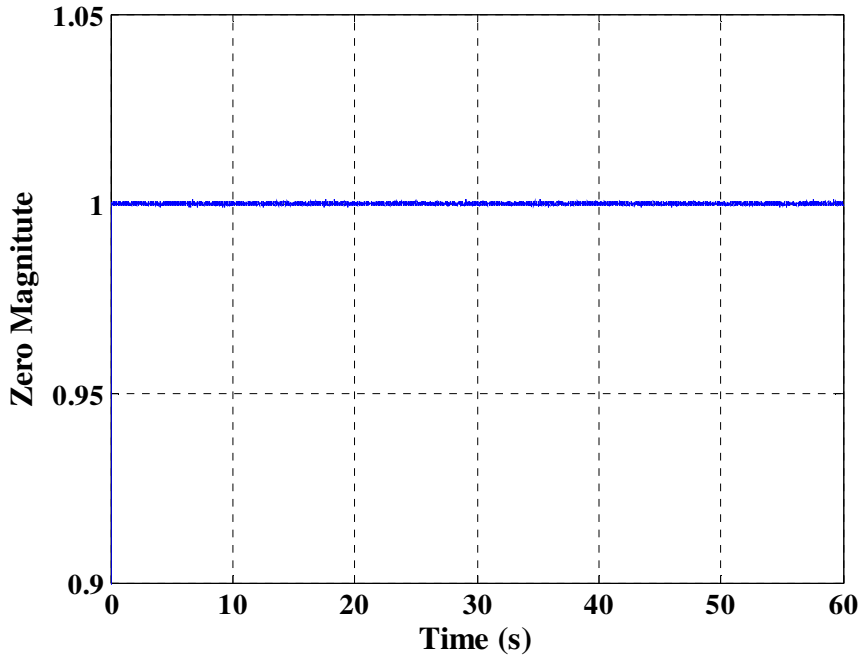

Figure 6.8: Magnitude of the estimate zero for 2-bit quantization (V_{rel} = 20 km/s)

6.5 CAF Results

The results of CAF values for different quantization configurations are shown in Figure 6.9. The correct cell is visible in the search space but its CAF level is lower than some intensely interference affected cells. Moreover, as the quantization resolution increases, the CAF value of the correct cell increases and the CAF plateau around it becomes sharper. While traditional schemes miss-detect the highly corrupted cells, the proposed schemes of Chapter Five will enable the receiver to detect the correct cell and acquire the desired GNSS signal.

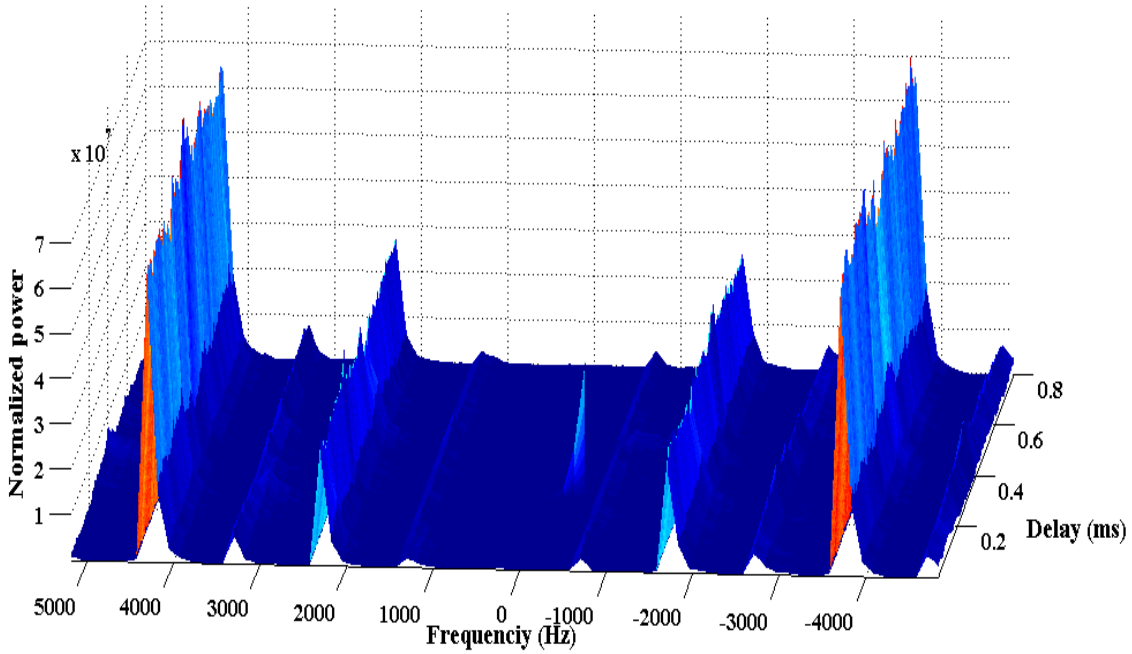

(a) No-quantized

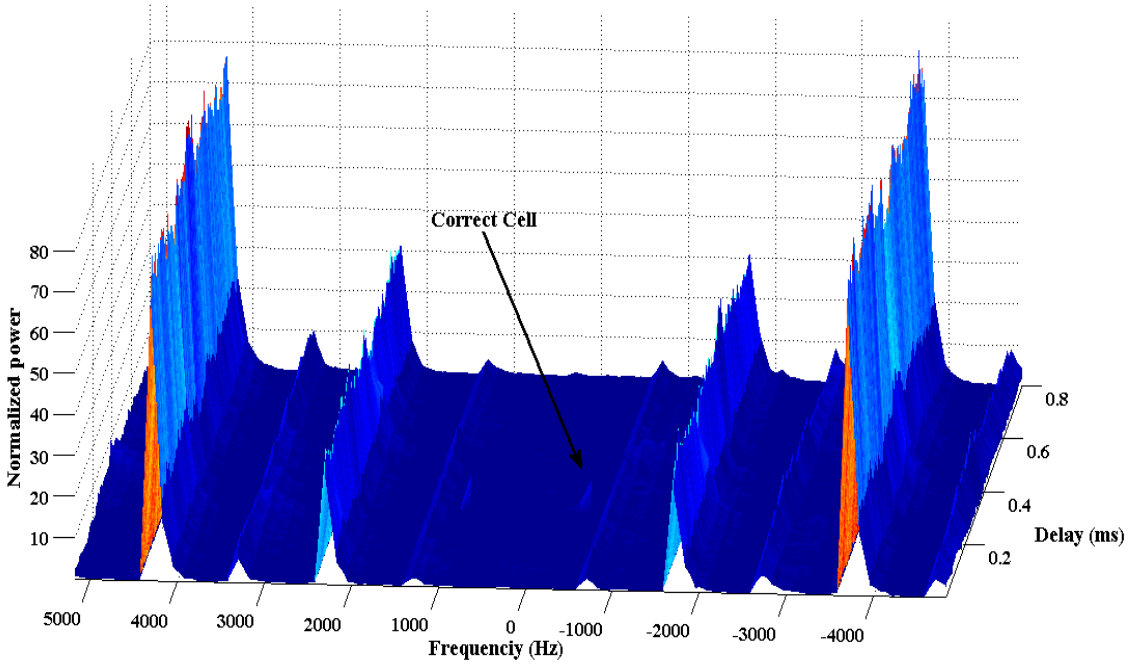

(b) 1-bit

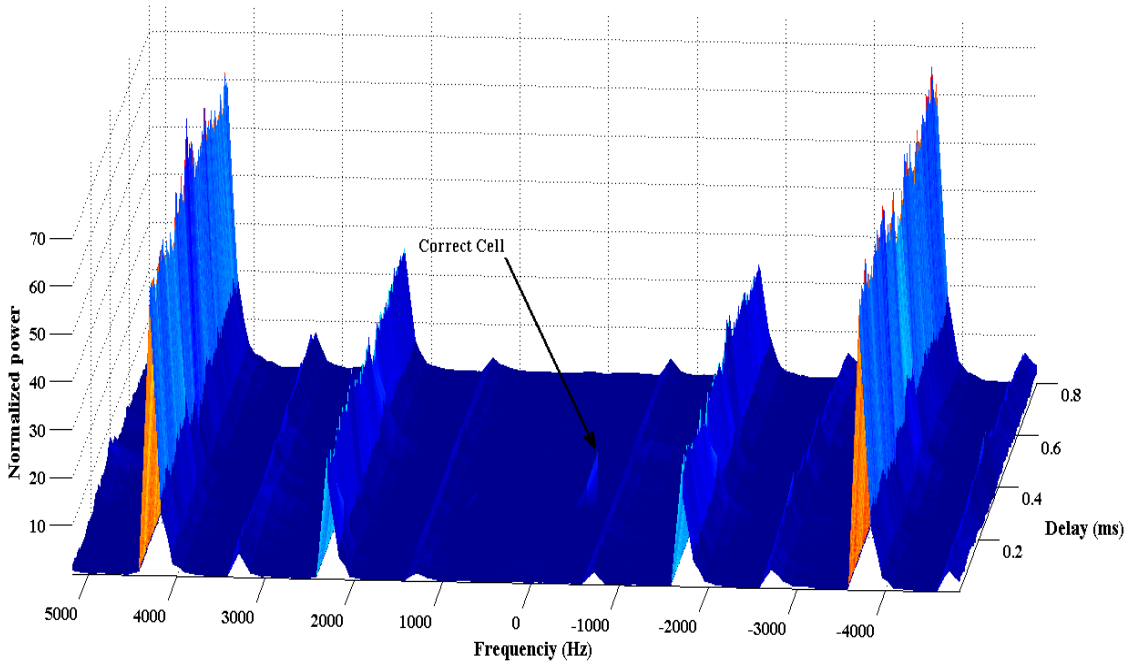

(c) 2-bit

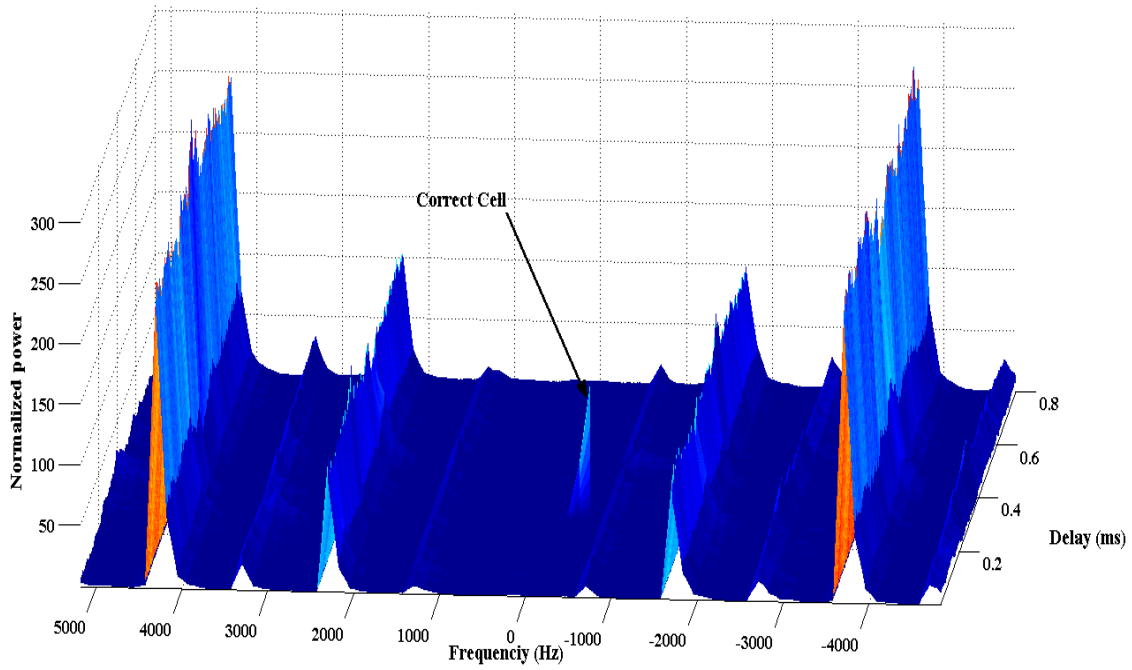

(d) 3-bit

Figure 6.9: CAF results for different quantization configurations

6.6 Cell-Level Performance

In this section, the acquisition performance of the proposed methods is studied using the data collected above. To compute cell-level false-alarm and detection probabilities, two sets of data are collected for each data collection scenarios: 1- without GNSS signal and 2- containing the desired GNSS signal. The GNSS signal free data is utilized to compute the false-alarm probability, while the other data set is used for detection probability computation. Moreover, to have the correct cell, the cell containing the GNSS signal, the first one minute of the data is set to be interference-free. By defining a high resolution search space as well as employing a long integration time, the position of the correct cell is determined. To compute the ROC performance, the coherent integration time is set to 1.0 ms, and thus, within a 60 s data set, 60×1000/7 separate integration intervals are available.

In the following, the ROC performance results are shown for no quantization, 1-bit and 2-bit quantization configurations. For the 2-bit quantization case, the optimum AGC gain (given in Chapter Three) is employed.

6.6.1 The Traditional Acquisition Scheme

Figure 6.10 shows the cell-level detection results of the traditional scheme for the first data scenario. In the first data set, the relative velocity is 20 km/h and the received *JNR* is about 75 dB. In this plot, the results of 1-bit, 2-bit and no quantization are shown for both the collected data and the MATLAB simulation results. This figure shows that the real data match the simulation results very well. However, particularly for lower quantization resolution, a disparity between the curves is evident. This is due to a non-ideal generation of the adjusted Doppler frequency precision of the simulator and data collection limitations of the NI.

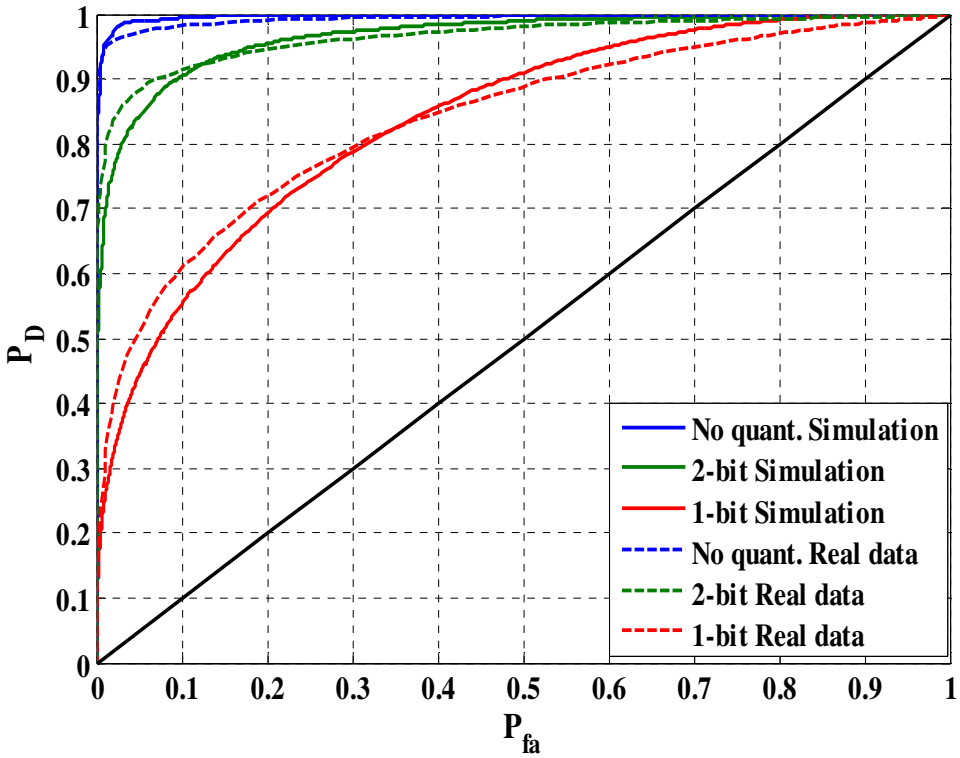

Figure 6.10: Cell-level detection results of the traditional scheme for the first data scenario

The cell-level detection results of the traditional scheme for the 8th data set are depicted in Figure 6.11. In the 8th data set, the relative velocity is 70 km/h and the received *JNR* is about 80 dB. Compared to Figure 6.10, the ROC performance decreases due to the presence of a higher interference power. Again, the disparity between the curves increases for lower quantization resolutions. Moreover, the sensitivity of the considered model for non-idealities increases for these quantization configurations.

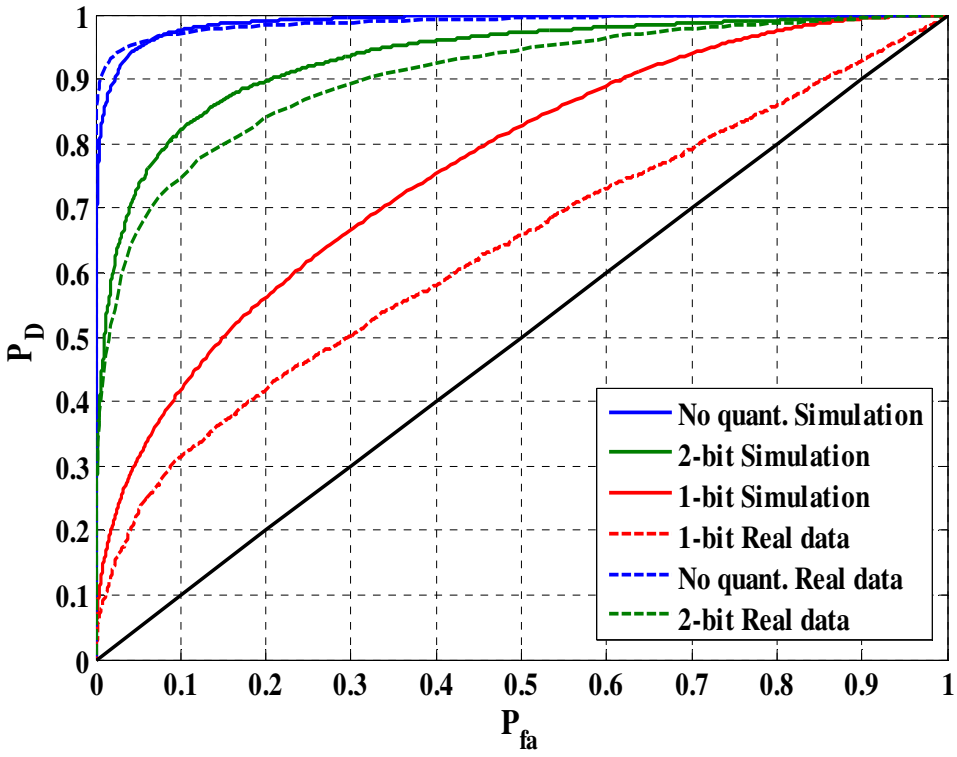

Figure 6.11: Cell-level detection results of traditional scheme for the third data scenario

6.6.2 Window-based Acquisition Scheme

The cell-level detection results of the window-based scheme for the first data are depicted in Figure 6.12. In this plot, the entire Doppler bin of search space (FFT) is considered to evaluate the window-based *decision variable*. As can be seen, the detection performance decreases compared to the traditional acquisition scheme. This is due to the fact that the *decision variable* of the window-based scheme contains more noise as compared to the traditional scheme. Moreover, the interference effect in cell-level acquisition of this metric might be increased due to averaging operation. However, it is expected that this method induces less noise term than the frequency-pair scheme due to averaging.

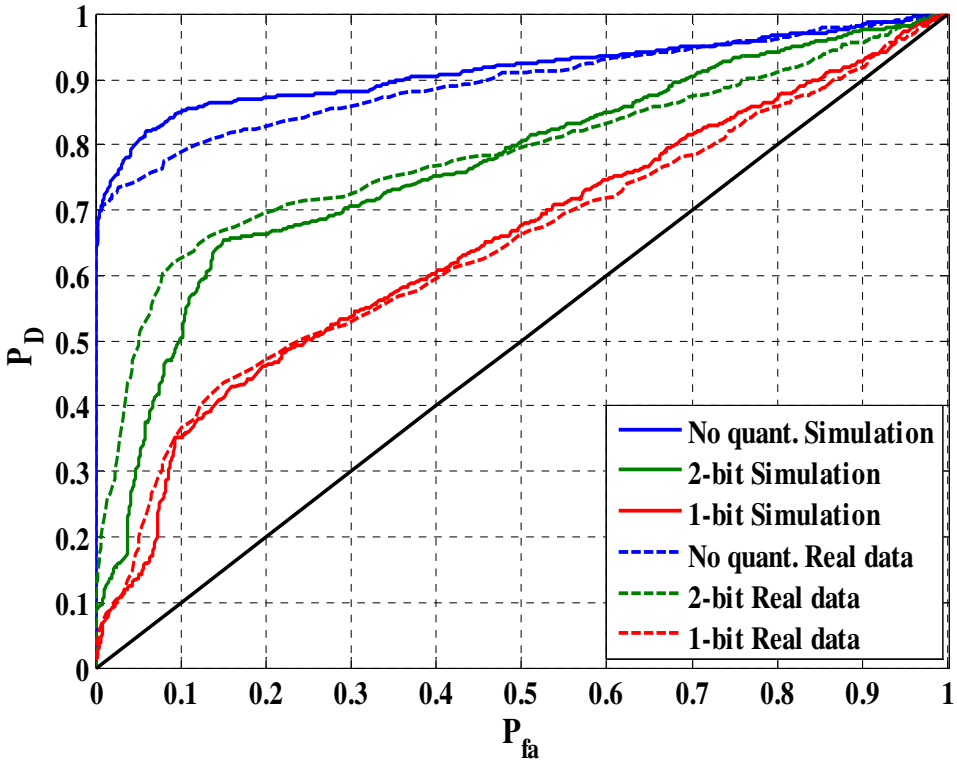

Figure 6.12: Cell-level detection results of window-based scheme for the first data scenario

The cell-level detection results of the window-based scheme for the third data are depicted in Figure 6.13. Again the performance degrades compared to the traditional acquisition scheme. Moreover, the shape of the ROC curves is slightly different from that of the traditional acquisition. This is because in window-based acquisition, the *decision variable* is a subtraction of two correlated random variables, and thus, has a different distribution function than that of the traditional *decision variable*.

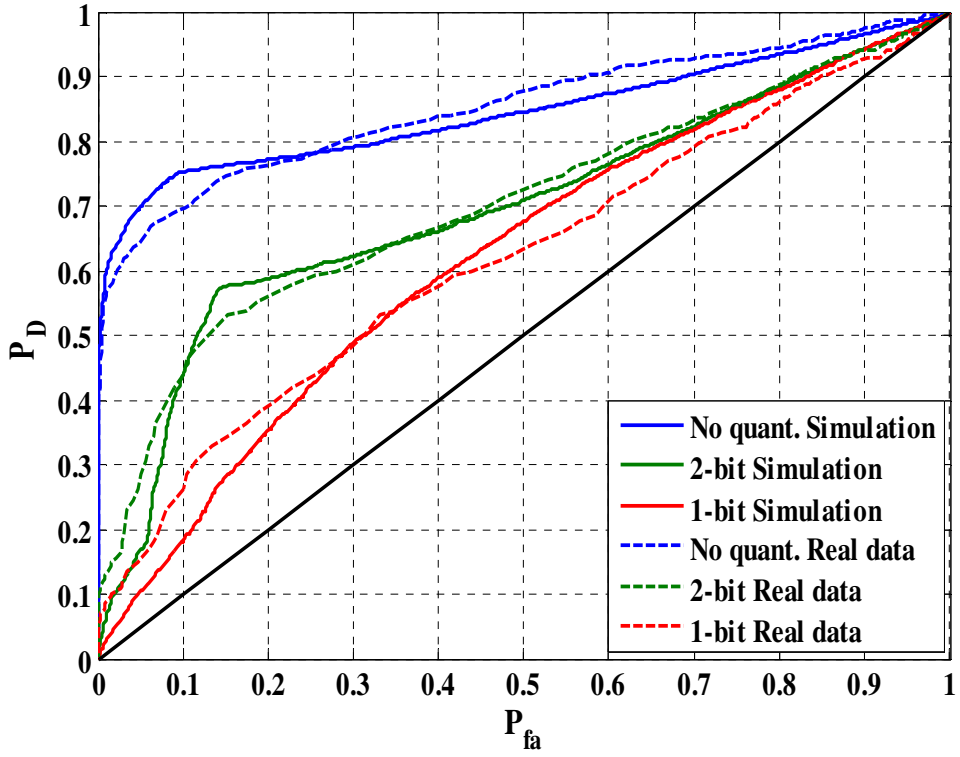

Figure 6.13: Cell-level detection results of window-based scheme for the third data scenario

6.6.3 The Frequency-Pair Acquisition Scheme

The cell-level detection results of frequency-pair acquisition scheme for the first data are shown in Figure 6.14. The overall performances of the acquisition for no quantization, 1-bit and 2-bit quantization decrease as compared to the traditional acquisition scheme. This is attributed to an increased *decision variable* noise. Compared to the window-based acquisition scheme, the performance of the frequency-pair scheme is slightly poorer.

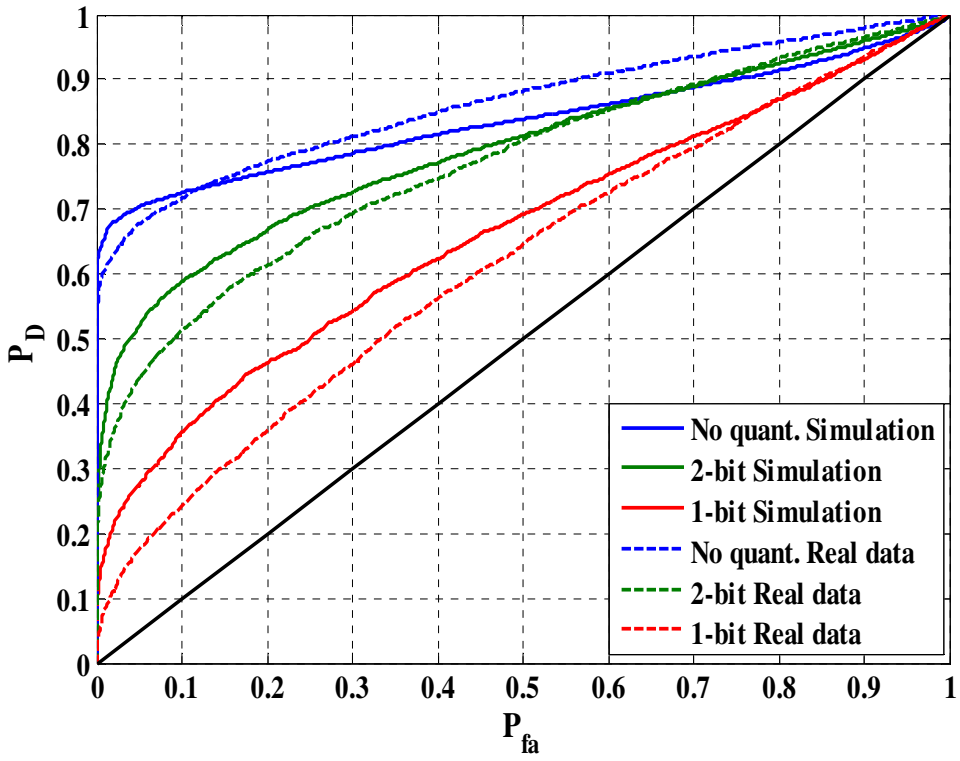

Figure 6.14: Cell-level detection results of frequency-pair scheme for the first data scenario

The cell-level detection results of frequency-pair acquisition scheme for the third data are depicted in Figure 6.15. Likewise, due to an increased *decision variable* noise, the overall performance of the acquisition decreases as compared to the traditional acquisition scheme. Moreover, the results almost match those given in Figure 6.14 in the presence of lower interference power. That is, this scheme is almost insensitive to the true interference amplitude, interference frequency and to errors in the receiver estimate of the interference amplitude. It is, however sensitive to errors in the receiver's estimate of the interference frequency as they will result in the incorrect pairing of cells. Indeed, if the interference frequency is sufficiently well known, this decision variable can significantly improve the detection performance, specifically at the system-level, albeit at the cost of increasing both the computational load and *decision variable* noise.

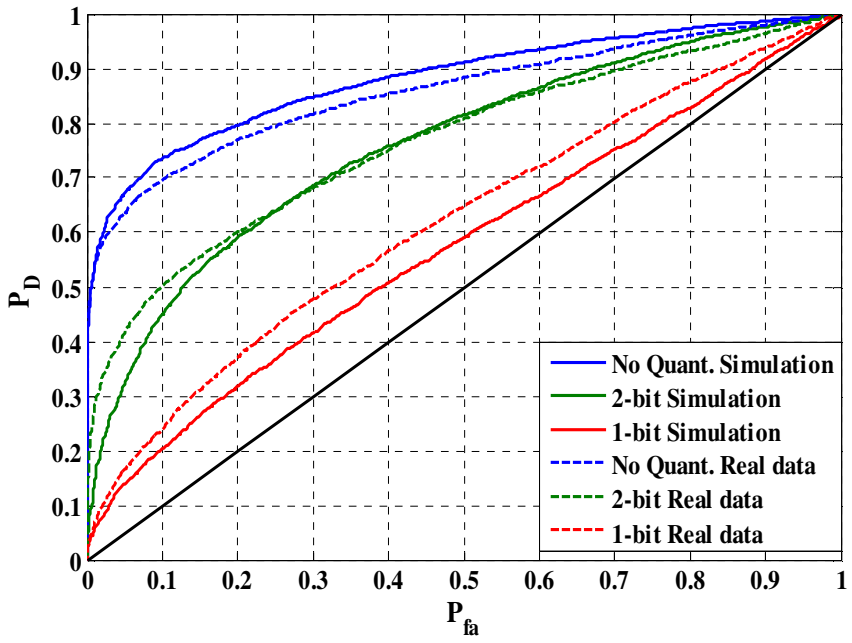

Figure 6.15: Cell-level detection results of frequency-pair scheme for the third data scenario

6.6.4 The Direct Interference Removal Acquisition Scheme

The cell-level detection results of the direct interference removal scheme for the first data are given in Figure 6.16. The performance of the direct interference removal acquisition scheme is slightly worse than traditional acquisition, except for the no quantization case. Therefore, although it is expected to have a better detection probability, induced quantization loss decreases the achieved performance. Compared to window-based and frequency-pair acquisition schemes, the direct interference removal presents higher ROC performance at the cost of increasing the computational load and required information of the interference.

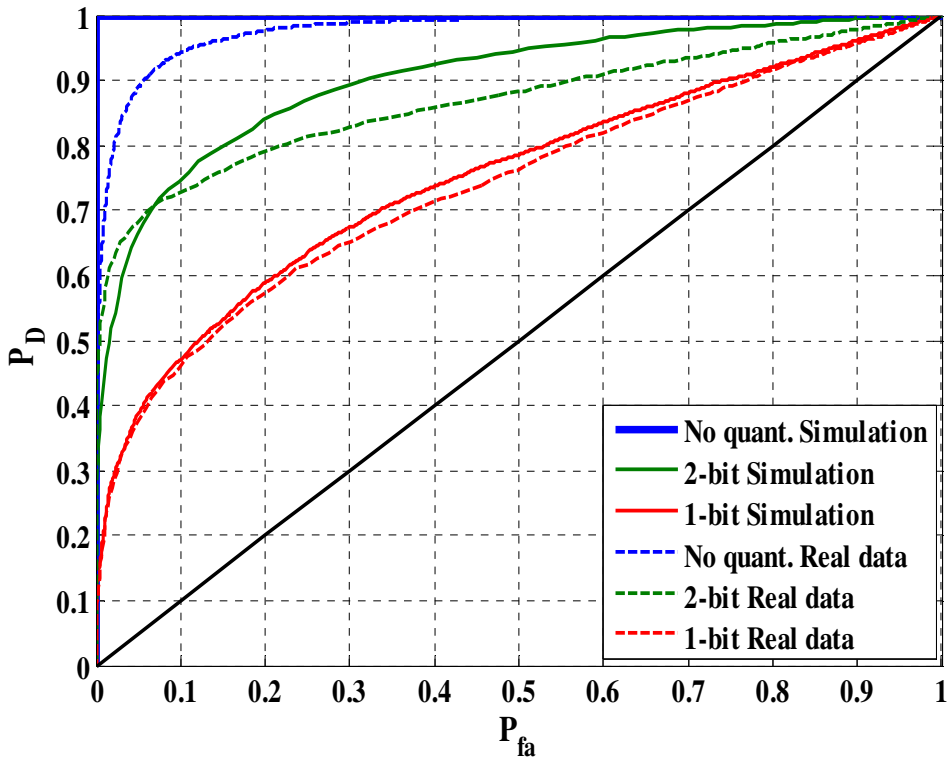

Figure 6.16: Cell-level detection results of direct interference removal for the first data scenario

The cell-level detection results of the direct interference removal scheme for the third data are depicted in Figure 6.17. As compared to Figure 6.16, as the interference power increases due to quantization loss, the difference between quantized generated interference and that of the received signal increases, which results in inferior detection performance.

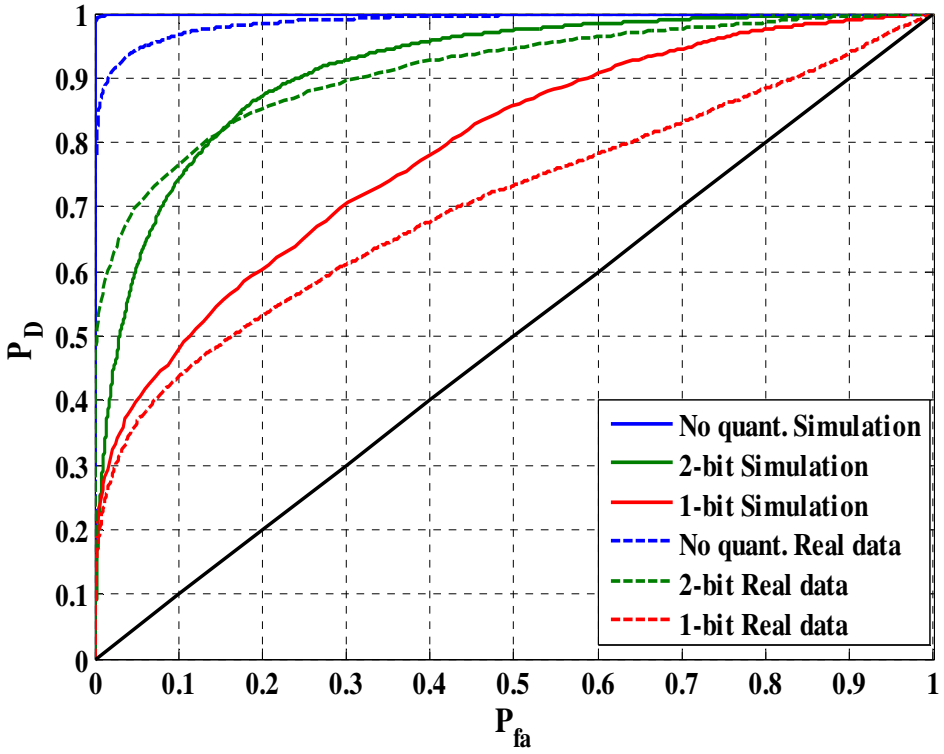

Figure 6.17: Cell-level detection results of direct interference removal for the third data scenario

6.7 System-Level Performance

Since the position of the desired signal in the collected data has a fixed Doppler frequency, system-level performance analysis is different from that of the Chapter Five. In fact, in order to evaluate the previous results for collected data, a large amount of data

collection would be required, wherein the relative frequencies of the interference and GPS signal were varied in each collection. However, to gain an insight into how the performance of the proposed acquisition schemes varies at the system-level, the value of the discussed *decision variables* are evaluated over the entire search space and the ROC results are shown.

Figure 6.18 shows the system-level ROC performance of the different *decision variables* for the no-quantizing and the 2-bit receiver. These results show that the traditional acquisition scheme fails to acquire the signal. This is because CAF values are highly corrupted due to interference (see Figure 6.9). If the receiver employs the traditional *decision variable*, it is highly probable that the receiver miss-detects the interference corrupted cells. On the other hand, the frequency-pair and direct interference removal schemes detect the correct cell most of the time. As discussed previously in Section 5.7.2, this improvement comes at the cost of having information about the interference characteristics. This may not be always possible, especially when the receiver blindly tries to acquire the GNSS signal or the interference characteristic estimates contain errors due to estimator accuracy limitations. Interestingly, as a tradeoff, the proposed window-based acquisition scheme provides acceptable detection probability. For example, the detection probability of this scheme is about 0.7 for $P_{\text{fa}} = 10^{-2}$ and 2-bit quantization.

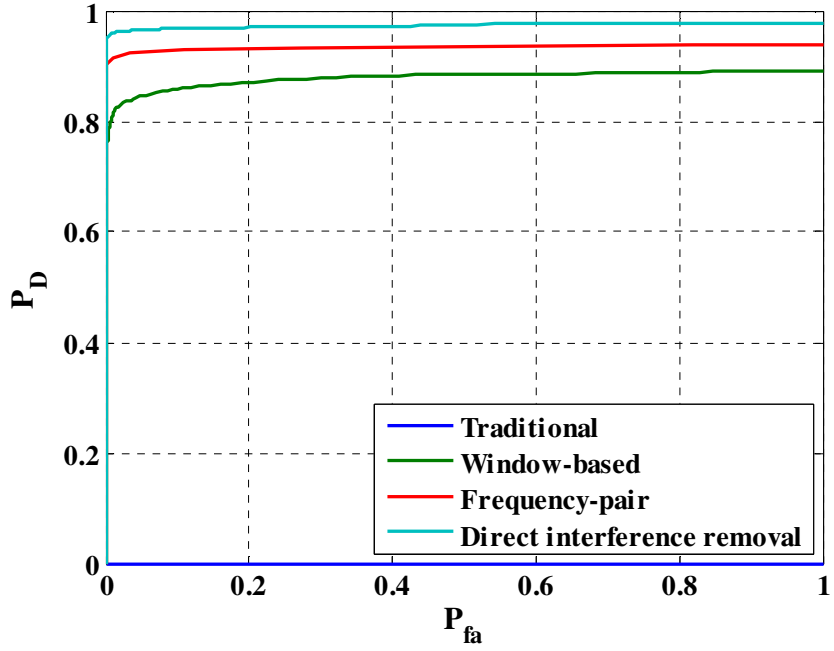

(a) System-level acquisition performance for no-quantizing receiver

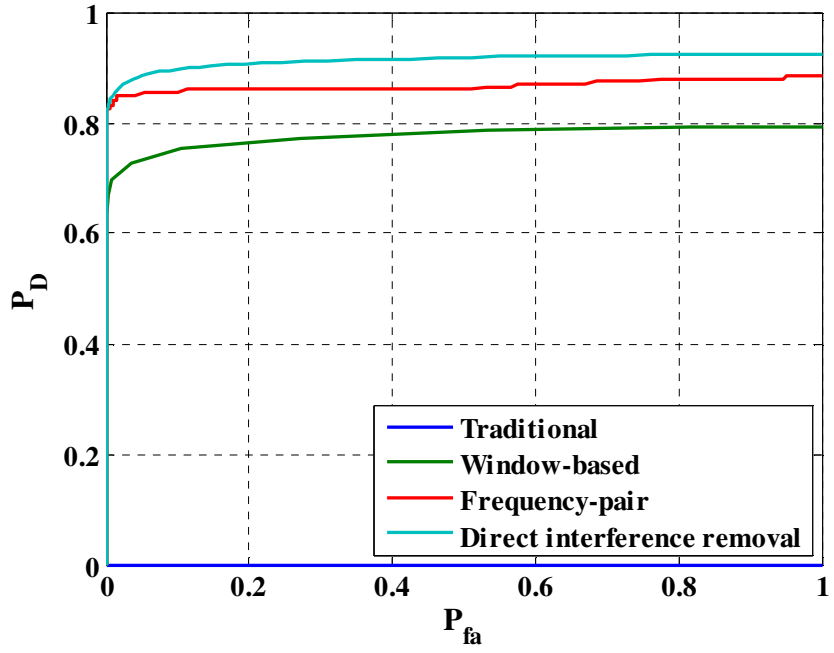

(b) System-level acquisition performance for 2-bit quantizer

Figure 6.18: System-level acquisition performance for the first data scenario

6.8 Summary and Conclusions

The overall performance of a consumer-grade GNSS receiver was investigated in this chapter. By employing a hardware simulator, interference corrupted GNSS signals were collected via NI digitalizer channels. Three practical cases of jamming were considered associated with jammer and the target vehicle's dynamics.

It was assumed that the receiver is equipped with an optimal AGC adjustment scheme, as well as notch filter based interference mitigation. The cell-level acquisition performances of the acquisition schemes (proposed in Chapter Five) was presented. It is shown that, generally, the proposed subtracting, averaging and pairing schemes decrease the performance of the acquisition process. An exception is when the receiver knows the exact interference power and frequency and can employ the direct interference removal scheme. In this case, for a high resolution quantizer, the performance is superior to that of a traditional acquisition scheme.

On the other hand, the system-level (global-level) acquisition performance of a GNSS receiver improves by employing the proposed schemes. The results of collected data confirm that, depending on how much information a receiver has, the acquisition performance can be improved. For example, it was shown that for $P_{fa} = 10^{-2}$ and 2-bit quantization, the detection probability improves from 0.0 to 0.7 by using the proposed window-based acquisition scheme under certain conditions (where the interference frequency is close to zero and *JNR* is about 75 dB). In this case, the receiver only knows that interference is present and the proposed window-based scheme often detects the correct cell, while the traditional scheme performs poorly in this considered scenario.

In a real GNSS application, the receiver needs to be adjusted in order to employ the proposed schemes. First of all, the quantization configuration should be adjusted. This improves the BER and detection performance of the receiver. Next, the acquisition scheme can be upgraded to one of the proposed schemes based on the available properties of the interference source.

Chapter Seven: Conclusions and Recommendations

Conclusions regarding GNSS signal acquisition in the presence of narrowband interference are presented in this chapter. Possible future work recommendations are also provided to further develop the proposed schemes.

7.1 Conclusions

7.1.1 The Quantization Process

Chapter Three examined the quantization performance of a typical consumer-grade GNSS in the presence of interference. It was shown that for strong interference signals, the bias introduced by interference in SINR metric can become significant. As an alternative, a measure of BER performance was introduced to alleviate this problem and measure the effect of interference on the quantizer and receiver performance.

An interesting observation drawn from the simulation results is that the ability of the low resolution quantizer to provide a given BER is limited by the interference power. For example, if a BER of less than 10^{-2} is required, then 2-bit quantization is not sufficient if the prevailing interference power is greater than -90 dBm.

Through an analysis of the effects of AGC configuration on the bit error rate and detection probability, it was shown that the optimum AGC gain that results in a minimum bit error rate will also maximize the cell-level acquisition performance. In addition, for a larger number of quantization bits, the range of AGC gain that provides near optimal performance is widened. That is, an increased quantization resolution not only provides

superior performance, it also reduces the sensitivity to AGC gain tuning in the quantizer design.

Due to the fact that the signal sampling and quantization process is performed prior to any digital interference mitigation schemes, the results demonstrate significant performance improvement for a GNSS receiver in terms of effective C/N_0, BER and acquisition performance. The results also show the limitations of low resolution quantizer configurations and present the maximum performance that can be achieved by each quantizer.

7.1.2 Interference Detection and Mitigation

The common approach in GNSS applications to eliminate the effect of narrowband interference is based on notch filtering. However, their Doppler frequency dependent bias induced into the pseudorange and autocorrelation function distortions should be compensated to improve the position domain results. In contrast, FIR notch filters provide guaranteed stability and insensitivity to coefficient rounding. Thus, a new adaptive FIR NF was proposed, implemented and in this work. Furthermore, FIR NF was modified to have a linear-phase response, in order to automatically remove the frequency dependent bias and distortion on the ACF.

Although NF-based schemes are efficient and simple to implement, for a typical consumer-grade receiver equipped with a low resolution quantizer, the number of harmonics induced in the receiver's digital bandwidth is large and, thus, employing a high number of NFs increases the NF side effect on the desired signal. In addition,

utilizing a low number of NF might not result in the desired performance. That is, in this kind of receiver, some other methods should be considered to help remove the effects of undesired narrowband interference. One possible method is using interference resistant acquisition schemes, which provide better detection performance due to having some information about the interference presence and its characteristics. For example, the estimate frequency given by NF, if precise enough, will enable the acquisition processor to employ the new detection methods studied in Chapter Five.

7.1.3 Signal Acquisition

Chapter Five considered the effect of quantization configuration on the detection performance in a consumer-grade GNSS receiver. The detection performance and cell-level ROC illustrate that the optimum AGC gain in terms of BER results in optimum ROC performance as well. That is, by adjusting AGC gain to its optimum value both the BER performance and the detection probability increase.

Moreover, the acquisition problem of a consumer-grade receiver in the presence of narrowband interference was also considered in Chapter Five. The drawbacks of traditional acquisition schemes were shown and to improve the acquisition performance, three new schemes were proposed and examined. These novel decision variables, which may utilize some information about interference characteristics, increase the acquisition robustness against narrowband interference.

The result of cell-level and system-level acquisition performance of these new *decision variables* illustrate that significant improvement specially by employing a window-based

scheme can be provided even in the presence of higher interference levels. For example, it was shown that, in some cases, by employing these new schemes, a receiver can operate under a *JNR* 20 dB higher than when using traditional schemes.

Although increasing the quantization resolution and employing a more efficient interference mitigation scheme are always promising in the presence of narrowband interference, the best receiver structure is to employ interference mitigation schemes along with new acquisition processors while the quantization configuration is optimally adjusted.

7.2 Future Research Recommendations

Further to the presented theoretical models and simulations-experimental results presented in this thesis, the following recommendation and notes can be considered for future research studies.

1- The system to evaluate the performance of the proposed models and schemes methods are limited to GPS L1 C/A code in this thesis. However due to the fact that the proposed schemes are system independent, they will be adequate for other GNSS systems, e.g. GPS L2, after some modifications and considerations. Specifically, the performance of proposed quantization configuration and new acquisition scheme for Galileo and GLONASS systems which are employing other modulation scheme rather than BPSK and CDMA will be interesting for evaluation and study.

2- Implementing the developed quantization configuration and proposed acquisition inside a GNSS receiver can be considered as a future work. As discussed in Chapter

Four, the proposed FIR and linear-phase FIR ANF were designed and implemented in a software receiver. The results of this implementation demonstrate their superior performance against IIR NF not only in pseudorange based navigation solutions but also to resolving the carrier ambiguities which were not presented in this chapter due to the fact that position domain analysis is outside the scope of this thesis. Interested readers are referred to (Lin et al 2011). The study and evaluation of the effect of the optimum quantization configuration and the proposed acquisition schemes in the position domain are recommended for future work.

3- The measure of C/N_0 as well as noise floor estimation is a well-documented research topic. However in the presence of receiver limitations such as low resolution quantization process and strong interference, the previous proposed methods would be inapplicable. As discussed and evaluated in Chapter Three, the C/N_0 measurement metric definition does not necessarily represents the actual C/N_0 of the received signal in the presence of strong interference. To remove the effect of interference on the C/N_0 metric, traditional C/N_0 measurement methods can be applied after interference mitigation schemes such as simple NF algorithms. As discussed in Chapter Three, the noise floor along with interference power estimation is of a great interest to set the optimum AGC gain. The study of the C/N_0 measurement/monitoring and noise floor estimation and their errors in the presence of quantization loss and interference distortion is recommended for future work, particularly for consumer-grade receivers.

4- In this work, the main focus was on a single CW type interference signal either fixed or swept. In practical situations, there might be more than an interference source

embedded in the received signal. To mitigate multiple CW interference, multi-pole notch filter, which is based on cascading two or more one-pole complex notch filter, were proposed in Chapter Four. However, the quantization configuration and acquisition schemes were not discussed under this condition. Of course in this situation, the optimum gain of the quantizer will be different from that of the single CW interference discussed in Chapter Three.

Moreover, the study of the GNSS performance in the presence of other type of interference signals, e.g. distance measuring equipment (DME), is one of currently interesting research topics and evaluating the effect of these interference sources on quantization loss and acquisition performance is of importance.

5- It was discussed in Chapter Four that the NF-based interference mitigation algorithms can be utilized to detect interference and to activate/deactivate NF. However, the investigation lacks a theoretical approach to illustrate the detection performance of this scheme. This theoretical approach can be based on two hypotheses of interference presence and absence. To simplify the detection problem, the assumption of normal distribution of the estimated zero can be considered in order to come up with two normally distributed PDF hypotheses. However, in the presence of a quantization loss or weak interference signal, the real scenario would be deviated from this simple assumed case. The study of detection performance of the NF-based interference mitigation and related capability is considered as future work in order to remove the unnecessarily NF algorithm activation that results in desired signal distortion. Moreover, convergence

error/speed analyses in terms of required procedure time as well as steady state estimation error would be of great interest specifically for higher accuracy application.

6- To adjust the quantization configuration and to employ the new acquisition schemes, the power and frequency of the narrowband interference are required as *a priori* information. This is the case when the receiver is equipped with some interference characteristics estimation schemes or where the data decoding is being performed in offline mode. However, to verify the applicability and effectiveness of the proposed schemes specifically in the position domain, evaluation of the accuracy of interference power and frequency estimator's performance is required. As discussed in Chapter 4, the power and frequency of the interference can be estimated by investigating the error output of the NF filter. However, the accuracy of these estimates might not be adequate for the acquisition problem considered in Chapter Five. Moreover, the estimate zero is biased in the studied NF algorithms and some bias removing schemes should be considered to improve the power and frequency estimates' accuracy. That is, the development of a simple yet efficient interference characteristics/feature extraction method remains as a future work.

7- The next step in a conventional GNSS receiver toward decoding the position domain results is the tracking loops. To have better position domain results, the reception process should be optimum in terms of tracking loops' metrics. Although the detection and BER metrics were considered in this thesis, to study the receiver's performance in terms of the tracking loop metrics such as jitter and noise remains as future work. It is predictable the quantization process will have an optimum configuration in order to satisfy tracking loop

requirements. This configuration may or may not be same as an optimum configuration in terms of BER and ROC performance. The study of tracking loops performance for different signal and interference power in the presence of quantization is recommended.

8- The quantizer configuration is considered to be an odd symmetric function in this thesis. However, there are other types of quantization constellation. For example, the quantization can be implemented to be non-uniform, which shows better results at low signal quality in terms of quantization loss (Koch & Lapidoth 2013). The quantization configuration and quantizer's constellation can be adjusted simultaneously in order to recover the quantization loss.

9- In this work, no method of threshold selection was provided for the proposed *decision variable*. Indeed, the choice of a detection threshold in this case is a function of many parameters and user-defined requirements. For each decision variable presented there, there may be a different selection of parameters upon which a detection threshold may depend on and, in turn, there may be a different set of user requirements (e.g. detection & false-alarm probabilities, and mean acquisition time) against which the value may be constrained. Admittedly, knowledge of a simple, tractable or even approximate expression for this threshold would be useful to a receiver designer; however this is not the focus of the work. Rather than presenting simple design guidelines for acquisition, this thesis intended to explore the best approach to acquisition by examining and developing novel decision variables. Rather than select one detection threshold for the purpose of Monte-Carlo simulations, an entire range of thresholds was evaluated in the form of cell-level ROC curves. Moreover, to provide an extensive and realistic

performance comparison of the presented decision variables, values for this detection threshold have been computed numerically for use in system-level experiments. The development of tuning guidelines, such as the detection threshold, is beyond the scope of this work and is left for future work.

10- This work focused on showing that, depending on how much information a receiver has, a different range of schemes could be used. However, the computational burden was considered to be beyond the scope of the research. Some of the schemes may however be optimized by performing some computational enhancements (for example, sharing the code-wipe off operation or employing FFT etc., all which will have some benefits/drawbacks).

In practice, thoroughly investigating the computational complexity would also require some choices as to the platform, the silicon process, the sample-rates and the exact floating/fixed point resolution of the correlators, the target platform (ASIC, FPGA, CPU), etc. Another real complication that may arise is the fact that some schemes require more a priori information that others (for example, direct interference removal and frequency-pair acquisition schemes). Using these schemes would require the use of additional signal processing algorithms to estimate interference parameters.

11- On of the current applications of the NF filtering is frequency estimation of a noise corrupted unknown sinusoidal signal. Previous work has only considered second order FIR NF. The frequency estimation performance of the proposed adaptive FIR NF scheme presented in Chapter Four can be considered as future work in order to investigate the

improvement of the signal characteristics estimation algorithm in term of bias and mean square errors.

References

Abdizadeh, M., J. T. Curran, and G. Lachapelle (2012) "Quantization Effects in GNSS Receivers in The Presence of Interference," in *ION International Technical Meeting*, 29 January- 2 February, Newport CA

Arribas, J., P. Closas, and C. Fernandez-Prades (2013) "Antenna Array Based GNSS Signal Acquisition for Interference Mitigation," *IEEE Transactions on Aerospace and Electronic Systems*, vol 49, no 1, pp. 223 -243

ATR063 (2011) *ATR063 datasheet,* http://www.atmel.com/Images/doc4928.pdf, last accessed April, 2011

Balaei, A. T., A. G. Dempster, and D. Akos (2008) "Quantization Degradation of GNSS Signal Quality in the Presence of CW RFI," in *IEEE 10th International Symposium on Spread Spectrum Techniques and Applications,* 25-28 August, pp. 42-47

Balaei, A. T., A. G. Dempster, and L. Lo Presti (2009) "Characterization of the Effects of CW and Pulse CW Interference on the GPS Signal Quality," *IEEE Transactions on Aerospace and Electronic Systems*, vol 45, no 4, October, pp. 1418-1431

Bastide, F., D. Akos, C. Macabiau, and B. Roturier (2003) "Automatic Gain Control AGC as an Interference Assessment Tool," in *Proceedings of the 16th International Technical Meeting of the Satellite Division of The Institute of Navigation (ION GPS/GNSS 2003)*, 9 - 12 September, pp. 2042-2053, Portland, OR

Bennett, W. R. (1948) "Spectra of Quantized Signals," *Bell System Technical Journal*, vol 27, July, pp. 446–472

Berger, T. (1972) "Optimum quantizers and permutation codes," *IEEE Transactions on Information Theory*, vol 18, no 6, November, pp. 759-765

Betz, J. W. (2000) “Effect of Narrowband Interference on GPS Code Tracking Accuracy,” in *Proceedings of the 2000 National Technical Meeting of The Institute of Navigation*, January, pp. 16–27, Anaheim, Calif., USA

Borio, D. (2010) “GNSS Acquisition in the Presence of Continuous Wave Interference”, *IEEE Transactions on Aerospace and Electronic Systems*, vol 46, no 1, January, pp. 47-60

Borio, D. (2008) *A Statistical Theory for GNSS Signal Acquisition*, Doctoral Thesis, Dipartimento di Elettronica, Politecnico di Torino, Italy (Available at http://plan.geomatics.ucalgary.ca)

Borio, D., L. Camoriano, and L. L. Presti (2008) “Two-Pole and Multi-Pole Notch Filters: A Computationally Effective Solution for GNSS Interference Detection and Mitigation,” *IEEE Systems Journal*, vol 2, no 1, March, pp. 38-47

Capozza, P. T., B. J. Holland, T. M. Hopkinson, and R. L. Landrau (2000) “A single-chip narrow-band frequency-domain excisor for a global positioning system (GPS) receiver,” *IEEE Journal of Solid state Circuits*, vol 35, no 3, March, pp. 401-411

Carusone, A. and D. D. Johns (1999) "Obtaining Digital Gradient Signals for Analog Adaptive Filters," in *Proc. IEEE Int. Symp. Circuits and Systems*, vol 3, May, pp. 54-57

Chang, H. (1982) “Resampling Filtering, Sampling and Quantisation Effects on Digital Matched Filter Performance,” in *International Telemetering Conference*, pp. 889–915, San Diego

Cherniakov, M. and J. Lo (1998) "Structural correlation between signal and CW interference in the spread spectrum systems," *Global Telecommunications Conference (GLOBECOM’98)*, vol 4, pp. 2162-2167

Corazza, G. E. and C. E. Caini (2004) “DS-CDMA code acquisition in the presence of correlated fading-Part I: Theoretical aspects,” *IEEE Transactions on Communications*, vol 52, no 7, July, pp. 1160–1168

Curran, J. T. (2010) *Weak Signal Digital GNSS Tracking Algorithms*, Doctoral Thesis, National University of Ireland, Cork (Available at http://plan.geomatics.ucalgary.ca)

Curran, J. T., D. Borio, G. Lachapelle, and C. C. Murphy (2010) “Reducing Front-End Bandwidth May Improve Digital GNSS Receiver Performance,” *IEEE Transactions on Signal Processing*, vol 58, no 4, April, pp. 2399 -2404

Deshpande, S. (2004) *Study of Interference Effects on GPS Signal Acquisition*, MSc Thesis, Department of Geomatics Engineering, University of Calgary, Canada (Available at http://plan.geomatics.ucalgary.ca)

Dierendonck, A. J. V., B. W. Parkinson, and J. J. Spliker (1996) “Global Positioning System: Theory and Applications,” [Chapter 8] in *Progress in Astronautics and Aeronautics, 1st edition*, pp. 329-408

Diggelen, F. V. (2009) "A-GPS: Assisted GPS, GNSS, and SBAS," [Chapter 6] in *GNSS Technology and Applications Series, 1st edition*, Artech House, pp. 163-186

Diniz, P. S. R. (2010) *Adaptive Filtering: Algorithms and Practical Implementation, 3rd edition*, Springer, 2010

Echard, J. D. (1992) "Quantization Noise Spectrum and Radar MTI Processing," *IEEE Transactions on Aerospace and Electronic Systems*, vol 28, no 2, April, pp. 588-596

Erlandson, R. and R. Frazier (2002), "An Updated Assessment of the GNSS L1 Radio Frequency Interference Environment," in *Proceedings of ION GPS 2002*, 24-27 September, Portland OR, pp. 591-599

Fasihuddin, M. K., K. George, R. Rajesh, R. Sharma, and A. Vengadarajan (2005) "An RLS-Based Adaptive Transversal Filter for GPS Narrowband Interference Cancellation," in *28th General Assembly of International Union of Radio Science*, New Delhi, India

FireHose (2012) GNSS Firehose CDU, Novatel Inc., December

Gandhi, P. P. (1996) "Data Quantization Effects In CFAR Signal Detection," *IEEE Transactions on Aerospace and Electronic Systems*, vol 32, no 4, October, pp. 1277-1289

Giordanengo, G. (2009) Impact of Notch Filtering on Tracking Loops for GNSS Applications, Master Thesis, Facoltà di Ingegneria dell'infromazione, Politecnico di Torino

Gold, R. (1967) “Optimal binary sequences for spread spectrum multiplexing,” *IEEE Transactions on Information Theory*, vol 13, no 4, October, pp. 619-621

Gonzalez, R. C and R. E. Woods (2006) *Digital Image Processing, 3rd edition*, Prentice-Hall Inc., Upper Saddle River, NJ, USA

Gray, R. M. (1990) “Quantization noise spectra,” *IEEE Transactions on Information Theory*, vol 36, no 6, November, pp. 1220-1244

Gray, R. M. and D. L. Neuhoff (1998) “Quantization,” *IEEE Transactions on Information Theory*, vol 44, no 6, October, pp. 2325-2383

Grewal, M. S., L. R. Weill, and A. P. Andrews (2007) *Global Positioning Systems, Inertial Navigation, and Integration, 2nd edition*, Wiley-Interscience

Groves, P. D. (2005) "GPS Signal to Noise Measurement in Weak Signal and High Interference Environments," in *Proceedings of the Proceedings of ION GNSS*, 3-16 September, Long Beach, CA, pp. 643-658

Haykin, S. O. (2001) *Adaptive Filter Theory, 4th edition*, Prentice Hall

Hegarty, C. J. (2011) “Analytical Model for GNSS Receiver Implementation Losses,” in *ION International Technical Meeting*, September

Host-Madsen, A. and P. Handel (2000) “Effects of sampling and quantization on single-tone frequency estimation,” *IEEE Transactions on Signal Processing*, vol 48, no 3, March, pp. 650-662

Kaplan, E. D. and C. J. Hegarty (2006) *Understanding GPS Principles and applications, 2nd edition*, Artech House, Boston, London

Koch, T. and A. Lapidoth (2013) “At Low SNR Asymmetric Quantizers Are Better,” *IEEE Transactions on Information Theory*, June

Kondoz, A. M. (2004) *Digital Speech: Coding for Low Bit Rate Communication Systems, 2nd edition*, Wiley

Kwan, T. and K. Martin (1989) "Adaptive Detection and Enhancement of Multiple Sinusoids Using a Cascade IIR Filter," *IEEE Trans. Circuits Syst.*, vol 36, no 7, July, pp. 937-947

Lin, T., M. Abdizadeh, A. Broumandan, D. Wang, K. O’Keefe, and G. Lachapelle (2011) “Interference Suppression for High Precision Navigation Using Vector-Based GNSS software Receivers,” in *Proceedings of GNSS’11*, September, U.S. Institute of Navigation. Portland, OR

Lo, J. and M. Cherniakov (1999) “Structural Correlation between Signal and CW Interference in DS/SS Systems with Non-Linearity,” in *Mobile and Personal Satellite Communications 3rd edition*, M. Ruggieri, ed., Springer , London, pp. 409-419

Mahata, K. and T. Soderstrom (2004) “ESPRIT-like estimation of real-valued sinusoidal frequencies,” *IEEE Transactions on Signal Processing*, vol 52, no 5, May, pp. 1161-1170

Marco, D. and D. L. Neuhoff (2005) "The validity of the additive noise model for uniform scalar quantizers," *IEEE Transactions on Information Theory*, vol 51, no 5, May, pp. 1739-1755

MATLAB (2013) *Periodogram power spectral density estimate*, http://www.mathworks.com/help/signal/ref/periodogram.html, last accessed August, 2013

Misra, P. and P. Enge (2010) *Global Positioning System, Signals, Measurements and Performance, 2nd edition*, Lincoln, Ganga-Jamuna Press, MA, December

Mitch, R. H., R. C. Dougherty, M. L. Psiaki, S. P. Powell, and B. W. O'Hanlon (2011) "Signal Characteristics of Civil GPS Jammers," in *Proceedings of GNSS'11*, September, U.S. Institute of Navigation. Portland, OR

Montloin, L. (2010) *Impact of Interference Mitigation Techniques on a GNSS Receiver*, MSc Thesis, Memoire de fin d'Etudes, Ecole Nationale de l'Aviation Civile, Toulouse (Available at http://plan.geomatics.ucalgary.ca)

Ndili, A. and P. Enge (1998) "GPS Receiver Autonomous Interference Detection," in *IEEE Position, Location and Navigation Symposium - PLANS'98*, April, Palm Springs, California, pp. 123-130

National Instruments (2013) http://www.ni.com/products/, last accessed July 25, 2013

Nishimura, S. and H. Y. Jiang (1998) "Simplified realization of cascaded adaptive notch filters using complex coefficients," in *Proceedings of the IEEE International Symposium on Circuits and Systems, ISCAS'98*, May, pp. 269-272

O'Driscoll, C. (2007) *Performance analysis of the parallel acquisition of weak GPS signals*, Doctoral Thesis, Department of Electrical and Electronic Engineering, National University of Ireland, Cork

Oppenheim, A. V. and R. W. Schafer (2009) *Discrete-Time Signal Processing, 3rd edition*, Prentice Hall, August

Pantazis, Y., O. Rosec, and Y. Stylianou (2010) "Iterative estimation of sinusoidal signal parameters," *IEEE Signal Processing Letters*, vol 17, no 5, May, p. 461-464

Parkinson, B. W. and J. J. Spilker (1996) *Global Positioning System: Theory and Applications, 1st edition*, American Institute of Aeronautics, 1996, vol 1

Pauluzzi, D. R. and N. C. Beaulieu (2000) "A Comparison of SNR Estimation Techniques for the AWGN Channel," *IEEE Transactions on Communications*, vol 48, no 10, October, pp. 1681-1691

Petovello, M. G., C. O'Driscoll, G. Lachapelle, D. Borio , and H. Murtaza (2008) "Architecture and Benefits of an Advanced GNSS Software Receiver," *Journal of Global Positioning Systems*, vol 7, no 2, pp. 156-168

Poisel, R. (2011) *Modern communications jamming principles and techniques,* 1st ed., Artech House, Boston, Massachusetts

Proakis, J. G. and M. Salehi (2007) *Digital Communications, 3rd edition*, McGraw Hill International Editions, November

Punchalard, R. (2012) "Mean square error analysis of unbiased modified plain gradient algorithm for second-order adaptive IIR notch filter," *Signal Processing*, vol 92, no 11, November, pp. 2815-2820

Punchalard, R., J. Koseeyaporn, and P. Wardkein (2009) "Adaptive IIR notch filter using a modified sign algorithm," *Signal Processing*, vol 89, no 2, February, pp. 239-243

Sarantel (2010) *Miniature Embedded GPS Antenna*, http://www.sarantel.com/products/index.php, last accessed August 5, 2010

Satyanarayana, S. (2011) *GNSS Channel Characterization and Enhanced Weak Signal Processing*, Doctoral Thesis, Department of Geomatics Engineering, University of Calgary, Canada (Available at http://plan.geomatics.ucalgary.ca)

Savasta, S., L. Lo Presti, and M. Rao (2013) "Interference Mitigation in GNSS Receivers by a Time-Frequency Approach," *IEEE Transactions on Aerospace and Electronic Systems*, vol 49, no 1, January, pp. 415-438

Sharawi, M. S., D. M. Akos, and D. N. Aloi (2007) "GPS C/N_0 estimation in the presence of interference and limited quantization levels," *IEEE Transactions on Aerospace and Electronic Systems*, vol 43, no 1, January, pp. 227-238

SiRF *GSC2x* (2011) *SiRF GSC2x specifications*, http://www.bgc.de/kunden/sirf/SiRFstarIIGSC.pdf, last accessed April, 2011

Smith, S. (2002) *Digital Signal Processing: A Practical Guide for Engineers and Scientists, 3rd edition*, Newnes, November

Soderstrand, M. A., T. G. Johnson, R. H. Strandberg, H. H. Loomis, and K. V. Rangarao (1997) "Suppression of multiple narrow-band interference using real-time adaptive notch filters," *IEEE Transactions on Circuits and Systems II: Analog and Digital Signal Processing*, vol 44, no 3, March, pp. 217-225

Spirent (2008) Spirent Communications Plc. SimGEN, User Manual

Songtao, L. and S. Jinping (2010) "A novel adaptive interference mitigation approach based on space time processing for global navigation system receiver arrays," in *IEEE 10th International Conference on Signal Processing (ICSP)*, 24-28 October, pp. 369-372

Thompson, R. J. R., E. Cetin, and A. G. Dempster (2011) "Detection and Jammer-to-Noise Ratio Estimation of Interferers Using the Automatic Gain Control," *International Global Navigation Satellite Systems Society IGNSS Symposium*, 15-17 September, Sydney, NSW, Australia

Tsui, J. (2004) *Fundamentals of Global Positioning System Receivers: A Software Approach, 2nd edition*, Wiley Series in Microwave and Optical Engineering, December

Wang, Y.-C. and L. B. Milstein (1988) "Rejection of multiple narrow-band interference in both BPSK and QPSK DS spread-spectrum systems," *IEEE Transactions on Communications*, vol 36, no 2, February, pp. 195-204

Widrow, B. and I. Kollar (2008) *Quantization noise- roundoff error in digital computation, signal processing, control, and communications,* Cambridge University Press, Cambridge, UK

Widrow, B., I. Kollar and M. C. Liu (1996) "Statistical Theory of Quantization," *IEEE Transactions of Instrumentations and Measurement*, vol 45, no 2, April, pp. 353-361

Zhe, H., C. Zhai, and X. Zhan (2008) "Signal Quantization Effects on Acquisition Process of GPS Receiver: The Analysis and Simulation," in *Congress on Image and Signal Processing (CISP'08)*, 27-30 May, pp. 197-200

Ziemer, R. E., R. L. Peterson, and D. E. Borth (1995) *Introduction to Spread Spectrum Communications, 1st edition*, Prentice Hall, Upper Saddle River, NJ, USA, March

Appendix A: Interference Sources Present in The GPS Band

Navigation solution reliability of a GPS receiver is strongly limited by radio frequency interference and jammers (Kaplan & Hegarty 2006). Radio frequency transmitters and their harmonics near the GNSS frequencies can cause unintentional interference. In the literature, interference sources are categorized in two different classes: intentional interference, e.g. jammers, and unintentional sources such as TV/FM/Radar emitters and Distance Measuring Equipment (DME)/ Tactical Air Navigation (TACAN) transceivers (Parkinson & Spilker 1996, Poisel 2011). A strong interference at the input of a GNSS receiver may adversely affect the performance, continuity, and integrity of receiver operation in different applications such as vehicle and pedestrian navigation, aviation and high precision surveying. Interference signals can be mainly categorized into four classes based on their statistical, spectral, and temporal characteristics as 1- Narrowband Gaussian interference, 2- Continuous Wave Interference, 3- Pulsed interference and 4- Swept interference (Poisel 2011).

A.1 Continuous Wave Interference

An undesired signal transmitted at a single frequency is considered as CW tone interference. CW interference causes degradation in the receiver performance by overcoming the processing gain of GNSS systems (Poisel 2011). A carrier tracking loop may lock onto the CW frequency and provide incorrect carrier phase and Doppler measurements (Deshapande 2004). This kind of interference is generated by intentional CW jammers or near-band unmodulated transmitter's carriers (Kaplan & Hegarty 2006).

A.2 Swept CW Interference

Swept interference is a narrowband signal which scans in time across a certain frequency band. Due to covering larger frequency band and Doppler frequencies, this kind of interference causes more deleterious effects than CW interference.

A.3 AM/FM Interference

The AM and FM radio transmitter signals broadcast high order harmonics close to the GPS L1 frequency and cause interference. These harmonics causes non-linear effect in the receiver. The strongest interference is the 15 to 18 order harmonics of the FM signal (Erlandson and Fraizer 2002).

Bauernfeind et al (2011) studied various types of in-car jammers within GPS bandwidth. An in-car jammer is an intentional jammer transmitting a high power, -10 to -20 dBm, fixed/swept narrowband continuous wave and chirp signal in the E1/L1 band. The bandwidth of these jammers is 0.1 – 50 MHz with a center frequency of 1575.42 ± 1 MHz. All of these jammers have linear and positive sweep function with different signal power, bandwidth, sweep time, and temperature characteristics. Only a few of them employ CW. These jammers degrade the carrier and tracking loop performance of the receiver until complete loss of lock.

Mitch et al (2011) investigates 18 commercially available GPS jammers based on experimental results. These devices were categorized into three groups 1- Cigarette Lighter Jammers, 2-SMA Battery Jammers, and 3-NonSMA-Battery Jammers.

Furthermore, the swept characteristics and mean power seen in the GPS L1/L2 band were measured and discussed. All the jammers generate saw tooth pattern swept interference signals with varying amplitude. Table A-1 summarizes the test results of 18 jammers of different groups reported in Mitch et al (2011).

Table A-1: Characteristics of the GPS jammers (Mitch et al 2011)

Group Number	Jammer Number	L1 Sweep Period (ms)	L1 Sweep Period (L1+/-MHz)	Power in band (mW) for 2MHz BW
1	4	26, 27, 9, 9	31.3/25.4, 31.3/31.3, 8.6/5.4, 9.6/4.4	1.7, 0.1, 5.8, 7.0
2	10	9, 12, 9, 9, 9, 1 9, 8, 9, 9	11.6/7.4, 19.6 / 21.4, 7.6 / 6.4, 6.6 / 9.4, 5.6/8.4, over/over, 5.6/6.4, 17.6/-5.6, 18.6/-4.6, 7.6 / 6.4	15, 6.3, 150, 87, 159, 1.2, 244, 0.00, 0.00, 18
3	4	9, 8, 9, 9	3.6/13.4, over/over, -5.4/16.4, 10.6/8.4	1.18, 0.01, 0.00, 1.39

Appendix B: Configuration of a Typical GPS Receiver

In this thesis, consumer grade GNSS receivers are considered due to their popularity and application. Consumer grade receivers are generally equipped with a low resolution quantizer and low sampling rate. One such example is the ANTARIS single-chip, ATR063 (ATR063 2011). The ATR063 is designed for use in mobile applications. This chip is employed in the Ublox 5 due to its low power consumption. It uses a 1.5-bit quantizer and a sampling frequency of 23.104 MHz with size of tiny 7 mm × 10 mm (ATR063 2011).

The Garmin 60Cx is equipped with a SiRF chipset (SiRF GSC2x 2011). The SiRF GSC2x chip employs one or two bit quantization with control gain up to 50 dB. A new version of this chipset, the SiRF Star IV GSD 4e GPS chipset, uses 2- or 4-bit quantizer with a sampling rate of about 8 MHz.

In this thesis, a realistic 2 MHz bandwidth consumer grade GPS receiver with a 1- to 4-bit quantizer resolution and sampling rate of 8 MHz is considered.

Appendix C: Coherent SINR for a 1-bit Quantizer

The expected value of $r_1[n]$ can be written as

$$\begin{aligned}\mathrm{E}[r_1[n]] = \frac{-1}{\sqrt{2\pi\sigma_n^2}}\int_{-s[n]-i[n]}^{s[n]-i[n]} \exp\left\{-\frac{z^2}{\sigma_n^2}\right\} dz \\ + \frac{1}{\sqrt{2\pi\sigma_n^2}}\int_{-s[n]+i[n]}^{s[n]+i[n]} \exp\left\{-\frac{z^2}{\sigma_n^2}\right\} dz\end{aligned} \tag{C.1}$$

Following a similar procedure to that of (Borio 2008), Chapter 6, Eq. (C.1) can be approximated by

$$\mathrm{E}[r_1[n]] \approx 2s[n]\frac{1}{\sqrt{2\pi\sigma_n^2}}\mathrm{E}\left[e^{-\frac{(i[n])^2}{2\sigma_n^2}}\right] \tag{C.2}$$

Using a similar procedure, the variance of $r_1[n]$ can be approximated as

$$\mathrm{Var}[r_1[n]] = \mathrm{E}[r_1^2[n]] - \mathrm{E}\big[r_1[n]\big]^2 \approx \mathrm{E}[1] - \frac{s^2[n]}{\pi\sigma_n^2}\mathrm{E}\left[e^{-\frac{(i[n])^2}{2\sigma_n^2}}\right] \tag{C.3}$$

The coherent SINR for 1-bit quantizer is given by

$$\rho_1 = \frac{\left(\mathrm{E}\left[\frac{1}{N}\sum_{n=0}^{N-1} r_1[n]h[n]\right]\right)^2}{\mathrm{Var}\left[\frac{1}{N}\sum_{n=0}^{N-1} r_1[n]h[n]\right]} \tag{C.4}$$

After some simplification, the numerator of Eq. (C.4) can be written as

$$\begin{aligned}\mathrm{E}\left[\frac{1}{N}\sum_{n=0}^{N-1} r_1[n]h[n]\right] &= \frac{2A_s}{N\sqrt{2\pi\sigma_n^2}}\sum_{n=0}^{N-1} c^2[n]\ \mathrm{E}\left[e^{-\frac{(i[n])^2}{2\sigma_n^2}}\right] \\ &= \frac{A_s}{\sqrt{2\pi\sigma_n^2}}\ \mathrm{E}\left[e^{-\frac{(i[n])^2}{2\sigma_n^2}}\right]\end{aligned} \tag{C.5}$$

and, the denominator can be written as

$$\mathrm{Var}\left[\frac{1}{N}\sum_{n=0}^{N-1} r_1[n]h[n]\right] = \frac{1}{N^2}\sum_{n=0}^{N-1} \mathrm{E}[r_1^2[n]|h[n]|^2] - E\left[\frac{1}{N}\sum_{n=0}^{N-1} r_1[n]h[n]\right]^2 \qquad \text{(C.6)}$$

If it is now assumed that successive samples of $r_1[n]$ are independent and it is assumed that $A_s/\sigma_n << 1$, then

$$\mathrm{Var}\left[\frac{1}{N}\sum_{n=0}^{N-1} r_1[n]h[n]\right] = \frac{1}{N^2}\sum_{n=0}^{N-1} \mathrm{c}^2[\mathrm{n}] - \left\{\frac{A_s}{\sqrt{2\pi\sigma_n^2}}\,\mathrm{E}\left[e^{-\frac{(i[n])^2}{2\sigma_n^2}}\right]\right\}^2 \approx \frac{1}{2N} \qquad \text{(C.7)}$$

And, from Appendix D, the coherent SINR for 1-bit quantizer is given by

$$\rho_1 = 2N\left\{\frac{A_s}{\sqrt{2\pi\sigma_n^2}}\,\mathrm{E}\left[e^{-\frac{(i[n])^2}{2\sigma_n^2}}\right]\right\}^2 = \frac{NA_s^2}{\pi\sigma_n^2}e^{-\frac{A_{\mathrm{int}}^2}{2\sigma_n^2}}I_0\left(\frac{A_{\mathrm{int}}^2}{4\sigma_n^2}\right)^2 \qquad \text{(C.8)}$$

Of course, in the absence of interference, the assumption that successive samples of $r_1[n]$ are independent is valid. As the power of the interference signal increases, however, samples of $r_1[n]$ become more correlated and this assumption becomes invalid, leading to inaccuracies in the prediction of the coherent SINR. This issue is discussed in the body of the thesis.

Appendix D: Calculation of Eq. (C.7)

If a narrowband CW interference is defined as:

$$i[n] = A_{\text{int}}\sin(2\pi f_{\text{int}} nT_s + \theta) \tag{D.1}$$

where θ is a random variable uniformly distributed on the interval [-π, π), then the following expected value can be written as

$$\mathrm{E}\left[e^{-\frac{(i[n])^2}{2\sigma_n^2}}\right] = \frac{1}{2\pi}\int_{\theta=-\pi}^{\pi} e^{-\frac{(i[n])^2}{2\sigma_n^2}}\,d\theta \tag{D.2}$$

which, after some simplification, reduces to

$$\mathrm{E}\left[e^{-\frac{(i[n])^2}{2\sigma_n^2}}\right] = \frac{e^{-\frac{A_{\text{int}}^2}{4\sigma_n^2}}}{2\pi}\int_{\theta=-\pi}^{\pi} e^{-\frac{A_{\text{int}}^2}{4\sigma_n^2}\cos(4\pi f_{\text{int}} nT_s + 2\theta)}\,d\theta \tag{D.3}$$

Recognizing the identity of the modified Bessel function of first kind, this simplifies further to

$$\mathrm{E}\left[e^{-\frac{(i[n])^2}{2\sigma_n^2}}\right] = e^{-\frac{A_{\text{int}}^2}{4\sigma_n^2}} I_0\left(\frac{A_{\text{int}}^2}{4\sigma_n^2}\right) \tag{D.4}$$

Appendix E: N^{th} Order One-Pole Adaptive IIR Notch Filter

The transfer function of one-pole N^{th} order IIR single notch frequency filter can be expressed as

$$H_{\mathrm{N-IIR}}(z) = \left(\frac{1 - z_0 z^{-1}}{1 - \rho z_0 z^{-1}}\right)^N \tag{E.1}$$

where z_0 is a complex number on unit circle and determines the notch frequency. The parameter ρ is the pole contraction factor and is less than one. The structure of the adaptive IIR notch filter is depicted in Figure E.1. As seen, this filter represents an autoregressive moving average (ARMA) structure composed of two blocks, namely 1- autoregressive (AR) and 2- moving average (MA) given by

$$H_{\mathrm{MA}}(z) = (1 - z_0 z^{-1})^N$$

$$H_{\mathrm{AR}}(z) = \frac{1}{(1 - \rho z_0 z^{-1})^N} \tag{E.2}$$

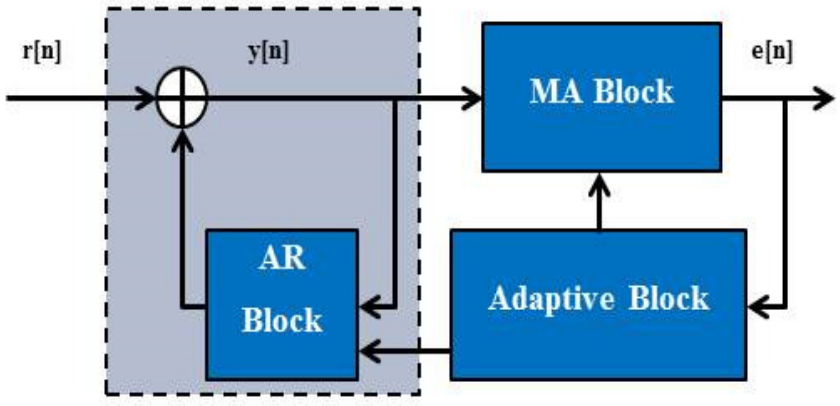

Figure E.1: Block diagram of adaptive IIR notch filter (Borio 2008)

E.1 The Adaptive Criterion

The adaptation block is considered to adaptively estimate and adjust the parameters of the IIR filter. This adaptation is performed based on minimizing the cost function given by

$$J[\mathrm{k}] = \mathrm{E}\big[e[k]e^{*}[k]\big] \tag{E.3}$$

where $e[k]$ is the filter output. Here, the cost function is defined as the energy of the output of the filter. The only free parameter for which minimization should be performed with respect to it is the notch filter's zero, which is a complex parameter. Again, an LMS algorithm is employed to iteratively minimize the cost function. The update for the parameter z_0 is given by the iterative rule of the LMS method as

$$\hat{z}_0[k+1] = \hat{z}_0[k] - \mu e[k]\left[\sum_{i=1}^{N} i\binom{N}{i}(-\hat{z}_0^{*})^{i-1}y^{*}[k-i]\right] \tag{E.4}$$

where μ is the LMS step size and $y[k]$ is shown in Figure E.1. The LMS step size parameter, μ, controls the convergence and accuracy characteristics of the LMS method and should be accurately chosen to have a proper convergence speed as well as a precise notch frequency estimation provided by LMS algorithm.

E.2 Bandwidth and Attenuation

Assume that estimate zero in the steady state can be written as $z_0 = Ze^{j\omega_{\mathrm{int}}}$. To find the minimum and maximum values of $|H(z)|$, the derivative of the function should be evaluated and be set equal to zero as

$$\frac{\partial}{\partial\omega}H_{\mathrm{N-IIR}}\big(Ze^{j\omega}\big) = 0 \tag{E.5}$$

For simplicity sake, we can use $|H(z)|^2$ as

$$\frac{\partial}{\partial\omega}\left(\frac{1-2Z\cos(\omega-\omega_{\text{int}})+Z^2}{1-2Z\rho\cos(\omega-\omega_{\text{int}})+Z^2}\right)^N=0 \tag{E.6}$$

which simplifies to

$$\sin(\omega-\omega_{\text{int}})=0 \tag{E.7}$$

The solution of this equation is given by

$$\omega=\omega_{\text{int}} \quad \text{or} \quad \omega=\omega_{\text{int}}+\pi \tag{E.8}$$

The maximum and minimum of $|H(z)|$ are therefore given respectively by

$$\begin{aligned} A_{\max} &= \left|H_{\text{N-IIR}}\left(z=Ze^{j(\omega_{\text{int}}+\pi)}\right)\right|=\left(\frac{1+Z}{1-\rho Z}\right)^N \\ A_{\min} &= \left|H_{\text{N-IIR}}\left(z=Ze^{j\omega_{\text{int}}}\right)\right|=\left(\frac{1-Z}{1-\rho Z}\right)^N \end{aligned} \tag{E.9}$$

Generally, the minimum values specify the attenuation of the filter. Figure E.2 shows the filter attenuation, i.e. $A_{\max}/A_{\min}$, for different values of *N* for given pole contraction factor $\rho = 0.9$. As can be seen, the filter attenuation increases as *N* increases.

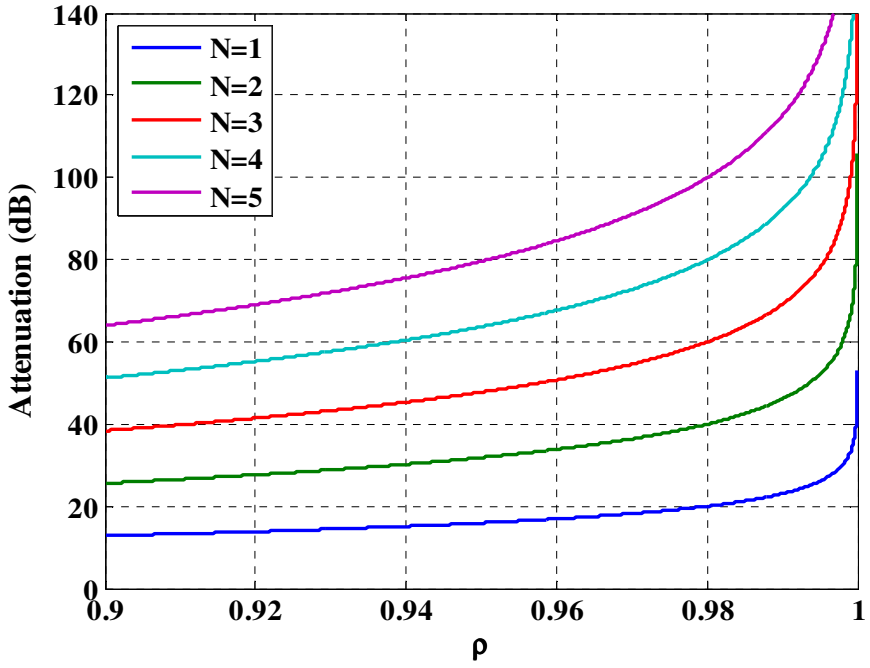

Figure E.2: Filter Attenuation for different values of *N*

To calculate the 3-dB bandwidth (BW), the solution of the following equation should be derived:

$$\left|H_{\mathrm{N-IIR}}\left(Ze^{j\omega}\right)\right|^2 = \frac{1}{2}A_{\max}^2 \tag{E.10}$$

After some simplifications, we have

$$\left(\frac{1-2Z\cos(\Delta\omega)+Z^2}{1-2Z\rho\cos(\Delta\omega)+Z^2}\right)^N = \frac{1}{2}\left(\frac{1+Z}{1+\rho\mathrm{Z}}\right)^{2N} = T^N \tag{E.11}$$

where

$$T = \frac{1}{\sqrt[N]{2}}\left(\frac{1+Z}{1+\rho\mathrm{Z}}\right)^2 \tag{E.12}$$

Then, if $\rho < \mathrm{Z}$, it can be written that

$$\cos(\Delta\omega) = \frac{T + T\rho^2 \mathrm{Z}^2 - 1 - Z^2}{2T\rho\mathrm{Z} - 2\mathrm{Z}} \tag{E.13}$$

As known, $\omega \approx \omega_{\mathrm{int}}$, and then $\Delta\omega \cong 0$. Hence, the approximation of cosine, i.e. $\cos(\Delta\omega) = 1 - 0.5\Delta\omega^2$, can be employed. Therefore, Eq. (E.13) can be expressed as

$$\Delta\omega^2 = 2 - \frac{T + T\rho^2 \mathrm{Z}^2 - 1 - Z^2}{T\rho\mathrm{Z} - \mathrm{Z}} \tag{E.14}$$

Or equivalently

$$\Delta\omega = \pm\sqrt{2 - \frac{T + T\rho^2 \mathrm{Z}^2 - 1 - Z^2}{T\rho\mathrm{Z} - \mathrm{Z}}} \tag{E.15}$$

Finally, the 3-dB bandwidth can be written as

$$BW = \frac{\Delta\omega_2 - \Delta\omega_1}{2\pi} = \frac{1}{\pi}\sqrt{2 - \frac{T + T\rho^2 \mathrm{Z}^2 - 1 - Z^2}{T\rho\mathrm{Z} - \mathrm{Z}}}. \tag{E.16}$$

For $\mathrm{Z} = 1$, Eq. (E.12) and Eq. (E.16) can be written as

$$\begin{aligned} T &= \frac{1}{\sqrt[N]{2}}\left(\frac{2}{1+\rho}\right)^2 \\ BW &= \frac{2}{\pi}\sqrt{\frac{(1-\rho)^2}{\sqrt[N]{2}(1+\rho)^2 - 4\rho}} \end{aligned} \tag{E.17}$$

which, for $N = 1$, simplifies to

$$BW = \frac{|1-\rho|}{\pi} \times \sqrt{\frac{2}{1+\rho^2}} \approx \frac{|1-\rho|}{\pi} \tag{E.18}$$

This is the same formula as given in Borio (2008).

Appendix F: Adaptive Linear-Phase FIR Notch Filter Impulse Response Function

To derive one-pole linear-phase adaptive complex FIR notch filter according to one-pole IIR notch filter, a finite number of IIR notch filter impulse response coefficients can be considered. The impulse response of complex IIR notch filter is given by

$$\frac{1 - z_0 z^{-1}}{1 - \rho z_0 z^{-1}} = (1 - z_0 z^{-1}) \sum_{n=0}^{\infty} (\rho z_0 z^{-1})^n \tag{F.1}$$

By keeping N significant terms of right expression, the transfer function of FIR notch filter can be written as

$$H_{\mathrm{FIR}}(z) = (1 - z_0 z^{-1}) \sum_{n=0}^{N-1} (\rho z_0 z^{-1})^n \tag{F.2}$$

After simplification, the transfer function can be expressed as

$$H_{\mathrm{FIR}}(z) = 1 + \sum_{n=0}^{N-1} (\rho^n - \rho^{n-1}) z_0^n z^{-n} - \rho^{N-1} z_0^{N-1} z^{-N} \tag{F.3}$$

where $H_{\mathrm{FIR}}(z)$ is the z-impulse response of the complex FIR filter.

In addition, in order to have a linear-phase FIR filter with a similar amplitude response to Eq. (F.3), the z-transfer function is given by using backward-forward filtering and can be applied as (Montloin 2010)

$$H_{\mathrm{LP-FIR}}(z) = H_{\mathrm{FIR}}(z)(H_{\mathrm{FIR}}(z^{*-1}) z^{*-N})^* \tag{F.4}$$

As can be seen, the second multiplication part in right term of Eq. (A.4) is a paraconjugate of first term. Moreover, the transfer function of the LP-FIR filter can be written using Eq. (4.2) as

$$H_{\mathrm{LP-FIR}}(z) = \left\{1 + \sum_{n=0}^{N-1} (\rho^n - \rho^{n-1}) z_0^n z^{-n} - \rho^{N-1} z_0^{N-1} z^{-N}\right\} \times \left\{1 + \sum_{n=0}^{N-1} (\rho^n - \rho^{n-1}) z_0^n z^n - \rho^{N-1} z_0^{N-1} z^N\right\} z^{-N} \tag{F.5}$$

And, Eq. (F.5) can be rewritten as

$$H_{\mathrm{LP-FIR}}(z) = \sum_{n=0}^{N} \sum_{m=0}^{N} \alpha_n \alpha_m z_0^n z_0^{*m} z^{-N-n+m} \tag{F.6}$$

where the coefficients α are given by Eq. (4.4).

Appendix G: Zero Update Equation for Adaptive Linear-Phase FIR Notch Filter

To find the adaptive LMS solution for Eq. (E.6), the error, $\mathrm{e}[k]$, and the cost function, *J*, are defined as

$$e[k] = x[k] \bigstar h[k] \tag{G.1}$$

$$J[\mathrm{k}] = \mathrm{E}[|e[k]|^2] \tag{G.2}$$

To minimize this cost function, the adaptation algorithm based on the Gradient algorithm is given by (Haykin 2001)

$$\hat{z}_0[k+1] = \hat{z}_0[k] - \mu \nabla_{z_0}\{|J|\} = \hat{z}_0[k] - \mu \left\{ \frac{\partial |e[k]|^2}{\partial z_0^*} \right\} \tag{G.3}$$

$$\hat{z}_0[k+1] = \hat{z}_0[k] - \mu \left\{ \frac{\partial |e[k]|^2}{\partial e^*[k]} \frac{\partial e^*[k]}{\partial z_0^*} \right\} \tag{G.4}$$

$$\hat{z}_0[k+1] = \hat{z}_0[k] - \mu e[k] \left\{ \frac{\partial e^*[k]}{\partial z_0^*} \right\} \tag{G.5}$$

$$\hat{z}_0[k+1] = \hat{z}_0[k] - \mu e[k] \left\{ \frac{\partial x[k] \bigstar h[k]}{\partial z_0} \right\}^* \tag{G.6}$$

After taking the derivative with respect to z_0, the update equation of the adaptation algorithm is given by

$$\hat{z}_0[k+1] = \hat{z}_0[k] - \mu e[k] \left\{ x[k] \bigstar \frac{\partial h[k]}{\partial z_0} \right\}^* \tag{G.7}$$

Interestingly, for high values of the filter order, *N*, the IIR corresponding adaptation model can be employed and is given by (Borio 2008)

$$\hat{z}_0[k+1] = \hat{z}_0[k] - \mu e[k] \left\{ \frac{\partial e[k]}{\partial z_0} \right\}^* \tag{G.8}$$

This decreases the computational complexity of the algorithm.

Appendix H: Wiener Solution for Adaptive FIR-NF

For an FIR notch filter, inserting Eq. (4.3) into Eq. (4.13) and using Eq. (4.14), Eq. (4.13) can be simplified to

$$\mathrm{E}\left[(x[k]\bigstar h[k])\left(x[k]\bigstar \frac{\partial h[k]}{\partial z_0}\right)^*\right]=0 \tag{H.1}$$

Each term in the bracket of Eq. (H.1) can be written as

$$x[k]\bigstar h[k]=\sum_{i=0}^{n}\Lambda_n\eta[k-i]+A_{\mathrm{int}}\sum_{i=0}^{n}\Lambda_n e^{j(2\pi(k-i)f_{\mathrm{int}}+\theta_{\mathrm{int}})} \tag{H.2}$$

$$x[k]\bigstar \frac{\partial h[k]}{\partial z_0}=\sum_{i=0}^{n}\Psi_n\eta[k-i]+A_{\mathrm{int}}\sum_{i=0}^{n}\Psi_n e^{j(2\pi(k-i)f_{\mathrm{int}}+\theta_{\mathrm{int}})} \tag{H.3}$$

Eq. (H.1) is presented as

$$\begin{aligned}&\mathrm{E}\left[(\eta[k]\bigstar h[k])\left(\eta[k]\bigstar \frac{\partial h[k]}{\partial z_0}\right)^*\right]\\&\qquad+\mathrm{E}\left[(i[k]\bigstar h[k])\left(i[k]\bigstar \frac{\partial h[k]}{\partial z_0}\right)^*\right]=0\end{aligned} \tag{H.4}$$

$$\Rightarrow\ \sigma_n^2\sum_{i=0}^{n}\Lambda_n\Psi_n+\mathrm{E}\left[(i[k]\bigstar h[k])\left(i[k]\bigstar \frac{\partial h[k]}{\partial z_0}\right)^*\right]=0 \tag{H.5}$$

In a convergence regime, the following can be written

$$\hat{z}_0=Ze^{j2\pi f_{\mathrm{int}}} \tag{H.6}$$

By inserting Eq. (H.6) in Eq. (H.2), Eq. (H.2) can be rewritten as

$$i[k]\bigstar h[k]=A_{\mathrm{int}}e^{j(2\pi kf_{\mathrm{int}}+\theta_{\mathrm{int}})}\left(1+(1-\rho^{-1})\sum_{i=1}^{N-1}(\rho Z)^i-\rho^{N-1}Z^N\right) \tag{H.7}$$

which simplifies to

$$i[k]\bigstar h[k] = A_{\text{int}}e^{j(2\pi k f_{\text{int}}+\theta_{\text{int}})}\left(1+(\rho-1)\frac{1-(\rho Z)^{N-1}}{1-\rho Z}Z-\rho^{N-1}Z^{N}\right) \tag{H.8}$$

The gradient output signal due to interference can be written as

$$i[k]\bigstar g[k] = A_{\text{int}}e^{j(2\pi k f_{\text{int}}+\theta_{\text{int}})}e^{-j2\pi f_{\text{int}}} \times\left(\frac{(1-\rho^{-1})}{Z}\sum_{i=1}^{N-1} i(\rho Z)^{i}-N(\rho Z)^{N-1}\right) \tag{H.9}$$

which is simplified to

$$i[k]\bigstar g[k] = A_{\text{int}}e^{j(2\pi k f_{\text{int}}+\theta_{\text{int}})}e^{-j2\pi f_{\text{int}}} \times\left((\rho-1)\frac{1-(N+1)(\rho Z)^{N}-N(\rho Z)^{N-1}}{(1-\rho Z)^{2}}-N(\rho Z)^{N-1}\right) \tag{H.10}$$

The first term of Eq. (D.5) can be written as

$$\sigma_n^2\sum_{i=0}^{n}\Lambda_n\Psi_n = \sigma_n^2\hat{z}_0^{*}\left((1-\rho^{-1})\sum_{i=1}^{N-1} i(\rho Z)^{2i}+N\frac{(\rho Z)^{2N}}{\rho^{2}}\right) \tag{H.11}$$

After simplification, the following can be written

$$\sigma_n^2\textstyle\sum_{i=0}^{n}\Lambda_n\Psi_n = \sigma_n^2\hat{z}_0^{*}\left((\rho-1)^{2}\frac{1-(N+1)(\rho Z)^{2N}-N(\rho Z)^{2N-2}}{(1-\rho^{2}Z^{2})^{2}}+N\frac{(\rho Z)^{2N}}{\rho^{2}}\right) \tag{H.12}$$

For $N \gg 1$, high order terms can be discarded, and Eq. (H.5) can be expressed as

$$\sigma_n^2 Z\frac{(\rho-1)^{2}}{(1-\rho^{2}Z^{2})^{2}}+A_{\text{int}}^{2}\left(1+\frac{\rho-1}{1-\rho Z}Z\right)\left(\frac{\rho-1}{(1-\rho Z)^{2}}\right)=0 \tag{H.13}$$

Or simply,

$$\frac{\sigma_n^2}{A_{\text{int}}^{2}}\frac{Z(\rho-1)}{(1+\rho Z)^{2}}+\left(\frac{1-Z}{1-\rho Z}\right)=0 \tag{H.14}$$

By defining γ as

$$\gamma = \frac{A_{\text{int}}^2}{\sigma_n^2(1-\rho)} \tag{H.15}$$

Eq. (H.14) can be written as

$$\rho Z^2 - (1+4\gamma)Z + 4\gamma = 0 \tag{H.16}$$

which has a solution in (0, 1] as

$$Z = \frac{1+4\gamma - \sqrt{(1+4\gamma)^2 - 16\rho\gamma}}{2\rho} \tag{H.17}$$

And the Wiener solution for the FIR notch filter is given by

$$Z_{0,\text{Wiener}}^{\text{FIR}} = \frac{1+4\gamma - \sqrt{(1+4\gamma)^2 - 16\rho\gamma}}{2\rho} e^{j2\pi f_{\text{int}}}. \tag{H.18}$$

Appendix I: Wiener Solution for Adaptive Linear-Phase FIR NF

In this case, each terms of Eq. (H.1) can be written as

$$x[k]\bigstar h_{\mathrm{LP}}[k] = \sum_{n=0}^{N}\sum_{m=0}^{N}\alpha_n\alpha_m z_0^n z_0^{*m}\eta[k-N+n-m] + A_{\mathrm{int}}\sum_{n=0}^{N}\sum_{m=0}^{N}\alpha_n\alpha_m z_0^n z_0^{*m}e^{j(2\pi(k-N+n-m)f_{\mathrm{int}}+\theta_{\mathrm{int}})} \tag{I.1}$$

and

$$\begin{aligned} &x[k]\bigstar g_{\mathrm{LP}}[k] \\ &= \sum_{n=0}^{N}\sum_{m=0}^{N} n\alpha_n\alpha_m z_0^{n-1} z_0^{*m}\eta[k-N+n-m] \\ &+ A_{\mathrm{int}}\sum_{n=0}^{N}\sum_{m=0}^{N} n\alpha_n\alpha_m z_0^{n-1} z_0^{*m}e^{j(2\pi(k-N+n-m)f_{\mathrm{int}}+\theta_{\mathrm{int}})} \end{aligned} \tag{I.2}$$

Thus, Eq. (H.1) is represented as

$$\mathrm{E}[(\eta[k]\bigstar h_{\mathrm{LP}}[k])(\eta[k]\bigstar g_{\mathrm{LP}}[k])^*] + \mathrm{E}[(i[k]\bigstar h_{\mathrm{LP}}[k])(i[k]\bigstar g_{\mathrm{LP}}[k])^*] = 0 \tag{I.3}$$

The first term in Eq. (H.3) can be approximately expressed as

$$\begin{aligned} &\mathrm{E}[(\eta[k]\bigstar h_{\mathrm{LP}}[k])(\eta[k]\bigstar g_{\mathrm{LP}}[k])^*] \\ &= \frac{\sigma_n^2}{z_0^*}\sum_{n=0}^{N}\sum_{m=0}^{N}\sum_{i=0}^{N}\sum_{j=0}^{N} n\alpha_n\alpha_m\alpha_i\alpha_j z_0^{n-1} z_0^{*m} Z^{n+m+i+j} \\ &\approx \frac{\sigma_n^2}{z_0^*}\sum_{n=0}^{N}\sum_{m=0}^{N} n(\rho Z)^{2n+2m} \end{aligned} \tag{I.4}$$

where Z is the magnitude of $\hat{z}_0$ as follows:

$$\hat{z}_0 = Ze^{j2\pi f_{\text{int}}} \tag{I.5}$$

After some simplifications, Eq. (I.3) can be expressed as

$$\sigma_n^2 \sum_{n=0}^{N} \sum_{m=0}^{N} n(\rho Z)^{2n+2m} + A_{\text{int}}^2 \left(\sum_{n=0}^{N} \alpha_n Z^n \right)^3 \left(\sum_{n=0}^{N} n\alpha_n Z^n \right) = 0 \tag{I.6}$$

For $N \gg 1$, high order terms can be discarded, and after some simplifications, Eq. (I.6) can be presented as

$$\frac{1}{4} = \gamma \left(\frac{1 - Z}{1 - \rho Z} \right)^3 \tag{I.7}$$

where γ is given by

$$\gamma = \frac{A_{\text{int}}^2}{\sigma_n^2 (1 - \rho)} \tag{I.8}$$

Finally, the Wiener solution for the linear-phase FIR NF is given by

$$z_{0,\text{Wiener}}^{\text{LP-FIR}} = \frac{\sqrt[3]{4\gamma} - 1}{\sqrt[3]{4\gamma} - \rho} e^{j2\pi f_{\text{int}}} \tag{I.9}$$

Appendix J: Steady State Solution for FIR NF

The impulse response of the adaptive FIR notch filter is given by

$$H(z,\hat{z}_0)=\sum_{i=0}^{N} a_i \hat{z}_0^i z^{-i} \tag{J.1}$$

where

$$\alpha_i=\begin{cases}1 & n=0\\ (\rho^n-\rho^{n-1})\hat{z}_0^n & 1\le n<N\\ -\rho^{N-1}\hat{z}_0^N & n=N\end{cases} \tag{J.2}$$

and

$$a_i=\begin{cases}1 & n=0\\ \rho^n-\rho^{n-1} & 1\le n<N\\ -\rho^{N-1} & n=N\end{cases} \tag{J.3}$$

When the filtering converges and the system is in steady state, the estimate of $\hat{z}_0$ is close to the true zero, z_0. Thus, Eq. (J.1) can be written as

$$H(z_0,\hat{z}_0)\approx\sum_{i=0}^{N} a_i \hat{z}_0^i z_0^{-i} \tag{J.4}$$

The zero estimation error is given by

$$\delta z_0[n]=\hat{z}_0[n]-z_0[n] \tag{J.5}$$

By substituting $\hat{z}_0[n]=z_0[n]+\delta z_0[n]$ in Eq. (F.4), the following is obtained:

$$H(z_0,\hat{z}_0)\approx\sum_{i=0}^{N} a_i (z_0+\delta z_0)^i z_0^{-i} \tag{J.6}$$

Employing Taylor expansion around $z=z_0$ and neglecting higher order terms, Eq. (J.4) can be simplified to

$$H(z_0, \hat{z}_0) \approx \sum_{i=0}^{N} a_i \left(z_0^i + i z_0^{i-1} \delta z_0 \right) z_0^{-i} \tag{J.7}$$

Now by using the following property of the FIR NF coefficients:

$$\sum_{i=0}^{N} a_i = 0, \quad \text{and} \quad \sum_{i=0}^{N} i a_i = -\frac{1-\rho^N}{1-\rho}, \tag{J.8}$$

Eq. (J.4) can be simplified to

$$H(z_0, \hat{z}_0) = \delta z_0 z_0^{-1} \sum_{i=0}^{N} i a_i = -\delta z_0 \frac{1-\rho^N}{1-\rho} z_0^{-1} \tag{J.9}$$

Similarly, the impulse response of the gradient function is given by

$$G(z_0, \hat{z}_0) = \sum_{i=0}^{N} i a_i \hat{z}_0^{i-1} z^{-i} \tag{J.10}$$

At the steady state, Eq. (J.10) can be written as

$$G(z_0, \hat{z}_0) = \sum_{i=0}^{N} i a_i \hat{z}_0^{i-1} z_0^{-i} \approx \sum_{i=0}^{N} i a_i (z_0 + \delta z_0)^{i-1} z_0^{-i} \tag{J.11}$$

Employing Taylor's expansion around $z = z_0$ and neglecting higher order terms, Eq. (J.10) simplifies to

$$G(z_0, \hat{z}_0) = \sum_{i=0}^{N} i a_i \left(z_0^{i-1} + (i-1) z_0^{i-2} \delta z_0 \right) z_0^{-i} \tag{J.12}$$

$$G(z_0, \hat{z}_0) = z_0^{-1} \sum_{i=0}^{N} i a_i = -\frac{1-\rho^N}{1-\rho} z_0^{-1} \tag{J.13}$$

By defining

$$\mathcal{A} = -\frac{1-\rho^N}{1-\rho} \tag{J.14}$$

Eq. (J.9) and Eq. (J.13) can be approximately presented as

$$\begin{aligned} H(z_0, \hat{z}_0) &\approx \mathcal{A}\delta z_0 z_0^{-1} \\ G(z_0, \hat{z}_0) &\approx \mathcal{A} z_0^{-1} \end{aligned} \tag{J.15}$$

Hence, the steady state output and gradient signal can be written as

$$\begin{aligned} e_s[k] &= \mathcal{A}\mathrm{A}_{\mathrm{int}}\delta z_0[k] e^{j(2\pi k f_{\mathrm{int}} + \theta_{int} - \varphi)} + \eta_1[k] \\ s_s[k] &= \mathcal{A}\mathrm{A}_{\mathrm{int}} e^{j(2\pi k f_{\mathrm{int}} + \theta_{int} - \varphi)} + \eta_2[k] \end{aligned} \tag{J.16}$$

where $\eta_1[k]$ and $\eta_2[k]$ are noise components introduced by $\eta[k]$ at the output of H and G filters, respectively. These noise components are assumed to be zero mean white Gaussian noises and variances of

$$\begin{aligned} \sigma_{\eta_1}^2 &= \mathrm{E}[\eta_1^2[k]] = \frac{\sigma_\eta^2}{2\pi}\int_{-\pi}^{\pi} \left|H\left(e^{j\omega}, \hat{z}_0\right)\right|^2 d\omega \\ \sigma_{\eta_2}^2 &= \mathrm{E}[\eta_2^2[k]] = \frac{\sigma_\eta^2}{2\pi}\int_{-\pi}^{\pi} \left|G\left(e^{j\omega}, \hat{z}_0\right)\right|^2 d\omega \end{aligned} \tag{J.17}$$

These variances can be calculated using Parseval's theorem as follows:

$$\begin{aligned} \sigma_{\eta_1}^2 &= \sigma_\eta^2 \sum_{i=0}^{N} |\alpha_i|^2 \\ \sigma_{\eta_2}^2 &= \sigma_\eta^2 \sum_{i=0}^{N} |\beta_i|^2 \end{aligned} \tag{J.18}$$

By substituting Eq. (J.16) in the zero estimation update equation Eq. (4.12), the following can be written:

$$\delta z_0[k+1] = \delta z_0[k] - \mu e_s[k] s_s^*[k] \tag{J.19}$$

By substituting Eq. (J.16) in Eq. (J.19), the zero estimation update equation simplifies to

$$\mathrm{E}\big[\delta z_0[k+1]\big] = \mathrm{E}\big[\delta z_0[k]\big] - \mu\mathcal{A}^2\mathrm{A}_{\mathrm{int}}^2\mathrm{E}\big[\delta z_0[k]\big] - \mu\mathrm{E}[\eta_1[k]\eta_2^*[k]] \tag{J.20}$$

The correlation between noise components, i.e. η_1 and η_2, is given by

$$\mathrm{E}[\eta_1[k]\eta_2^*[k]] = R_{\eta_1,\eta_2} = \frac{\sigma_\eta^2}{2\pi j}\oint_C H(z,\hat{z}_0)G^*(z^{-1},\hat{z}_0)z^{-1}dz \tag{J.21}$$

By using the Residue theorem, the correlation value is given by

$$\begin{aligned} R_{\eta_1,\eta_2} &= \sigma_\eta^2 \sum_{i=0}^{N} \alpha_i \beta_i^* \\ &= \sigma_\eta^2 \hat{z}_0 \left((\rho-1)^2 \frac{1-(N+1)(\rho\hat{z}_0)^{2N} - N(\rho\hat{z}_0)^{2N-2}}{(1-(\rho\hat{z}_0)^2)^2} + N(\rho\hat{z}_0)^{2N-2} \right) \\ &\cong \sigma_\eta^2 \hat{z}_0 \left(\frac{1-\rho}{1-(\rho\hat{z}_0)^2} \right)^2 \end{aligned} \tag{J.22}$$

Thus, Eq. (J.20) can be rewritten as

$$\mathrm{E}\big[\delta z_0[k+1]\big] = \big(1-\mu\mathcal{A}^2\mathrm{A}_{\mathrm{int}}^2\big)\mathrm{E}\big[\delta z_0[k]\big] - \mu R_{\eta_1,\eta_2} \tag{J.23}$$

Eq. (J.23) represents the difference equation of the convergence in the mean for the zero estimation problem. The final value of the discrete differential equation is given by

$$\begin{aligned} &\mathrm{E}\big[\delta z_0[\infty]\big] = \lim_{k\to\infty} \mathrm{E}\big[\delta z_0[k+1]\big] = \lim_{k\to\infty} \mathrm{E}\big[\delta z_0[k]\big] \\ &\Rightarrow \lim_{k\to\infty} \mathrm{E}\big[\delta z_0[k]\big] \cong -\frac{R_{\eta_1,\eta_2}}{\mathcal{A}^2\mathrm{A}_{\mathrm{int}}^2}, \text{and, } \lim_{k\to\infty} \mathrm{E}\big[z_0[k]\big] \cong z_0 - \frac{R_{\eta_1,\eta_2}}{\mathcal{A}^2\mathrm{A}_{\mathrm{int}}^2} \end{aligned} \tag{J.24}$$

Appendix K: MSE of FIR NF Solution

By employing Eq. (4.12), the following can be written

$$\mathrm{E}[|\delta z_0[k+1]|^2] = \mathrm{E}[|\delta z_0[k] - \mu e[k]s^*[k]|^2] \tag{K.1}$$

which can be presented as

$$\mathrm{E}[|\delta z_0[k+1]|^2] = \mathrm{E}[|\delta z_0[k]|^2] + \mu^2 \mathrm{M}_1 - \mu \mathrm{E}[|\delta z_0[k]|^2] \mathrm{M}_2 \tag{K.2}$$

where, after long calculation, M_1 and M_2 are given by

$$\begin{aligned} M_1 = {} & \left(\mathcal{A}^2 A_{\mathrm{int}}^2 \mathrm{E}[|\delta z_0[k]|^2] + \sigma_{\eta_1}^2\right)\left(\mathcal{A}^2 A_{\mathrm{int}}^2 + \sigma_{\eta_2}^2\right) \\ & + 2\mathcal{A}^2 A_{\mathrm{int}}^2 R\mathrm{e}\left\{R_{\eta_1,\eta_2} \mathrm{E}[\delta z_0^*[k]]\right\} + 2\left|R_{\eta_1,\eta_2}\right|^2 \end{aligned} \tag{K.3}$$

and

$$M_2 = 2\mathcal{A}^2 A_{\mathrm{int}}^2 + 2R\mathrm{e}\left\{R_{\eta_1,\eta_2}\right\} \tag{K.4}$$

By employing steady state results given by Eq. (J.16), the steady state MSE of Eq. (K.1) can be simplified to

$$\lim_{k\to\infty} \mathrm{E}[|\delta z_0[k]|^2] = \frac{\mu\sigma_{\eta_1}^2\left(\mathcal{A}^2 \mathrm{A}_{\mathrm{int}}^2 + \sigma_{\eta_2}^2\right)}{2\left(\mathcal{A}^2 A_{\mathrm{int}}^2 + R\mathrm{e}\left\{R_{\eta_1,\eta_2}\right\}\right) - \mu\mathcal{A}^2 \mathrm{A}_{\mathrm{int}}^2\left(\mathcal{A}^2 \mathrm{A}_{\mathrm{int}}^2 + \sigma_{\eta_2}^2\right)} \tag{K.5}$$

By considering Eq. (K.5) and taking into account that the MSE estimator is always positive, the LMS step size following can be written as

$$0 < \mu < \frac{2\left(\mathcal{A}^2 A_{\mathrm{int}}^2 + R\mathrm{e}\left\{R_{\eta_1,\eta_2}\right\}\right)}{\mathcal{A}^2 \mathrm{A}_{\mathrm{int}}^2\left(\mathcal{A}^2 \mathrm{A}_{\mathrm{int}}^2 + \sigma_{\eta_2}^2\right)} \tag{K.6}$$

Appendix L: BER performance for different quantization resolutions

Figure L.1 shows the BER results for the 1-bit quantization case. The effective C/N_0 values can be easily calculated using these plots and Eq. (3.18). As can be seen, BER increases as the jammer approaches the target receiver, where for the worst case, the BER is about 0.2. The performance improvement employing NF is small in terms of BER. This is due to this fact that, although the strongest harmonic is removed, due to the high levels of other harmonics, the performance degradation is the same as that of an NF-free case. To improve the performance, either the quantization resolution or the number of NFs should be increased.

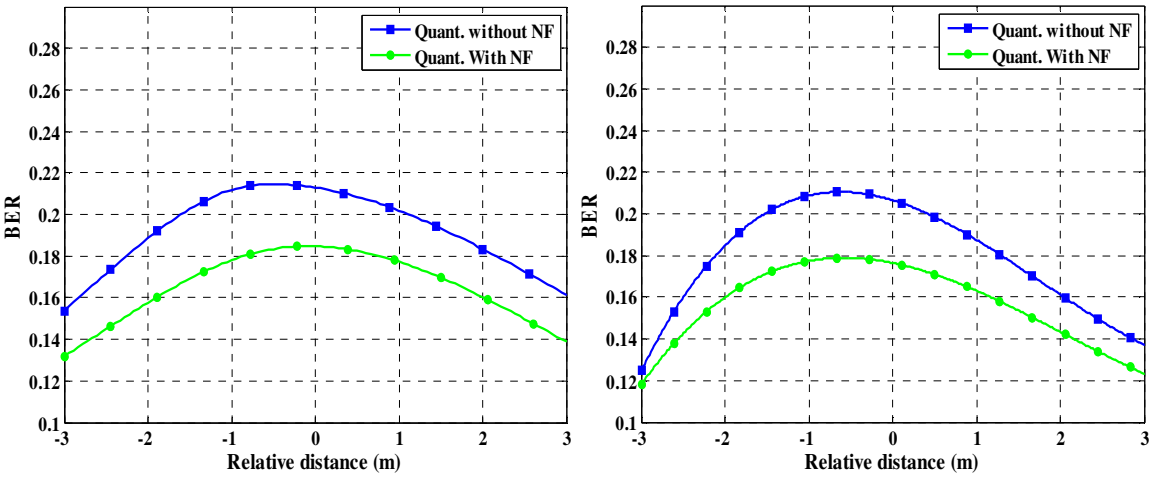

(a) 20 km/h relative velocity (b) 70 km/h relative velocity

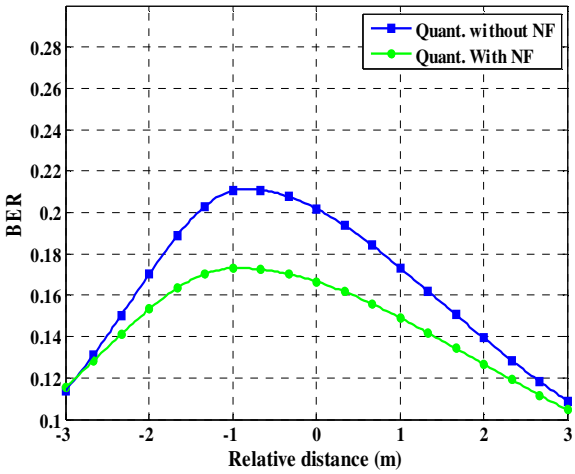

(c) 120 km/h relative velocity

Figure L.1: BER results for 1-bit quantization

Figure L.2 demonstrates the BER results for the 3-bit quantization case. As it can be seen, BER performance in the worst case is approximately 3×10^{-3}, which improves to 3×10^{-4} by employing a single NF.

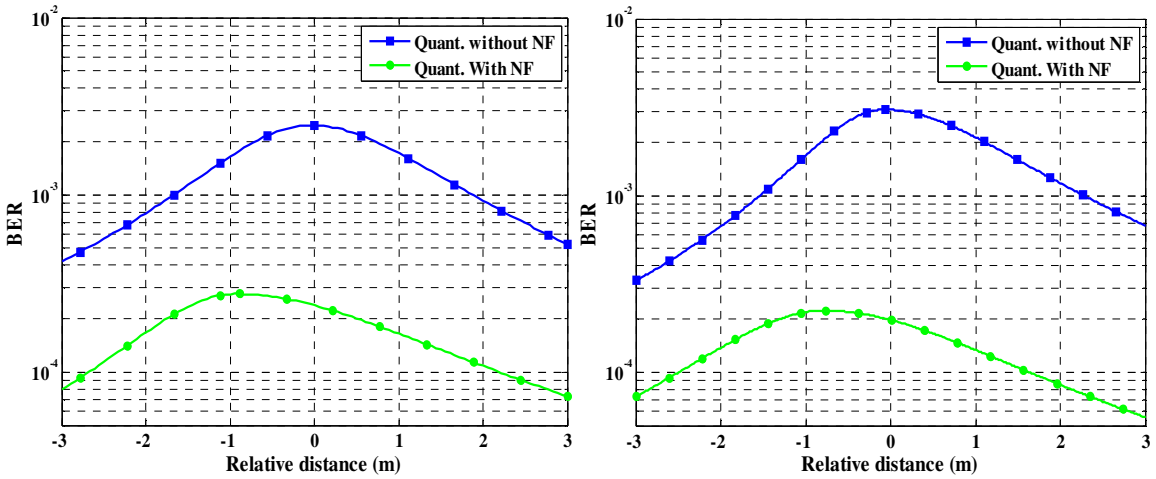

(a) 20 km/h relative velocity (b) 70 km/h relative velocity

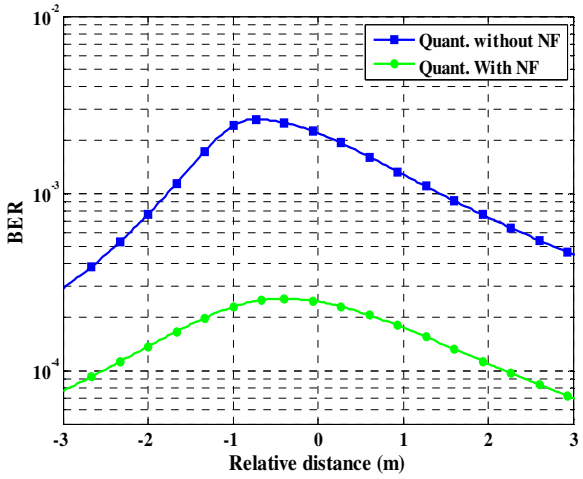

(c) 120 km/h relative velocity

Figure L.2: BER results for 3-bit quantization

Figure L.3 shows the BER results for the 4-bit quantization case for the different scenarios. In this case, BER performance in the worst case is approximately 2×10^{-3}, which improves to 3×10^{-4} by employing a single NF. Because the interference power is high, the performances of 3-bit and 4-bit are close to each other (See Chapter Three).

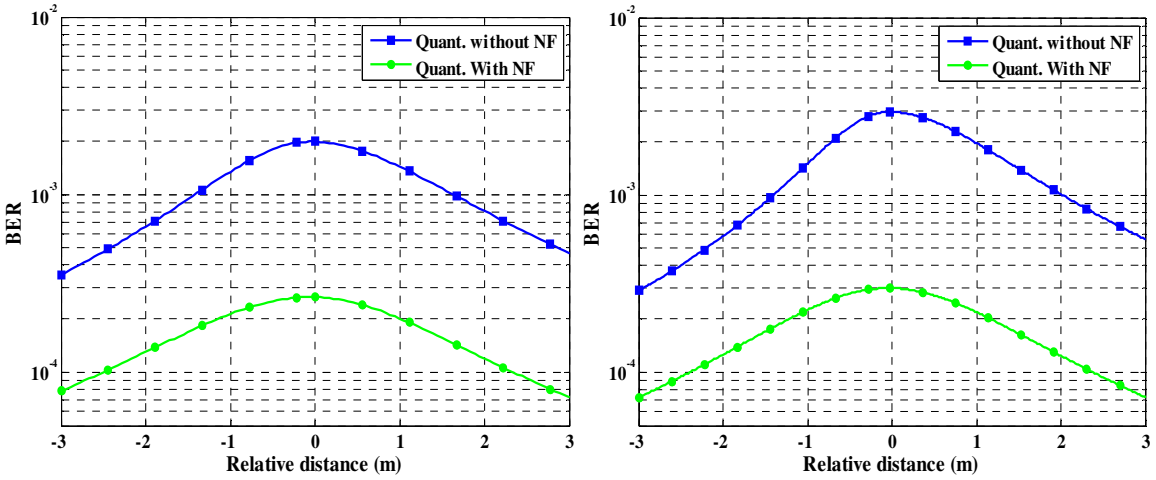

(a) 20 km/h relative velocity (b) 70 km/h relative velocity

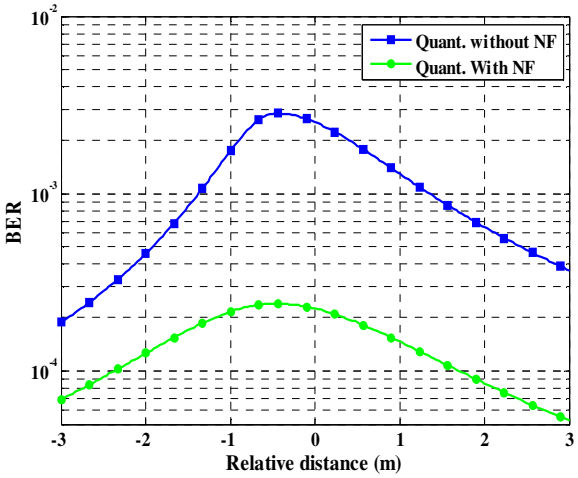

(c) 120 km/h relative velocity

Figure L.3: BER results for 4-bit quantization